2000

Dynamic behavior characterization of fine powders consisting of a homogeneous emulsion, and, Synthesis and decomposition of methane gas hydrate: A reaction engineering study.

Sridhar Narasimhan
West Virginia University

DYNAMIC BEHAVIOR CHARACTERIZATION OF FINE POWDERS CONSISTING OF A HOMOGENEOUS EMULSION

&

SYNTHESIS AND DECOMPOSITION OF METHANE GAS HYDRATE
< A REACTION ENGINEERING STUDY>

Sridhar Narasimhan

Thesis submitted to the
College of Engineering and Mineral Resources
at West Virginia University
in partial fulfillment of the requirements
for the degree of

Master of Science
in
Chemical Engineering

Hisashi O. Kono. Ph.D., Chair
Alfred H. Stiller, Ph.D.
Charter D. Stinespring, Ph.D.

Department of Chemical Engineering

Morgantown, West Virginia
2000

Keywords: Rheological Parameters, Viscosity, Methane Gas Hydrate, Sediments

ABSTRACT

SECTION I

This work quantitatively characterizes the flow and mixing properties of aerated bulk fine powders between the minimum fluidization and minimum bubbling velocities ($U_{mf} < U < U_{mb}$). In order to accomplish this characterization, the viscosity of the emulsion phase was measured using the Maxwell's model for the rheological behavior of complex bodies along with the set of rheological parameters proposed by Kono et al (1994). A unique property of the bulk fine powder called the relaxation time (τ) was measured experimentally and this property was combined with another rheological parameter called the plastic deformation coefficient (Y) to give the viscosity of the emulsion phase as $\mu = Y\tau$.

SECTION II

This work describes the first homogeneous formation and decomposition of methane gas hydrates within several different synthetic sediments by using a high-pressure batch reaction system. The pressure of the formation reaction was varied in the range of 6.8 – 13.6 MPa while the temperature was maintained constant at 273.5 K Decomposition of hydrate was accomplished through controlled depressurization starting at a pressure of 2.7 MPa, maintaining the temperature constant at 273.5 K. Overall reaction order, both for the formation and decomposition were also determined.

DEDICATED TO MY PARENTS

ACKNOWLEDGEMENTS

The author expresses his sincere thanks to his research advisor, Prof. H. O. Kono, whose guidance in accomplishing this research work was beyond words. The author would like to mention that Dr. Kono always adds a fourth dimension to his research, which is excellence.

The author also expresses his gratitude to the examining committee members, Dr. A. H. Stiller and Dr. C. D. Stinespring, for their valuable questioning and suggestions. He would also like to thank Dr. Dady B. Dadyburjor for the help he offered by providing a teaching assistantship in the department. The author would like to thank Mr. James Hall for all the help provided in view of repairing old and designing new equipment.

TABLE OF CONTENTS

NOMENCLATURE

SECTION I

A : cross-sectional area of cylindrical column [m^2]

d* : effective particle diameter [m]

F : contact force at a single contact point [N]

g : gravitational acceleration = 9.8 m/s^2

G : dead zone formation number [-]

k : co-ordination number [-]

M : mass of particles [kg]

N : number of unit layers [-]

S : strain on the bulk powder [-]

U : superficial gas velocity [cm/s]

Y : plastic deformation coefficient [Pa]

ΔP^{**} : gas pressure drop across the unit layer [Pa]

Subscript

mf : at minimum fluidization

mb : at minimum bubbling

p : particle

f : fluid

Greek Letters

σ : fracture strength of the bulk powder [Pa]

μ : viscosity of the emulsion phase [Pa-s]

ε : porosity of the bulk powder [-]

τ : relaxation time of the bulk powder [sec]

SECTION II

H : hydrate

k : overall reaction rate constant $[min]^{-1}$ or [moles/min]

L : liquid

n : number of moles of methane [moles]

n* : overall order of reaction [-]

P : pressure [MPa]

T : temperature [K]

V : volume $[m^3]$

Subscript

f : at formation

d : at decomposition

e : at equilibrium

gs : gas space

LIST OF TABLES

SECTION I

SECTION II

LIST OF FIGURES

SECTION I

SECTION II

SECTION I

CHAPTER I

INTRODUCTION

1.1 Objectives

Development of the method and the theory to measure the viscosity of the emulsion phase or particulate phase (μ) of homogeneously aerated or expanded fine powders within the well-defined gas velocity range $U_{mf} < U < U_{mb}$. The effect of viscosity on the flow characteristics of the bulk powder is also investigated.

Development of a novel dimensionless number to characterize the particle behavior in a fluidized bed as against the gravitational force acting on the particles. This dimensionless number, called the dead zone formation number (G) is defined and measured at the minimum fluidization velocity U_{mf}.

1.2 Background

Generally, any research in Powder Characterization starts with the question ”What are Particles?” Discrete particles have conventionally been defined by simply specifying their properties such as particle size (d_p), density (ρ_p) and shape factor (ϕ_s). The next step is to answer the question “What is Powder?”. The fact that each powder researcher has a different view makes the definition of ‘powder’ very difficult. ‘Powder’, as defined by the Webster’s dictionary is “matter in a finely divided state, a form of fine particles”. According to Rietema (1991) in his book “The Dynamics of Fine Powders”, he defined ‘powder’ as “a collection of small discrete solid particles in close contact with each other…”

For predicting the flow properties of dry bulk fine powders in solid-gas system, static powder properties such as particle size (d_p), density (ρ_p), shape factor (ϕ_s) and their distribution, have been traditionally measured since long. However, it seems that the dynamic characteristics of these bulk fine powders could not always be quantitatively

obtained from the above static powder properties, which have rather been used only as some indexes.

Hence in this work, we have introduced the specific concept of "Bulk Fine Powder" based on a series of publications by Kono et al (1994). Bulk Fine Powder, as defined here, is a collection of very large numbers of small discrete solid particles in close contact with each other, maintaining empty space of the void fraction (ε) between the particles. In case of gas-solid system, this void space is occupied by the gas. In this work, the bulk fine powder is modeled as a single quasi-solid body and it consists of infinite numbers (N) of fine particles where for example N could be in the range $10^5 \sim 10^{15}$ per liter of the bulk fine powder.

The characterization of the flow properties of this bulk fine powder involves the basic consideration of several important fundamental principles of powder rheology. As a first step in characterizing the flow properties of bulk fine powder, the flow regime of the bulk fine powder must be specified. The flow regime considered in this work is the regime between the minimum fluidization (U_{mf}) and minimum bubbling (U_{mb}) velocities. This flow regime is represented as $U_{mf} < U < U_{mb}$ and the bulk fine powder in this regime is said to consist of a homogeneous emulsion phase. This emulsion phase satisfying the above condition could be characterized by a dimensionless number $G = \Delta P_{Umf} / \tau_g$; τ_g being the gravitational stress of the bed given by the ratio Mg/A. For sample powders considered in this work, G is close to unity.

For bulk fine powder that satisfies all the above conditions Kono et al (1994) defined rheological parameters to completely characterize its flow and mixing properties. These rheological parameters defined within the well-defined gas velocity range $U_{mf} < U < U_{mb}$ are

1. Plastic deformation coefficient (Y) measured within the range $U_{mf} < U < U_{mb}$.
2. Fracture strength ($\sigma_{f,mb}$) measured at Umb.

The theory and the experimental measurement methods required to determine Y and $\sigma_{f,mb}$ have already been outlined by Kono et al (1994) in another paper.

Although Kono et al (1994) proposed to measure two rheological parameters of aerated fine powders such as plastic deformation coefficient (Y) and fracture strength ($\sigma_{f,mb}$) in the homogeneously aerated bed between the gas velocity range of minimum fluidization (U_{mf}) and minimum bubbling (U_{mb}) at ambient and elevated temperature, the measurement of the viscosity of the emulsion phase (μ) was achieved and reported in this work within the gas velocity range $U_{mf} < U < U_{mb}$. It should be noted that the viscosity of the emulsion phase defined here be the viscosity of the emulsion phase relevant to the Maxwell body for the rheological behavior of complex bodies, which is different from the so-called eddy viscosity.

The method of estimation for the viscosity of the homogeneous emulsion phase of the bulk fine powder bed is based on the Maxwell's model for the rheological behavior of complex bodies. The fundamental premise behind this estimation method is that certain bulk fine powder beds behave like a viscoplastic body when subjected to aeration and subsequent relaxation. A unique parameter of the bulk powder called the relaxation time is measured experimentally. This relaxation time is defined as the time required for the stress to relax to 1/e of its initial value when the strain is held constant. Here the variation of stress with time is measured in terms of the variation of ΔH with time. Since the bed height decreases exponentially, the relaxation time τ is the time when $H = (1/e)(\Delta H)_{initial}$. Hence by knowing τ and Y, the viscosity of the homogeneous emulsion phase (μ) could

be calculated as $\mu = Y\tau$. If the bulk fine powder bed follows the Maxwell's model described above, then the bulk fine powder bed is said to be viscoplastic in nature.

In order to further understand the significance of these rheological parameters, two dimensionless numbers are defined and these numbers are referred to as the Viscoplastic numbers of the bulk fine powder bed and are defined as shown below

$$Vn(I) = \frac{s_{f,mb}}{Y}$$

$$Vn(II) = \frac{m}{Yt}$$

Hence, by knowing the viscosity through the experimental method described in this paper, together with two other rheological parameters of plastic deformation coefficient (Y) and fracture strength ($\sigma_{f,mb}$), the viscoplastic characteristics of the emulsion phase could completely be described.

Therefore, it could be realized that the viscoplastic characteristics of the emulsion phase within the gas velocity range $U_{mf} < U < U_{mb}$ seems to be the necessary and satisfactory condition for the good fluidization of dry bulk fine powders. As sample powders, starch with three different mean diameters of 15, 20 and 40 microns was used for all the experiments.

1.3 Significance of Research

Quantitative characterization of the hydrodynamics of aerated beds is required for the design and scale-up of efficient new reactors in several chemical industries. It is well known that rheological parameters strongly influence the hydrodynamic behavior of aerated gas-solid beds. Flows of particulate materials are encountered in numerous

commercial industries including metallurgical, chemical, agricultural, pharmaceutical, plastics and food processing industries.

Viscosity, a dynamic rheological property is useful in characterizing quantitatively these flow and mixing properties of fine powders. The use of numerical simulation in fluidized beds also requires reliable values of this rheological property. The importance of viscosity could also be realized from certain dimensionless numbers encountered in fluid dynamics such as Reynolds number, Archimedes number, etc. Viscosity also plays a key role in heat and mass transfer applications as is evident from the dimensionless numbers such as Prandtl number and Schmidt number respectively.

In general, for liquids, better heat, mass and momentum transport could be achieved by lowering the viscosity of the liquid. Considering the key role-played by viscosity in these transport processes, it could be seen that measuring the viscosity of the emulsion phase in fluidized beds becomes important and useful. Therefore, we propose to study the rheological parameters of aerated fine powders, in particular, the viscosity of the homogeneous emulsion phase. Furthermore, the effect of varying the viscosity of the emulsion phase on the flow characteristics of fine powders is also studied in order to find a new insight into the fluidization phenomenon.

CHAPTER II

BASIC CONSIDERATION
&
LITERATURE REVIEW

2.1 Previous Research

Schügerl (1960) measured the viscosity of fluidized beds by using the well-known couette viscometer, which has conventionally been utilized for measuring the viscosity of liquids. The viscometer used rotates inside the fluidized bed and the obtained results were dependent upon the rotation speed of the rotor. The drawback of this method is that the rotor created heterogeneity in the bed destroying the homogeneous powder structure.

Grace (1970) proposed a method where the viscosity of fluidized beds was estimated from the shape of the bubbles in the fluidized bed. This method correlated empirically, the bubble Reynolds number with the included angle in a bubble, from which the viscosity was measured. The drawback of this method is that the interparticle interactions were not taken into account.

Edwards (1990) proposed a mathematical model to predict the viscosity for the slow flow of powders based on the compactivity of powders. The model equation relates compactivity and viscosity over a wide range of velocities. Equations to describe the stress tensor required for the determination of viscosity were also proposed. The drawback of this method is that the results given by the model equation were not verified experimentally.

Khakhar et al (1995) measured the apparent shear viscosity of gas – fluidized beds containing glass beads in the size range 400 – 1000 microns. The fluidized bed was experimentally verified to behave like a Bingham plastic. The well-known Brookfield viscometer was used to measure the viscosity.

Overfelt et al (1998) proposed a method where the viscosity of fluidized beds was measured using a Brookfield viscometer under reduced gravity. The particles used were silica sand with the particle size range 150-700 microns. The viscometer used had a

rotating spindle, which was allowed to rotate inside the fluidized bed during measurements. In this method, the spindle created heterogeneity in the bed, thereby destroying the powder structure, which is a serious drawback.

Cazenave et al (1999) measured the viscosity of powder beds containing glass beads with three different particle sizes namely 600, 60 and 6 microns by subjecting the bed to vertical vibrations. A known torque was imposed on the powder bed using a rotating vane and the resulting angular displacement was measured. The viscosity was obtained from this torque-angular displacement data.

2.2 Basic Consideration

2.2.1 Powder Classification

In 1973, Geldart classified powders by particle diameter and particle density and divided the classification into four different Geldart type powders. Group A powders have a diameter ranging between 40μm and 500μm, density less than 1400kg/m^3, and are aeratable. Group B powders are similar in size to Group A, but are sand-like and have a density between 1400kg/m^3 and 4000kg/m^3. Group B powder fluidizes well but bubbles vigorously. Group D powders are large and dense. Group D powders do not fluidize very well because they normally lead to channeling. Group C powders have a diameter smaller than 15μm. They have very high interparticle force and could not be fluidized.

Considering the recent advances in the branch of Powder Technology, conventional characterization based on simple particle properties is not always adequate. There are also other important determining factors in powder classification which are outlined in Table 1. This classification has been derived from the conclusions of a series of publications by Kono et al over the past several years.

Properties of Bulk Powders	**Coarse Particles**	**Fine Powders**	**Very Fine Powders**
Particle diameter, d_p	$d_p > 100\mu m$	$40\mu m < d_p < 100\mu m$	$d_p < 5\mu m$
Aeration condition	$U_{mf} = U_{mb}$	$U_{mb} > U_{mf}$	U_{mf} and U_{mb} could not be defined
Homogeneous Aeration without bubble	Impossible	Possible	Impossible
Fluidization Quality at $U = 15U_{mb}$	Bad due to dead zone formation	Generally Good	Generally impossible due to channeling
Compressibility	No	No or very small	Yes
Time averaged Porosity, ε_{mf}	Constant	Changes slightly	Changes drastically
Cohesiveness	Non-Cohesive	Slightly Cohesive	Cohesive
Fracture Strength, σ_f at U_{mb}	Approximately zero	Small to very small	Significant and relatively large
Plastic Deformation Coefficient, Y at $U_{mf} < U < U_{mb}$	Very Large	Large	Small

Table 2.1 Powder classification as a function of several important physical properties

2.2.2 Rheological Approach

The rheological approach proposed by Kono et al (1994) is based on the concept of “Bulk Fine Powder”. The behavior of this bulk fine powder needs to be explained in order to understand the rheological approach. Generally, for coarse particles, the behavior of the bulk powder is considered to be very unstable. Fine powders (with appropriate rheological parameters) are considered to be stable because the bulk powder bed expands homogeneously in height when fluidized. The bed height increases until the point of minimum fluidization where the bed has a porosity ε_{mf}. With additional aeration, the porosity increases to a point ε_{mb} where the first bubble appears.

It was experimentally observed by Kono et al (1994) that, the powder starch ($d_p = 15\mu m$, $\rho_p = 1550 kg/m^3$) could be fluidized well although it is a Geldart’s Group C powder. Therefore, the classical static parameters such as particle size and density are not enough to predict the quality of fluidization. Kono et al (1994) found an empirical equation, later found to be theoretical, which states that if a powder lies on the line $\sigma_{f,\,mb} = 0.11Y^{0.9}$, then the powder is fluidizable where $\sigma_{f,\,mb}$ and Y are called the *rheological parameters of aerated fine powders*. In this empirical equation, Y is known as the plastic deformation coefficient of the bulk fine powder defined within the gas velocity range $U_{mf} < U < U_{mb}$, while $\sigma_{f,\,mb}$ is known as the fracture strength of the bulk fine powder defined at the minimum bubbling point, U_{mb}.

2.2.3 InterParticle Force

The tensile strength of individual spherical particles of uniform size has been defined by Rumpf (1958) as

$$s_f = \frac{1-e}{p} k \frac{F}{d^{*2}} \qquad (2.1)$$

Where:

$\sigma_{f:}$ tensile strength of the powder compact, [Pa]

ε : porosity (voidage) of the powder compact, [-]

k: coordination number, [-]

F: contact force at a single contact point, [N]

d*: effective particle diameter (assuming uniformity in size), [m]

The coordination number of a single particle in a packing is defined as the total number of points of contact with surrounding particles. It should be noted that though the contact force F is a constant, it is specific to a certain powder.

2.2.4 Significance of Rheological Parameters (Y, $\sigma_{f,mb}$, μ)

The plastic deformation coefficient Y is defined as the ratio of the stress the powder is under, to the strain the powder undergoes. In other words, Y measures the amount of energy input required for a known expansion of the powder bed. The parameter Y could also be visualized as a volume expansion index of the aerated powders.

The fracture strength $\sigma_{f,mb}$ is a measure of the adhesive forces within the powder particulates. The fracture strength is measured at the minimum bubbling point and the first fracture in the powder bed marks the birth of the first bubble.

The viscosity of the emulsion phase μ is a measure of the fluidity or mobility of the bulk powder bed. The viscosity measured is a strong property of the material. This viscosity is applicable only for powders that exhibit viscoplastic behavior following the Maxwell's model for the rheological behavior of complex bodies.

2.2.5 Measurement of Rheological Parameters

The fracture strength $\sigma_{f,\,mb}$ and the plastic deformation coefficient Y for fine powders could be directly measured by aeration experiments. In general, under the aerated or fluidized state, there exists two phases. One is the phase containing both the gas and the solid particles in suspension called the emulsion or dense or particulate phase and the other is the bubble phase, which contains solid free gas envelopes called bubbles.

Fine powders could be fluidized without the formation of bubbles in the gas velocity range between U_{mf} and U_{mb}. When the gas velocity reaches the minimum fluidization velocity, the gravitational force is compensated by the drag force of the flowing gas. After the point of minimum fluidization velocity, the pressure drop across the bed remains nearly constant with additional flow of gas. At the minimum bubbling point, the homogeneity of the bed is disturbed and the first bubble appears.

The expansion of the powder bed could be expressed in terms of an equivalent unit layer for conditions at U_{mf} and U_{mb}. The physical changes occurring in a bed of fine powder within the gas velocity range, $U_{mf} < U < U_{mb}$ are very important to be able to make an energy balance for the equivalent unit layer of the powder bed.

By making an energy balance on the equivalent unit layer of the powder bed and by combining this energy balance with the Rumpf's definition equation, the fracture strength of the bulk powder at U_{mb} could be derived as

$$s_{f,mb} = \frac{\Delta P^{**}}{1+\left(\frac{e_{mb}}{e_{mf}}\right)\frac{(1-e_{mf})}{(1-e_{mb})}} \qquad (2.2)$$

Where,

$\sigma_{f,\,mb}$: fracture strength at the minimum bubbling point, [Pa]

ΔP^{**}: pressure drop across a unit layer of powder, [Pa]

ε_{mf}: porosity at minimum fluidization point, [-]

ε_{mb}: porosity at minimum bubbling point, [-]

For the deformation of the powder bed in the range between U_{mf} and U_{mb} the strain in the unit powder layer, assuming homogeneous expansion, could be expressed as

$$S = \frac{h_{mb} - h_{mf}}{h_{mf}} = \frac{N(h_{mb} - h_{mf})}{N h_{mf}} = \frac{H_{mb} - H_{mf}}{H_{mf}} \tag{2.3}$$

Therefore, the plastic deformation coefficient Y of the aerated powder structure could be defined as

$$Y = \frac{\Delta P^{*} / N}{(h_{mb} - h_{mf}) / h_{mf}} = \frac{\Delta P^{**}}{(H_{mb} - H_{mf}) / H_{mf}} = \frac{\Delta P^{**}}{\left(\frac{\Delta H}{H}\right)} \tag{2.4}$$

CHAPTER III

THEORETICAL BACKGROUND

3.1 Viscosity Estimation

3.1.1 Methodology

The viscosity as estimated here, is a property of the powder and describes the physical nature of the material. The viscosity defined here is applicable only to the emulsion phase of the bed. The concept of viscosity resulting from gas-particle or particle-particle shearing forces is only applicable to the emulsion phase of the bed. By measuring the viscosity, the viscoplastic behavior of the powder could be completely characterized. The term viscoplastic is strictly restricted to those materials whose response to a sudden relaxation obeys the Maxwell's model for the rheological behavior of complex bodies.

The estimation method proposed in this work for the viscosity of aerated fine powders is based on the Maxwell's model for the rheological behavior of complex bodies. The fundamental premise behind this estimation method is that certain specific bulk powder beds behave like a viscoplastic body when subjected to aeration and subsequent relaxation. A unique parameter of the bulk powder called the relaxation time, is measured experimentally. This experimentally obtained relaxation time is combined with the Maxwell's model to give the viscosity of the emulsion phase as $\mu = Y\tau$. This methodology is schematically represented in Fig 3.1. The Maxwell's model for the rheological behavior of complex bodies as applied to the case of aerated fine powders is as shown in Fig 3.2.

The relaxation experiment is conducted in the velocity range $U_{mf} < U < U_{mb}$ so that there is nearly no influence of the gravitational force in the powder bed. Because, under this velocity condition, the gravitational force acting on the particles is nearly

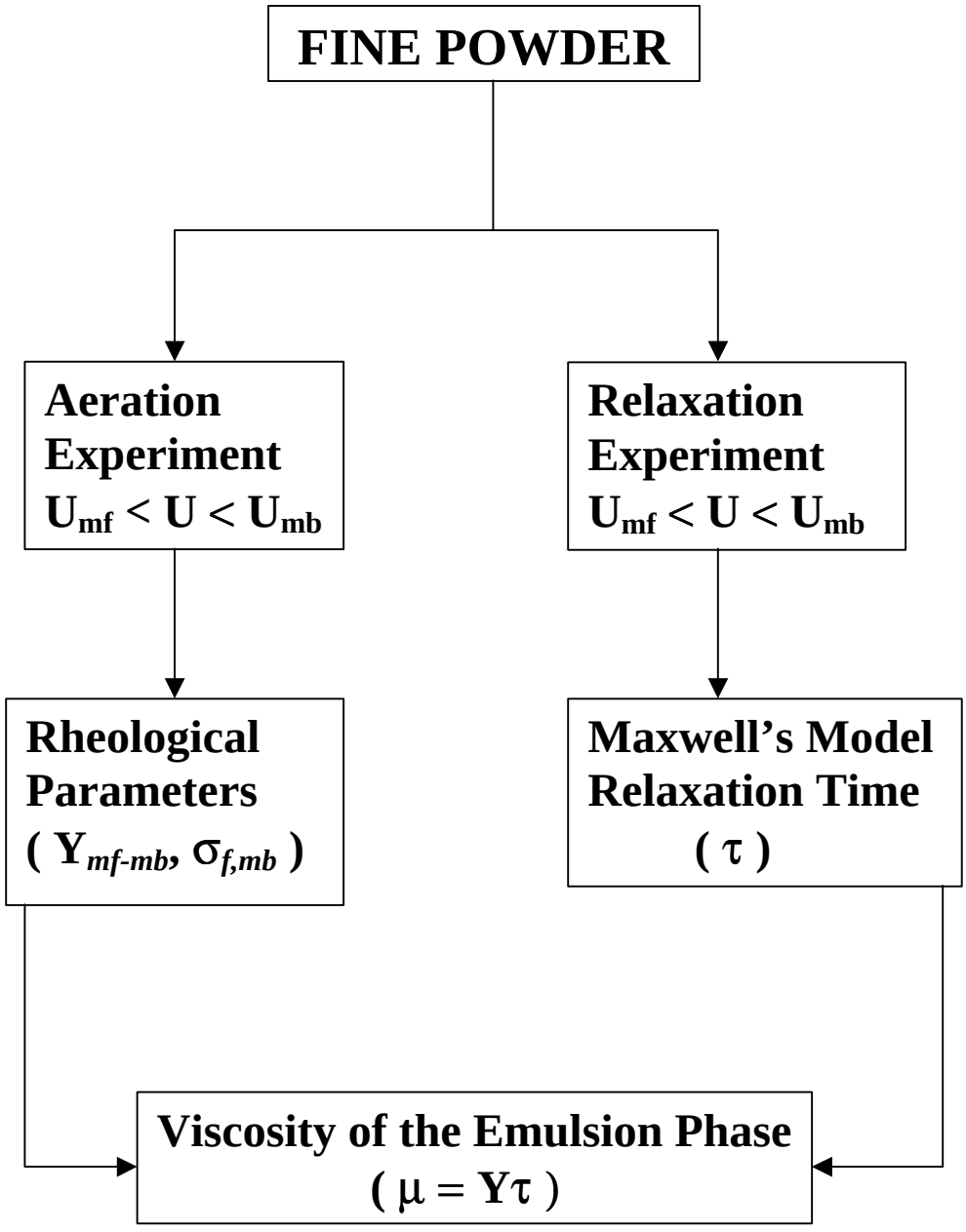

Figure 3.1 Methodology for the estimation of viscosity of the emulsion phase.

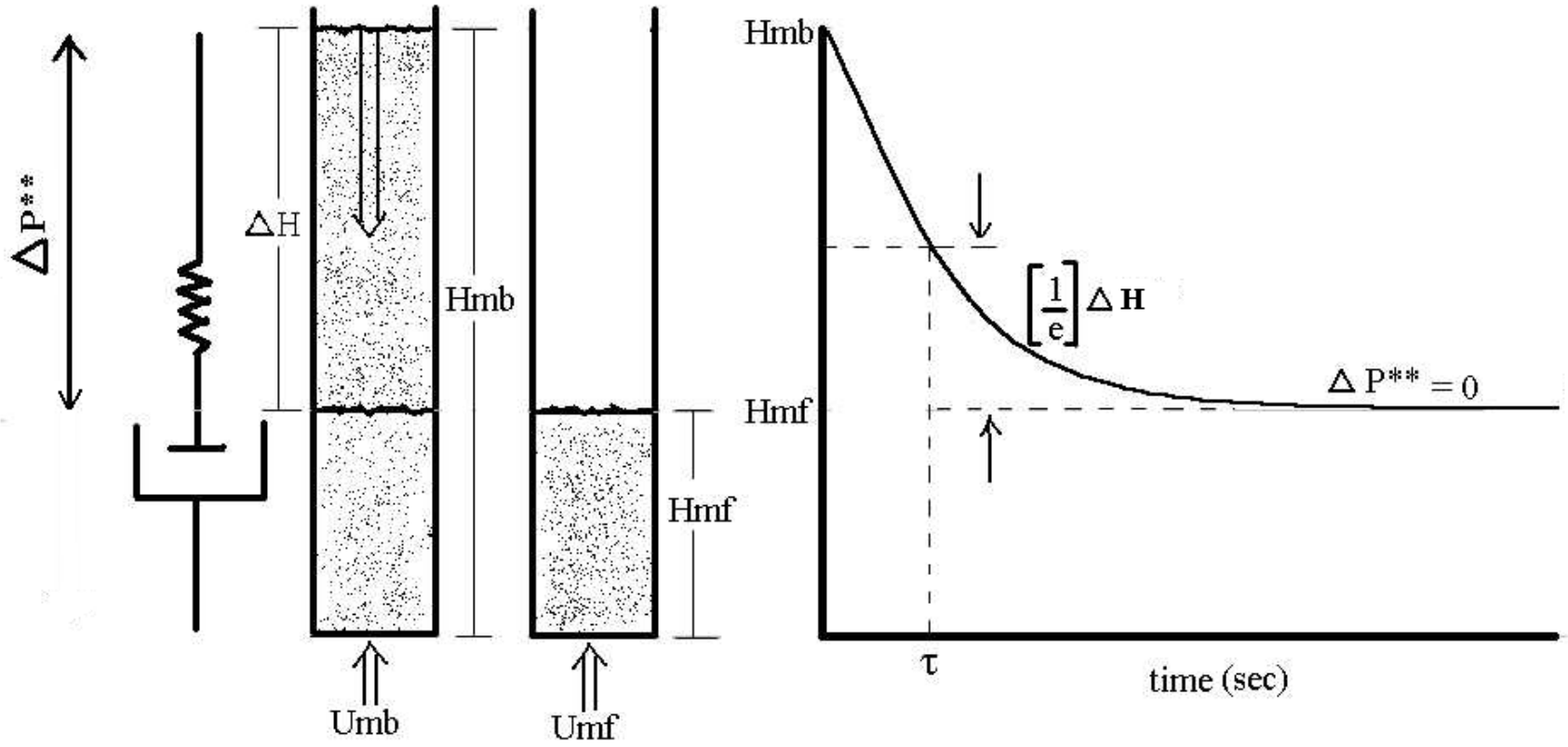

Figure 3.2 Maxwell's model for the rheological behavior of complex bodies.

compensated by the drag force of the flowing gas. Under these circumstances, the only other force that needs consideration is the interparticle force. Hence, the elimination of the effect of gravitational force is one major advantage of the proposed method in comparison with other methods, which are existing, in open literature.

3.1.2 Model description

The viscosity of the emulsion phase (μ) of aerated fine powders without bubbles, i.e., at the gas velocity (U) between the minimum fluidization (U_{mf}) and minimum bubbling (U_{mb}) points, with homogeneous, well-defined fine powder packing structures could be estimated by the method outlined below for the case of fluidizable powders.

The method of determination of viscosity of the emulsion phase starts with the determination of the plastic deformation coefficient (Y) of the emulsion phase, followed by the estimation of the relaxation time (τ). These experimentally determined parameters are combined together to give the viscosity of the emulsion phase.

The plastic deformation coefficient is defined between the minimum fluidization and minimum bubbling points and could be expressed by Eqn (3.1).

$$Y_{mf-mb} = \frac{\Delta P^{**}}{\left(\frac{\Delta H}{H}\right)} \tag{3.1}$$

The estimation of the relaxation time is based on the Maxwell's model for the rheological behavior of complex bodies. This model could be physically visualized as shown in Fig 3.2. The Maxwell's model consists of a spring (elastic element) with a

modulus Y and a dashpot (viscous element) with a viscosity μ, connected in series. Under any external force, the total strain is the sum of the strain in the spring and in the dashpot,

$$S = S_1 + S_2 \tag{3.2}$$

where

S_1: strain in the elastic spring, [-]

S_2: strain in the viscous dashpot, [-]

The stress on the spring is

$$F = YS_1 \tag{3.3}$$

The stress on the dashpot is

$$F = \mu \frac{dS_2}{dt} \tag{3.4}$$

Differentiating Equation (3.2) with respect to time on both sides,

$$\frac{dS}{dt} = \frac{dS_1}{dt} + \frac{dS_2}{dt} \tag{3.5}$$

Replacing for the terms in Equation (3.5) and since the stress F corresponds to ΔP^{**} the model equation could be derived as

$$\frac{dS}{dt} = \frac{1}{m}\Delta P^{**}(t) + \frac{1}{Y}\frac{d(\Delta P^{**})}{dt} \tag{3.6}$$

At time t = 0, $\frac{dS}{dt} = 0$ and hence Equation (3.6) becomes

$$\frac{1}{m}\Delta P^{**}(t) + \frac{1}{Y}\frac{d(\Delta P^{**})}{dt} = 0 \tag{3.7}$$

The solution of Equation (3.7) is

$$\Delta P^{**} = \left(\Delta P^{**}\right)_{U_{mb}} \exp\left(-\frac{t}{t}\right) \tag{3.8}$$

Where $t = \frac{m}{Y}$ is the relaxation time for the bulk powder, [sec]

The derivation of Eqn. (3.8) is outlined in the Appendix.

The relaxation time is defined as the time required for the stress to relax to 1/e of its initial value when the strain is held constant. From Equation (3.1), it is evident that ΔP** is directly proportional to ΔH. Hence the variation of ΔP** with time could be measured in terms of the variation of ΔH with time. Since the bed height decreases exponentially, the relaxation time τ is the time when $H = (1/e)(\Delta H)_{initial}$. Hence by knowing τ and Y, the viscosity of the emulsion phase μ could be calculated as $\mu = Y\tau$.

3.2 Novel Dimensionless Number

Many conventional fluidization dimensionless numbers for gas-particle systems were proposed to characterize fluidization phenomena since 1960s. These dimensionless numbers are for example Reynolds Number (Re), Archimedes Number (Ar), Froude Number (Fr), and other simpler empirical numbers such as U / U_{mf}, U_{mb} / U_{mf}, ρ_p / ρ_f, etc.

By reviewing the application history of these dimensionless numbers, it seems that these dimensionless numbers could not much effectively predict the behavior of fluidization phenomena observed either in laboratory or in industrial processes. Instead, these dimensionless numbers have rather been utilized as a kind of convenient

classification index numbers almost in the same way to classify the aerated powder as types of A, B, C and D particles (Geldart, 1973).

In order to find the most appropriate dimensionless number, the force balance relation between the gas drag force by gas flow and gravitational force acting on the particles in a unit volume at the minimum fluidization velocity is to be reviewed to find whether the set-up of classical approach could really be acceptable in terms of the existing experimental evidence. In this work, we found a significant oversimplification of experimental facts, which had created various misleading conclusions. This significant oversimplification is the assumption that “the drag force exerted by the upward moving gas for a volume element in a fluidized bed be always equal to the gravitational force exerted by the solid particles”.

In any fluidization process, the main purpose is to completely aerate all the particles in the bed in order to achieve desired heat and mass transfer characteristics which is required for the efficient operation of a fluidized bed. Hence, in order to characterize the efficient operation of a fluidized bed, a novel dimensionless number is proposed here that describes the aeration behavior of particles as against the gravitational force acting on the particles. This dimensionless number is the ratio of the experimental pressure drop across the bed at U_{mf} to the buoyant weight of the particles based on the mass of particles in the bed. This number is referred to as the dead zone formation number and could be represented as

$$G = \frac{DP_{U\,mf}}{\left(\frac{Mg}{A}\right)}$$

The value of this number could be less than or equal to 1.0 for any fluidized bed. The physical meaning of this number could be explained by considering the following cases:

(1) If G = 1.0, then it means that the fluidized bed has reached the theoretical pressure drop. All particles are completely aerated by the gas and the particles are freely floating, one particle not touching the other. This free floating condition is an ideal situation that is very difficult to achieve in actual operating fluidized beds. In other words, all the particles are in a suspended state. Under this condition the fluidized bed could be said to be in a homogeneous state (homogeneous emulsion phase).

(2) If G << 1.0, then it means that all the particles are not being aerated by the flowing gas. There are isolated groups of particles existing in the column on top of the gas distributor. These isolated groups of particles are called dead zones. These are called dead zones because the particles do not move. Under this condition the fluidized bed could be said to be in a heterogeneous state.

CHAPTER IV

RESULTS & DISCUSSION

4.1 Experimental Method

4.1.1 Experimental Apparatus

The experimental parameters, i.e., plastic deformation coefficient (Y) and the relaxation time (τ), that are necessary to obtain the viscosity of the emulsion phase were obtained through the experimental procedure described below.

The experimental apparatus is shown schematically in Fig. 4.1. The cylindrical fluidized bed used was 10.16 cm in diameter and was transparent to allow for visualization of the structural changes occurring in aeration and relaxation. Through preliminary experimentation, this size of fluidized bed was found to be appropriate to avoid the wall effect in the experiments. The gas distributor used was a sintered porous plate. The fluidizing gas was supplied from a dry low-pressure airline via a flowmeter. The change of height of the powder bed was visually monitored and recorded as a function of time.

4.1.2 Experimental procedure

The column was filled with the sample powder to a specific height before starting the experiment. The experiments were carried out within the gas velocity range, $U_{mf} < U < U_{mb}$. For the case of fluidizable powders, the metered air was allowed to enter the bottom of the column. At first, the gas velocity was increased to U_{mb}. i.e. at time t = 0, $U = U_{mb}$. Then the gas velocity was instantaneously reduced to U_{mf}. The bed height reduces from H_{mb} to H_{mf} due to the effect of the interparticle force. The reduction in bed height from H_{mb} to H_{mf} was recorded as a function of time. For the case of powders that exhibit viscoplastic behavior, this reduction in bed height is an exponential decay following the Maxwell's model. From this plot, the time required for the stress to reduce to 1/e of its initial value is obtained and this time is defined as the relaxation time (τ).

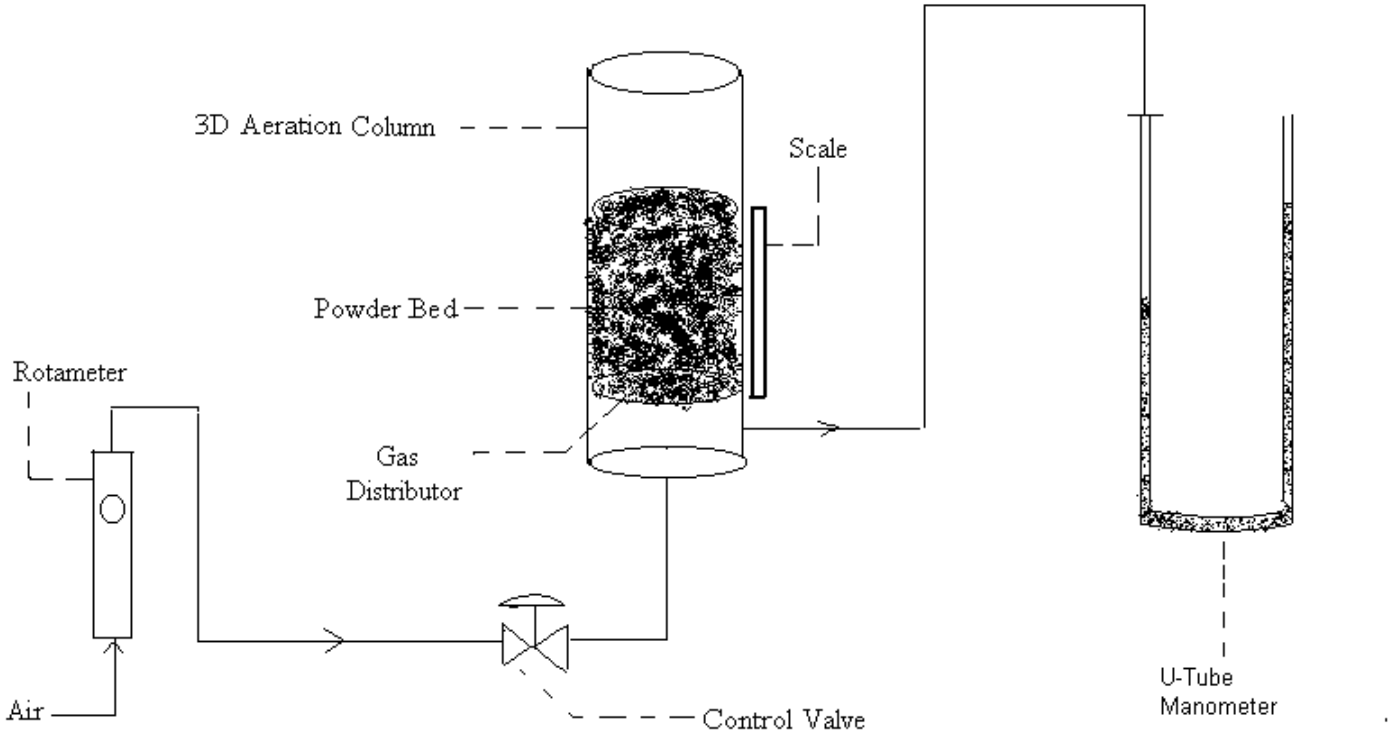

Figure 4.1 Experimental Apparatus for Aeration and Relaxation Experiments

4.2 Characteristic Aeration Regimes

The determination of viscosity of the emulsion phase is described using a specific example of starch powder (fine powder) with three different mean diameters of 15, 20 and 40 microns. These three starch powders are referred to as Starch (S), Starch (M) and Starch (L) respectively. In general, different powders exhibit different expansion characteristics when subjected to aeration. This difference in expansion behavior is very important to be understood in view of the different physical nature of the powder. Atleast, two different characteristic regimes are conceivable for fine powders. The two regimes are defined based on the magnitude of the superficial gas velocity of operation as below.

1) The regime where $U_{mf} < U < U_{mb}$, signifies a homogeneous emulsion phase without bubbles. The homogeneous powder bed in this regime is modeled as a single quasi-solid body.
2) The regime where $U >> U_{mb}$, signifies a heterogeneous powder bed with bubbles.

These two regimes of aeration are shown in Figures 4.2, 4.3 and 4.4 for the case of Starch S, M and L respectively for a wide range of superficial gas velocities. It could be observed from Figs. 4.2, 4.3 and 4.4 that, in general the bed height increases as the gas velocity is increased. For small values of gas velocity the bed height remains nearly a constant and after a specific point the bed height starts to increase sharply. The velocity at this point is called the minimum fluidization velocity (U_{mf}). At this velocity the downward gravitational force acting on the particles is nearly compensated by the upward drag force of the flowing gas thereby keeping the solid particles in a suspended state. At this point, the bed is modeled to consist of a homogeneous emulsion phase. When the gas velocity is increased further, the bed height continues to increase until a point and

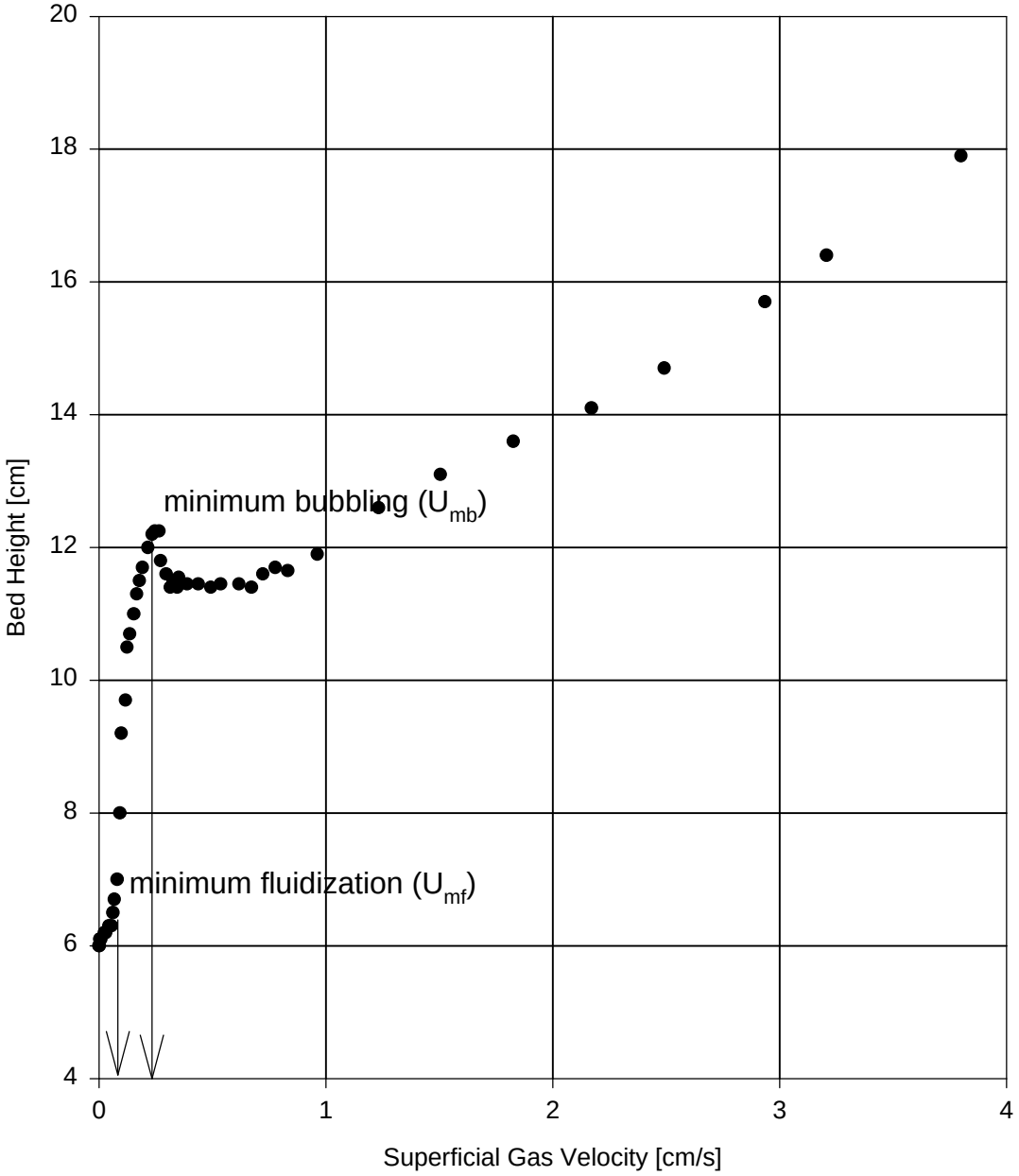

Figure 4.2 Bed Height vs Superficial Gas Velocity for Starch (S)

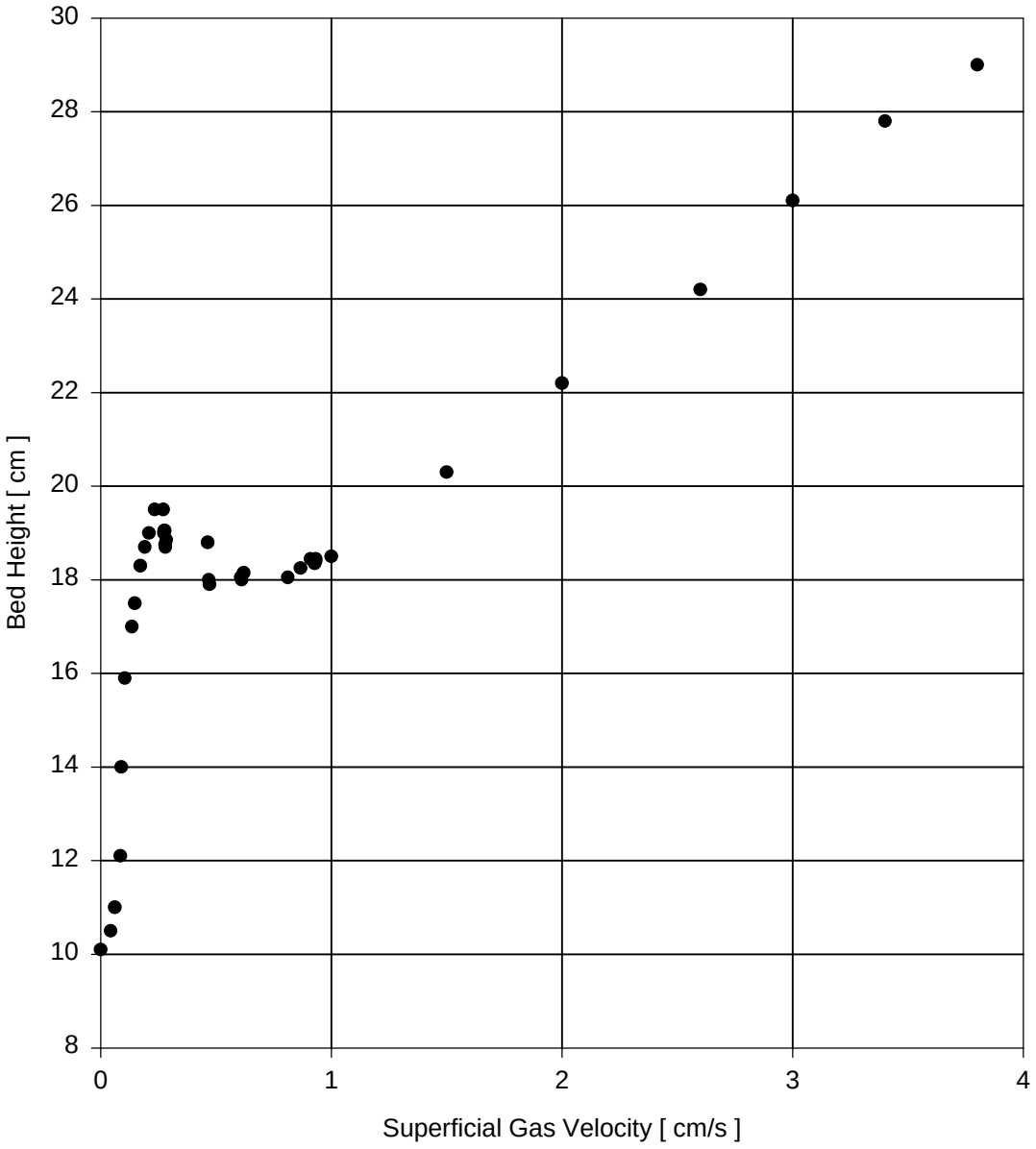

Figure 4.3 Bed Height vs Superficial Gas Velocity for Starch (M)

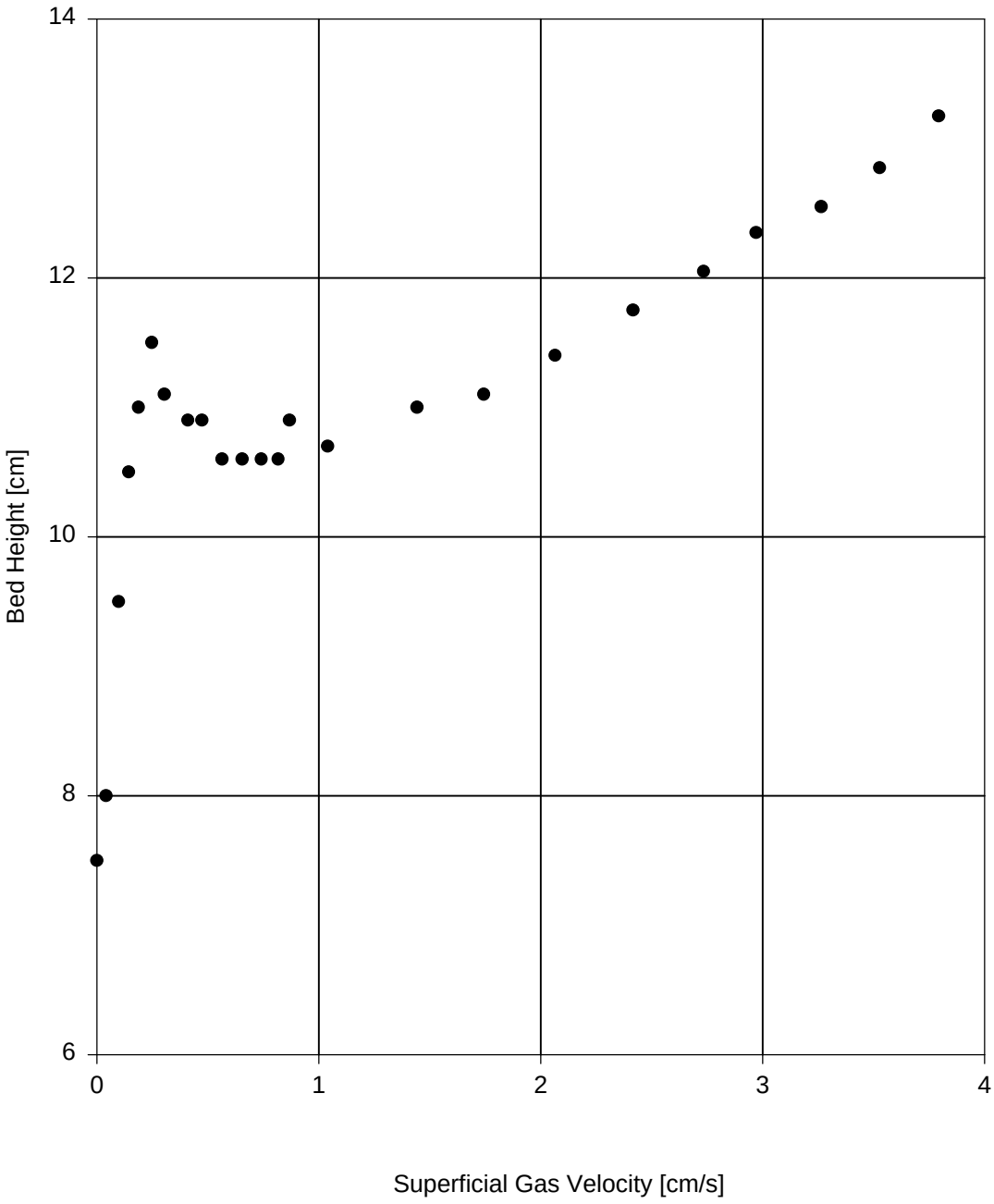

Figure 4.4 Bed Height vs Superficial Gas Velocity for Starch (L)

decreases for a while and shows an increasing trend again. The velocity at which the bed height starts to decrease is defined as the minimum bubbling velocity (U_{mb}) at which the first fracture in the powder structure takes place. According to the Quasi-Solid fracture model of Kono et al (1996), the first fracture of the powder bed marks the birth of the first bubble giving rise to a heterogeneous emulsion phase.

It is vitally important to understand the relationship between the rheological parameters (Y, $\sigma_{f,mb}$) to charcterize the viscosity of the emulsion phase of fine powders. Fig 4.5 shows the relationship between the rheological parameters of plastic deformation coefficient Y and fracture strength $\sigma_{f,mb}$ for samples starch S, M & L within the well-defined gas velocity range $U_{mf} < U < U_{mb}$. From this plot it could be seen that for all the samples, the rheological parameter sets (Y, $\sigma_{f,mb}$) lie on the same line which could be represented as $\sigma_{f,\,mb} = 0.11Y^{0.9}$. This is the flow characteristic line that determines the quality of aeration in a fluidized bed. Fine powders exhibiting this behavior are defined as aeratable or fluidizable and the viscosity measured here should be applicable only for powders that follow this flow characteristic line.

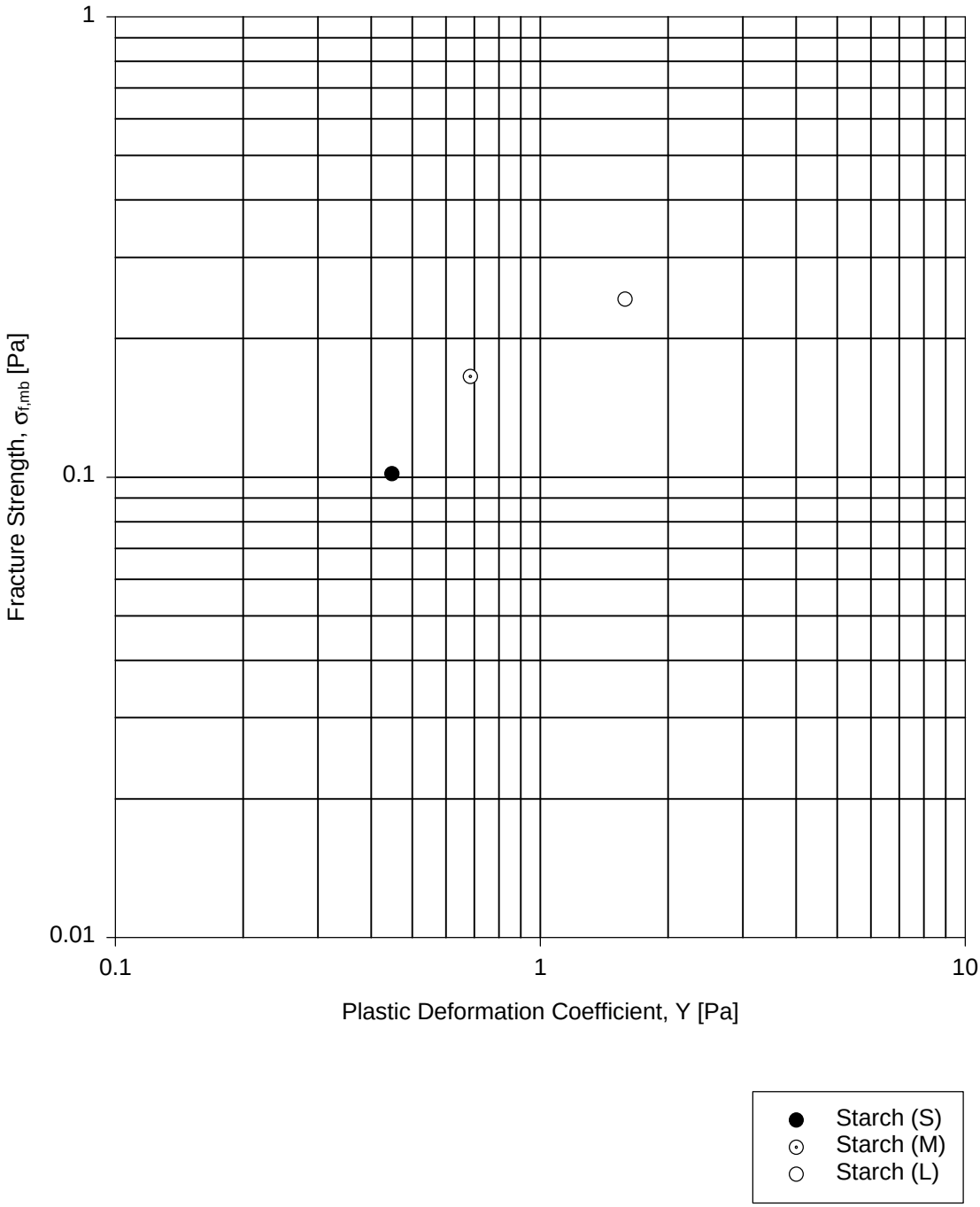

Figure 4.5 Rheological Parameters of Sample Fine Powders

4.3 Relaxation Behavior

Relaxation is a unique property of fine powders that are expandable or aeratable within the well-defined gas velocity range $U_{mf} < U < U_{mb}$. Utilizing the relaxation property of the powder, the viscosity is determined through the Maxwell's model for the rheological behavior of complex bodies.

The relaxation behavior of a powder could be confirmed by monitoring the response of the powder bed surface to a sudden step-wise decrease in the superficial gas velocity. For the case of samples starch S, M and L, this response was found to be an exponential decay. i.e. the bed height decreases exponentially with time. This exponential decay is shown in Figs. 4.6, 4.7 and 4.8 for samples starch S, M and L respectively. It could be observed from Figs. 4.6, 4.7 and 4.8 that as the gas velocity is instantaneously reduced from U_{mb} to U_{mf}, the bed height decreases smoothly following an exponential function given by $\Delta P^{**} = (\Delta P^{**})_{Umb} e^{-t/\tau}$. It should be understood that this decrease in bed height is not due to the gravitational force but because of the interparticle force acting between the particles. It could also be readily seen that when $t = 0$, $\Delta P^{**} = (\Delta P^{**})_{Umb}$, which is a constant and this condition corresponds to the start of the relaxation process where the bed is under a constant strain. In other words, when $\Delta P^{**} = (1/e)(\Delta P^{**})_{Umb}$, $t = \tau$, where τ is called the relaxation time of the powder bed and is defined as the time required for the stress to reduce to 1/e of its initial value, $(\Delta P^{**})_{Umb}$.

From these relaxation graphs, i.e. Figs. 4.6, 4.7 and 4.8, the relaxation time of the powder bed, τ was determined by making a tangent to the exponential decay curve at time $t = 0$.

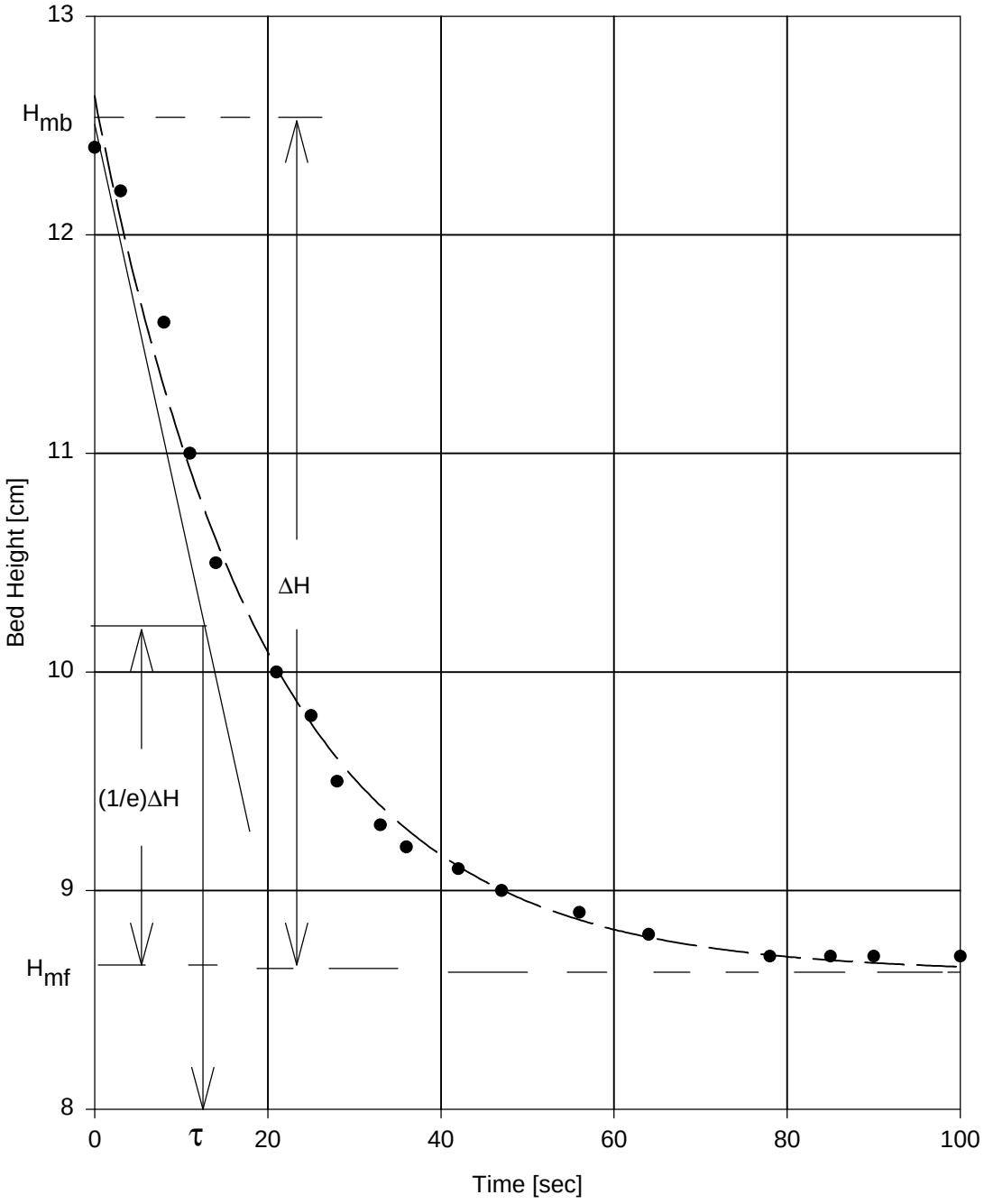

Figure 4.6 Relaxation behavior for Starch (S) within the range $U_{mf} < U < U_{mb}$.

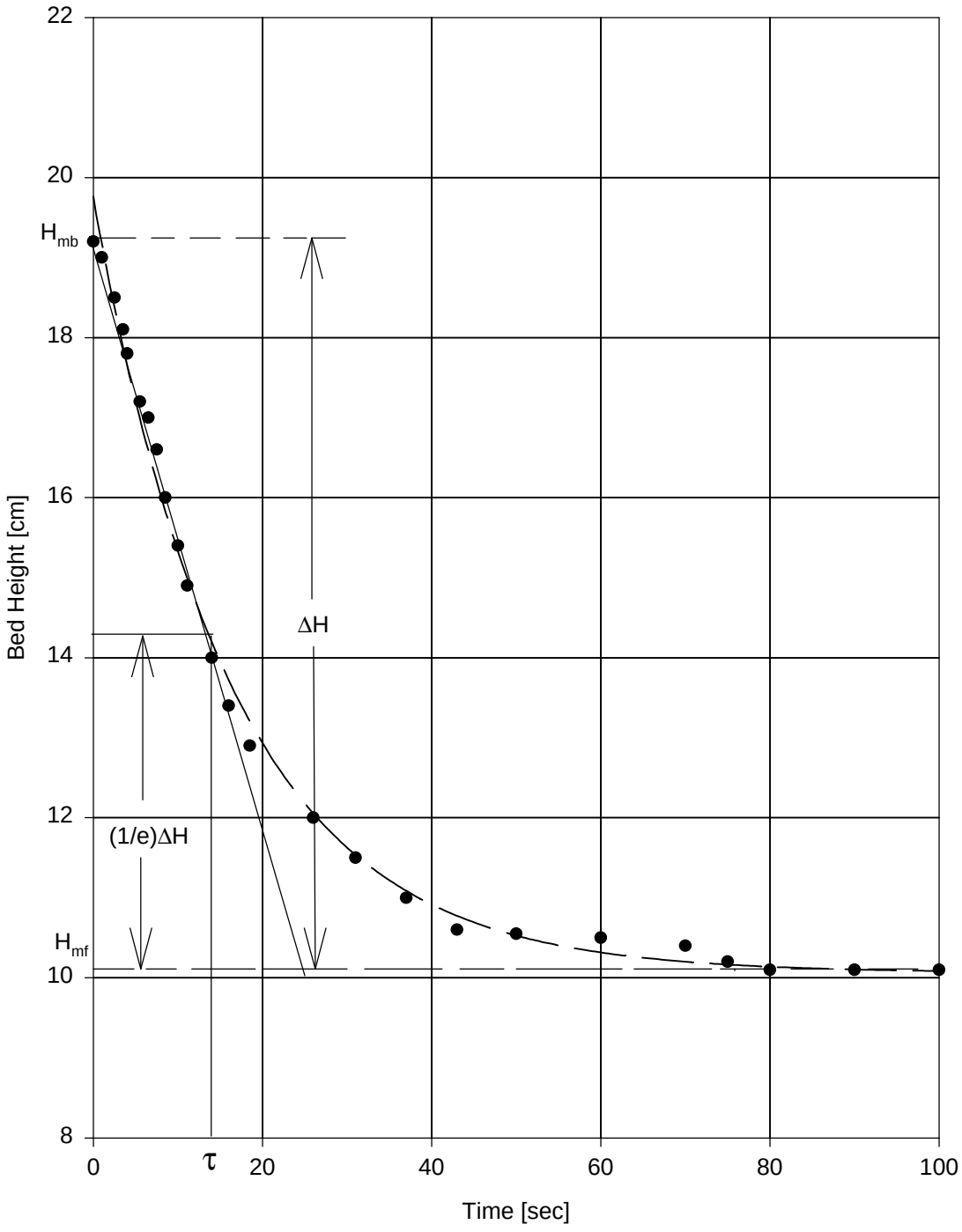

Figure 4.7 Relaxation behavior for Starch (M) within the range $U_{mf} < U < U_{mb}$.

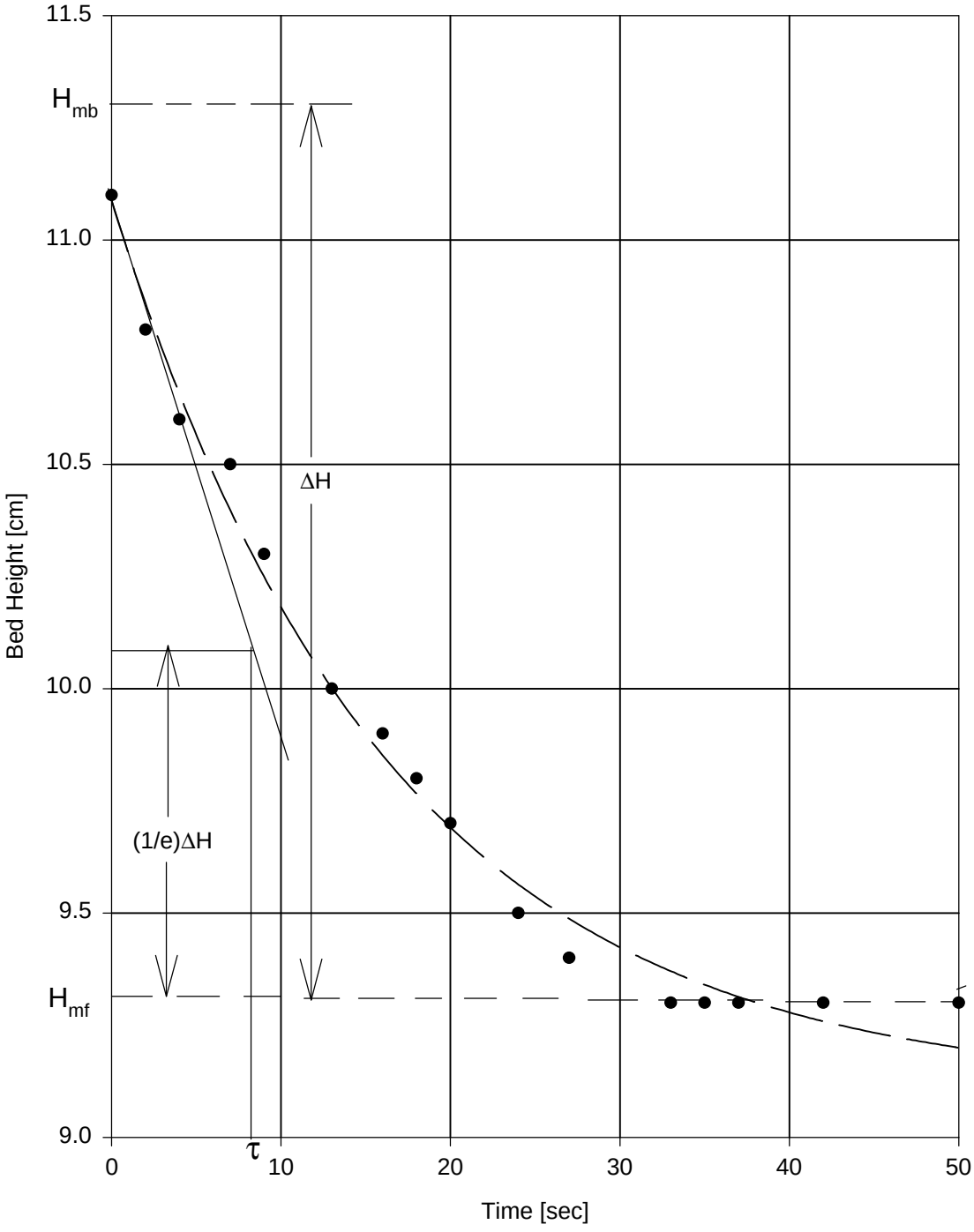

Figure 4.8 Relaxation behavior for Starch (L) within the range $U_{mf} < U < U_{mb}$.

The value of the plastic deformation coefficient for each powder was then combined with this relaxation time from Maxwell's model to determine the viscosity of the emulsion phase as $\mu = Y\tau$ within the well-defined gas velocity range $U_{mf} < U < U_{mb}$.

Table 4.1 shows the comprehensive experimental data of the rheological parameters Y, $\sigma_{f,mb}$ and μ for the case of sample fine powders of Starch (S), Starch (M) and Starch (L).

Fig 4.9 shows the relationship between the plastic deformation coefficient Y and the viscosity of the emulsion phase μ for the sample powders Starch S, M and L. It could be clearly observed from this plot that as the value of the plastic deformation coefficient increases, the viscosity of the emulsion phase also increases. This behavior is expected because as the plastic deformation coefficient increases, the bulk powder structure becomes harder and hence a higher value for the viscosity. In other words, softer the structure, lower is the viscosity and harder the structure, higher is the viscosity. This trend could be readily observed in Fig 4.9. Hence it could be inferred that the viscosity reported here is the intrinsic property of the material itself.

In addition to the Maxwell's model, the estimation of viscosity could also be done using the Kelvin-Voigt model (Eirich 1956). This estimation method is currently under investigation.

Parameter	Starch (S)	Starch (M)	Starch (L)
Mean Diameter, d_p [m]	15×10^{-6}	20×10^{-6}	40×10^{-6}
Column Diameter [m]	0.1016	0.1016	0.1016
Mass of Particles [kg]	0.3731	0.6141	0.4950
U_{mf} [m/s]	0.80×10^{-3}	0.85×10^{-3}	0.63×10^{-3}
U_{mb} [m/s]	2.64×10^{-3}	2.64×10^{-3}	2.28×10^{-3}
H_{mf} [m]	7.0×10^{-2}	10.1×10^{-2}	7.8×10^{-2}
H_{mb} [m]	12.4×10^{-2}	19.2×10^{-2}	11.6×10^{-2}
ΔP^* [Pa]	1610	3136	1655
N [–]	4667	5025	2325
ΔP^{**} [Pa]	0.3449	0.6241	0.7119
ε_{mf} [-]	0.5537	0.5137	0.5017
ε_{mb} [-]	0.7481	0.7455	0.6599
$Y_{mf\text{-}mb}$ [Pa]	0.4471	0.6854	1.582
$\sigma_{f,mb}$ [Pa]	0.1016	0.1654	0.2432
τ [sec]	17.0	14.0	14.0
$\mu_{mf\text{-}mb}$ [Pa-s]	7.60	9.60	22.15

Table 4.1 Experimental Data of Rheological Parameters $Y_{mf\text{-}mb}$, $\sigma_{f,mb}$ and $\mu_{mf\text{-}mb}$ for samples Starch (S), Starch (M) and Starch (L).

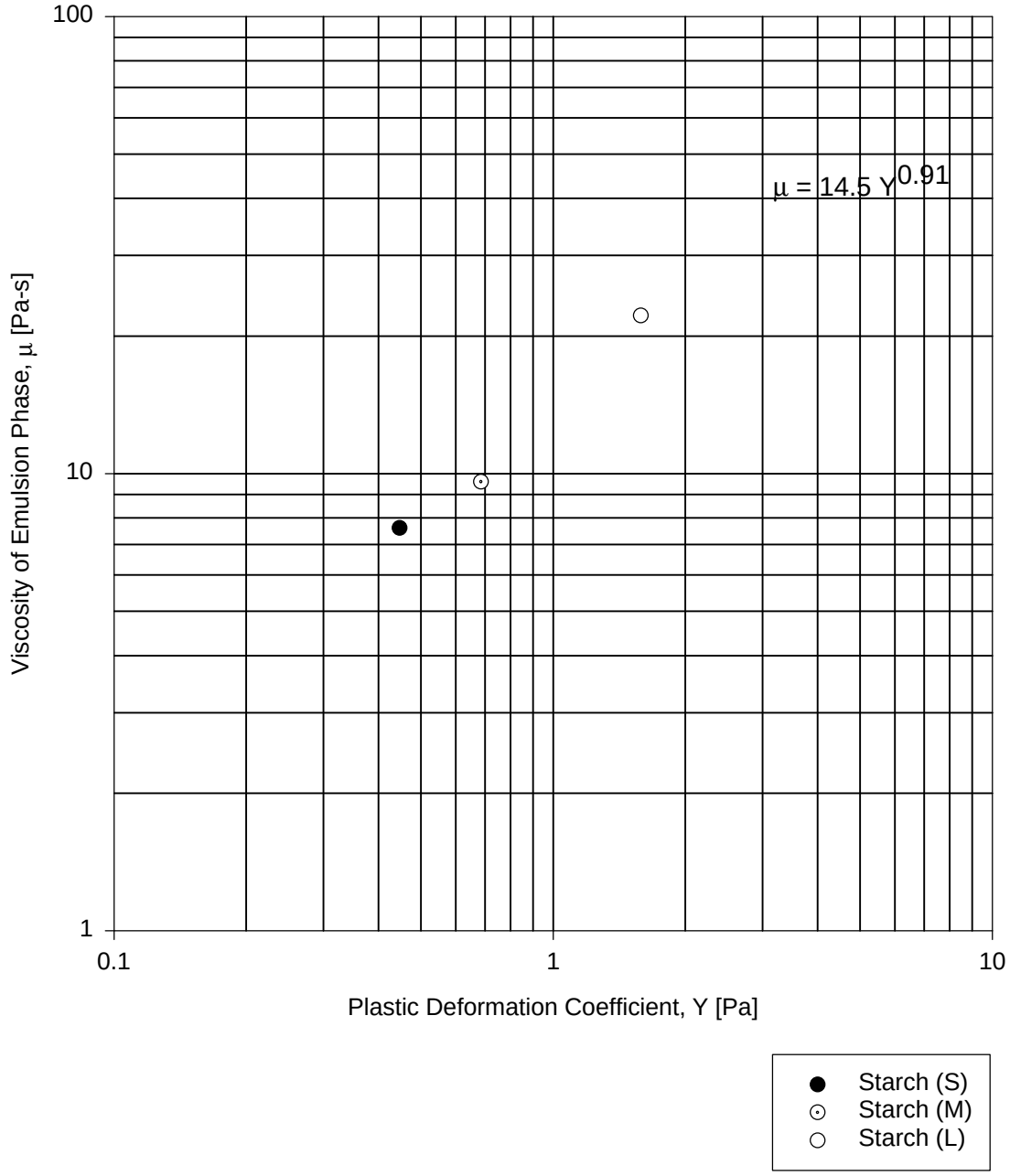

Figure 4.9 Viscosity as a function of Plastic Deformation Coefficient for the sample powders.

4.4 Dead Zone Formation Number

Figures 4.10, 4.11 and 4.12 show the behavior of the pressure drop across the bed as a function of superficial gas velocity for samples Starch (S), Starch (M) and Starch (L). It could be clearly seen from these graphs that the pressure drop increases until U_{mf} and then levels off at higher gas velocities. This behavior is expected because the voidage of the bed increases as the bed starts to expand homogeneously beyond U_{mf}.

The values of the dead zone formation number for all the sample powders have been calculated and reported in figures 4.10, 4.11 and 4.12. It could be observed that the values of G for all the sample powders are greater than 0.9. Since the value of G is close to unity, it could be concluded that the fine powder behaves like a homogeneous body without any dead zone formation. However since $G < 1.0$, the assumption of force balance at U_{mf} could not hold true. This axiomatic assumption could be stated as below: "In a fluidized bed, at the minimum fluidization velocity, the upward drag force exerted by the flowing gas is completely compensated by the downward gravitational force acting on the solid particles".

Richardson et al (1971) also performed similar experiments for diakon particles with a mean diameter of 126 microns, where the value of G is again less than unity. This is another experimental evidence denying the axiomatic assumption of force balance at the minimum fluidization point. This experimental data is as shown in Fig 4.13.

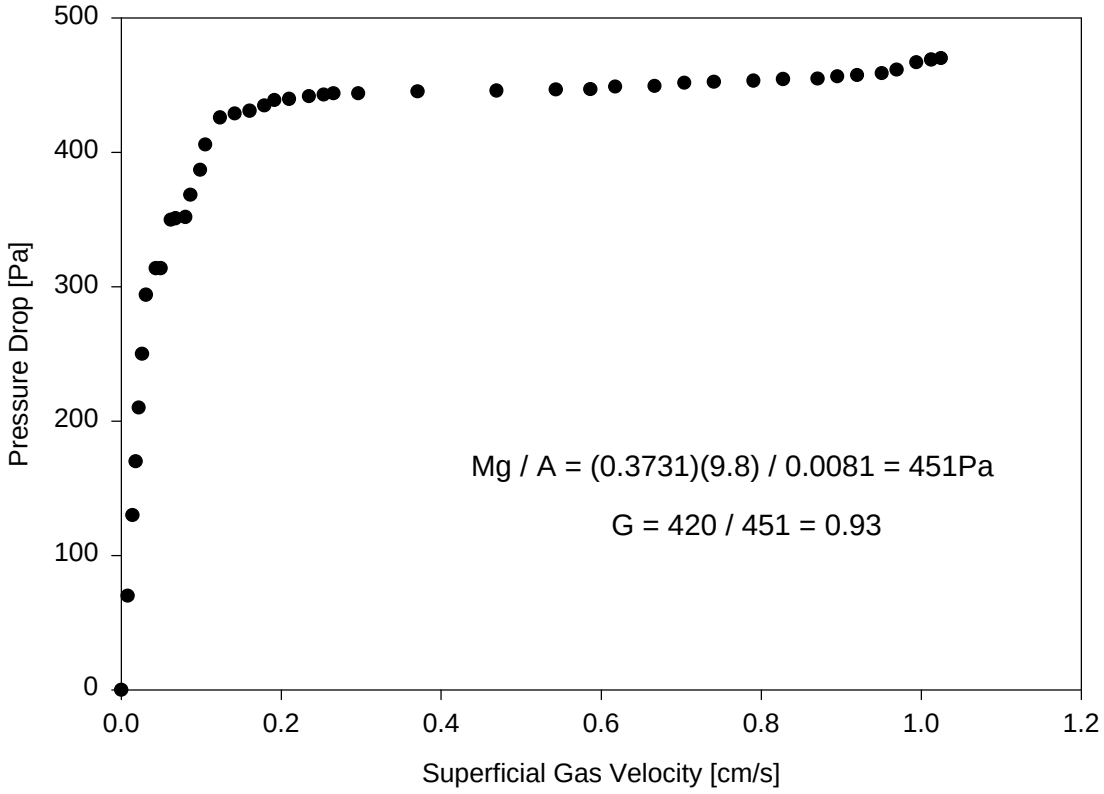

Figure 4.10 Pressure Drop vs Superficial Gas Velocity for Starch (S)

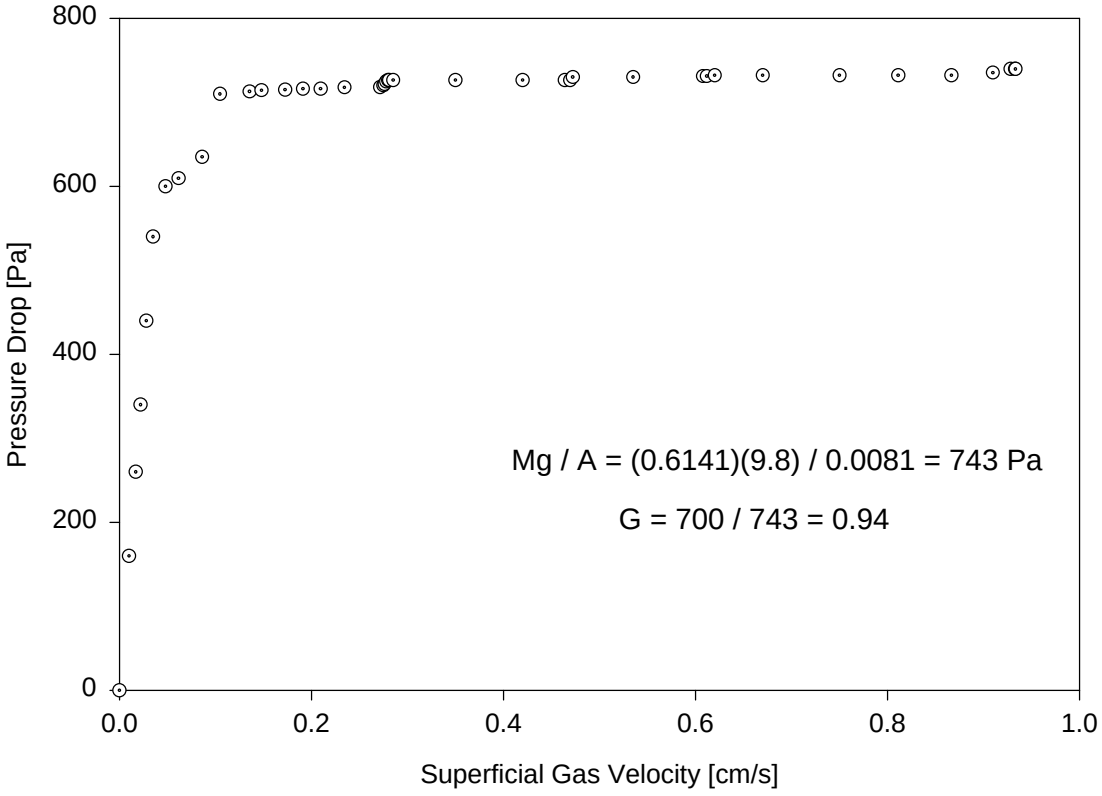

Figure 4.11 Pressure Drop vs Gas Velocity for Starch (M)

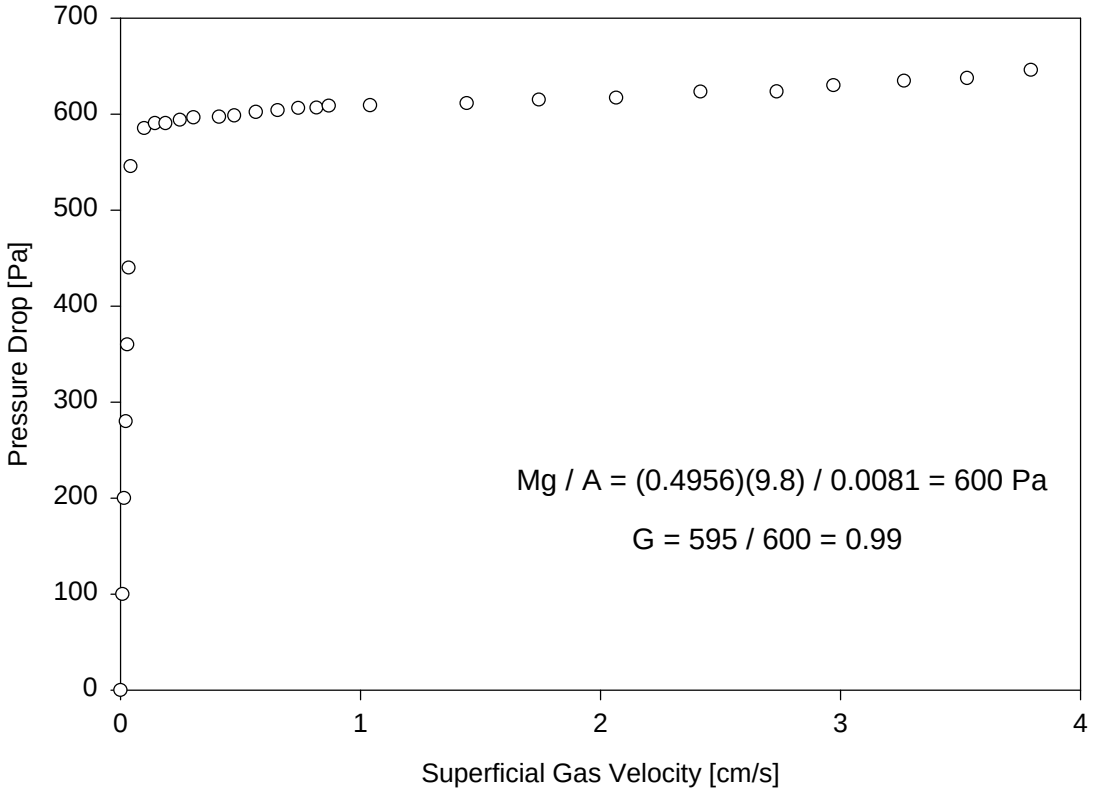

Figure 4.12 Pressure Drop vs Superficial Gas Velocity for Starch (L)

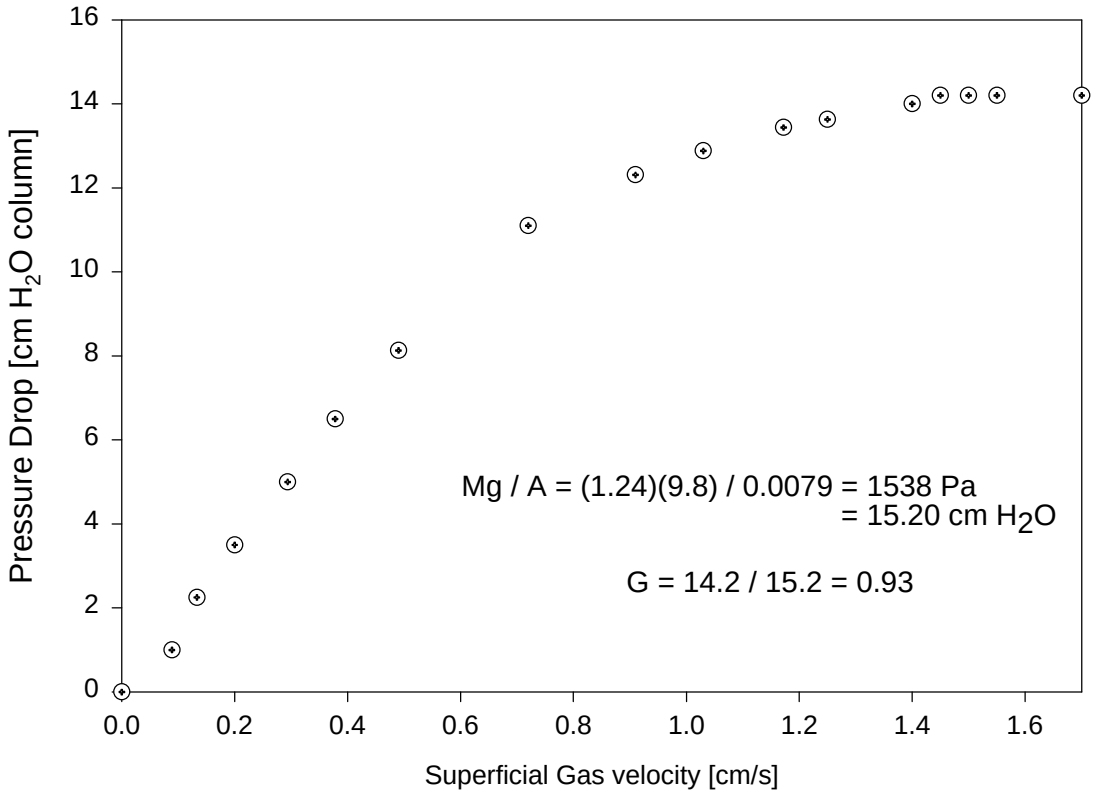

Figure 4.13 Pressure Drop vs Superficial Gas Velocity for diakon particles. (reproduced from Richardson et al, 1971)

CHAPTER V

CONCLUSION

Conclusion

A novel measurement method and its theory have been developed for the determination of the viscosity of the emulsion phase of aerated fine powder beds, within the gas velocity range $U_{mf} < U < U_{mb}$. The viscosity of the emulsion phase was measured without disturbing the homogeneous powder structure in a fundamental way. Flowability of solids is an important characteristic in any powder transport process. The viscosity of the powder bed decides the flowability and hence it becomes important to estimate and control this rheological parameter in any industrial or pilot-plant scale powder transport process. By measuring the viscosity of aerated fine powders, quantitative characterization of the flow behavior of fine powders could be achieved.

The behavior of aerated fine powders within the scope of this study was found to be nearly viscoplastic in nature. This conclusion was obtained by applying the Maxwell's model for the rheological behavior of complex bodies to characterize the flow behavior in aerated beds. In conclusion, it is emphasized that the flow characterization method proposed here could be useful in understanding several powder handling or transport processes like cyclone separators, mechanical mixing, aerated mixing, fluidized bed, pneumatic conveying, grinding, etc.

In addition to the above flow characterization, a novel dimensionless number called the dead zone formation number was defined and experimentally measured to quantitatively characterize the particle behavior in a gas-solid fluidized bed as against the gravitational force acting on the particles. This dimensionless number measures the quality of aeration at the minimum fluidization point in a fluidized bed. Hence it could be realized that it is useful to estimate this dimensionless number before scaling up any commercial fluidized bed process.

In conclusion it should be noted that by estimating this dimensionless number, the axiomatic assumption of the force balance between the gas drag and the gravitational force acting on the particles in a fluidized bed at U_{mf} could be quantitatively verified.

CHAPTER VI

REFERENCES

References

1. Bairos-Cazenave, A., et al, "Experimental Study of Powder Rheological Behavior", *Powder Technology*, 103, 58-64 (1999).
2. Brian J. Briscoe, "Interaction Laws and the Rheology of Assemblies", 88, 255-259 (1996).
3. Edwards, S.F., "The Rheology of Powders", *Rheologica Acta*, 29, 493-499 (1990).
4. Eirich, F.R., "Rheology: Theory and Applications", vol.2, 387-397, Academic Press, New York (1956).
5. Grace, J.R., "The Viscosity of Fluidized Beds", *The Canadian Journal of Chemical Engineering*, 48, 30-33 (1970).
6. Haddad Y., et al, "Rheological Properties of Wheat Endosperm with a view on Grinding Behavior", *Powder Technology*, 105, 89-94 (1999).
7. Kono, H.O., et al., "Quantitative Criteria for Emulsion Phase Characteristics and for the Transition between Particulate and Bubbling Fluidization", *Powder Technology*, 52, 69-72 (1987).
8. Kono, H.O., et al, "Measurement and Applications of the Rheological Parameters of Aerated Fine Powders - A Novel Characterization Approach to Powder Flow Properties", *Powder Technology*, 81, 177-187 (1994).
9. Kono, H.O., et al, "Characterization of Fluidization Properties of Fine Powder FCC Catalyst at Elevated Temperature", *AIChE Symp. Ser., Fluidization and Fluid-Particle Systems No. 308*, 91 , 170-179 (1995).
10. Kono, H.O., et al, "Characterization of Fine Powder Properties for Fluidization at Ambient and Elevated Temperatures", *Fluidization VIII*, ed. By G.Lagueri and J.Large, 723-736, Engineering Foundation, New York (1995c).

11. Kono, H.O., et al, "Characteristic Criterion of Rheological Parameters to Predict Flow Properties of Fine Powders", *AIChE Symp. Ser. No. 313*, 92 , 114-119 (1996).
12. Kono, H.O., et al, "Flow and Mixing Properties of Fine and Ultra Fine Powders",*AIChE Symp. Ser. No. 317*, 93, 141-146 (1997).
13. Kono, H.O., et al, "Development on Flow Property Characterization of Aggregated Fine Powders in Gas Flow", *Chemical Engineering*, Japan, 62, 654-657 (1998).
14. Kramers, H., "On the Viscosity of a Bed of Fluidized Solids", *Chemical Engineering Science*, 1, 35-37 (1951).
15. Matheson, G.L., "Characteristics of Fluid-Solid Systems", *Industrial and Engineering Chemistry*, 41, 1099-1104 (1949).
16. Noda, K., "Flow Patterns of Fine Particles in a Vibrated Fluidized Bed under Atmospheric or Reduced Pressure", *Powder Technology*, 99, 11-14 (1998).
17. Richardson, J.F., Fluidization (1st ed.), p 25-64, ed. by Davidson et al, Academic Press, London, 1971.
18. Robert Diekman, et al, "Laboratory Prediction of Flow Properties of Fluidized Solids", *Industrial and Engineering Chemistry*, 45, 1174-1176 (1953).
19. Ruel A. Overfelt, et al, "Fluidized Bed Viscosity Measurements in Reduced Gravity", *Powder Technology*, 99, 53-59 (1998).
20. Schügerl K., "Rheological Behavior of Fluidized Systems" in *Fluidization*, 2nd edition, edited by Davidson J.F., et al, Academic Press, London (1985).
21. Schügerl K., *Chem Tech*, 18, 544 (1966).
22. William W. Shuster, et al, "Point Viscosity Measurements in a Fluidized Bed", *Journal of Chemical and Engineering Data*, 5, 525-530 (1960).

APPENDIX

Solution to the Maxwell's model for the rheological behavior of complex bodies as applied to the aerated fine powder bed.

Under any external force, the total strain on the Maxwell element is

$$S = S_1 + S_2$$

Differentiating with respect to time on both sides

$$\frac{dS}{dt} = \frac{dS_1}{dt} + \frac{dS_2}{dt} .....(A)$$

For the spring

$$F = YS_1$$

$$Hence \frac{dS_1}{dt} = \frac{1}{Y}\frac{dF}{dt}$$

For the dashpot

$$F = m\frac{dS_2}{dt}$$

$$Hence \frac{dS_2}{dt} = \frac{F}{m}$$

Since F = ΔP^{**} and replacing for the terms in Eqn. A

$$\frac{dS}{dt} = \frac{1}{Y}\frac{d}{dt}(\Delta P^{**}) + \frac{1}{m}(\Delta P^{**})$$

Initial condition: At t = 0, dS/dt = 0, U = U_{mb}, H = H_{mb}, $\varepsilon = \varepsilon_{mb}$ and $\Delta P^{**} = (\Delta P^{**})_{Umb}$

Then the governing equation becomes

$$\frac{1}{Y}\frac{d}{dt}(\Delta P^{**}) + \frac{1}{m}(\Delta P^{**}) = 0$$

$$\frac{d}{dt}(\Delta P^{**}) + \frac{Y}{m}\Delta P^{**} = 0$$

$$\frac{d}{dt}(\Delta P^{**}) + \frac{1}{t}\Delta P^{**} = 0$$

where $\tau = \mu / Y$.

Multiplying both sides of the equation by $e^{\frac{t}{t}}$

$$\frac{d}{dt}(\Delta P^{**})e^{t/t} + \frac{1}{t}(\Delta P^{**})e^{t/t} = 0$$

From the product rule of differentiation we could readily see that

$$\frac{d}{dt}(\Delta P^{**}e^{t/t}) = \frac{d}{dt}(\Delta P^{**})e^{t/t} + \frac{1}{t}(\Delta P^{**})e^{t/t}$$

Hence

$$\frac{d}{dt}(\Delta P^{**}e^{t/t}) = 0$$

Integrating the above equation yields

$$\Delta P^{**}e^{t/t} = (\Delta P^{**})_{U_{mb}}$$

$$\Delta P^{**} = (\Delta P^{**})_{U_{mb}} e^{-t/t}$$

SECTION II

CHAPTER I

INTRODUCTION

1.1 Objective

Investigation of the kinetics of synthesis and decomposition of Natural Gas Hydrates, specifically methane gas hydrate using porous sediments comprising of several different fine powders.

1.2 Background

Natural Gas Hydrates (NGH) are solid, porous, ice-like crystalline inclusion compounds (also called clathrates) of a host water lattice with cavities which contain guest gases. They are frequently referred to as solid solutions and are bonded by Van der Waals forces under low temperature and high pressure. The guest molecule is necessary to support the cavities in the water lattice. The host water molecules on account of hydrogen bonding form a three-dimensional lattice into whose voids the guest gas molecules penetrate.

In general, Natural Gas Hydrate (NGH) consists of a family of clathrate compounds such as methane-, ethane- and propane gas hydrates. However, this study is limited only to the kinetics of Methane Gas Hydrate (MGH) formation and decomposition. Methane gas hydrate ($CH_4.nH_2O$) has a crystalline structure of the category sI. Further detailed description of the characteristics and nature of gas hydrates is explained in the next chapter.

In the past, several investigators have studied the thermodynamics and crystal structures of natural gas hydrates including methane gas hydrates and the corresponding conclusions were well understood. However, the reaction engineering kinetics together with heat and mass transfer considerations have not yet been completely clarified. Hence in this work, a systematic study of the reaction engineering kinetics of methane hydrates has been attempted.

1.3 Formation and Decomposition Reactions

This work describes the first homogeneous formation and decomposition of methane gas hydrates within several different synthetic sediments by using our custom built high-pressure batch and semi-continuous reactors (patent application in process). These synthetic sediments are very well defined in terms of their powder packing structures and chemical surface characteristics. The formation of gas hydrates is a very complex exothermic (heat generating) reaction that is carried out at high pressure (6.8 – 13.6 MPa) and low temperature (273.5 K). The decomposition of hydrates is a very complex endothermic (heat absorbing) reaction that is carried out at pressures below the equilibrium pressure on the three phase diagram. Decomposition of hydrate was accomplished through a controlled depressurization technique starting at a pressure of 2.7 MPa, maintaining the temperature constant at 273.5 K.

The entire reactor assembly consisted of methane gas feeding system, various custom designed sediments, methane hydrate formation rate measuring system and decomposition rate measuring system.

Overall kinetic rate constants both for the formation and decomposition reactions were determined from experiments including the overall order of the reaction for several different sediments. Based on the experimental results, we obtained a reaction engineering rate equation of the quasi-first order type $n = n_o\left(1 - e^{-k_f t}\right)$ for the formation reaction where the rate constant k_f is a function of the pressure, temperature, sediment type and their corresponding catalytic reactivity. During decomposition, two types of rate behavior were observed depending on the type of sediment used. In some cases, the

decomposition followed a zero-order reaction rate while in others a first order reaction rate was observed.

1.3 Significance of this work

In view of the production of natural gas from the underground strata either in the tundra land or in offshore fields, it becomes practically important to understand and control the decomposition rates of natural gas hydrate samples by the depressurizing technique. In the past, decomposition rates were studied by several investigators (Bishnoi (1983), Englezos (1987) and Kim et al (1987)), in which the hydrate samples were actually suspended in a bulk volume of water. The decomposition was accomplished by increasing the temperature at a certain pressure. In the studies of the above investigators, the reaction system consisted of either [CH_4(g) - H_2O(l) - MGH(s)] or [CH_4(g) - H_2O(l) - H_2O(s) - MGH(s)] in contrast to our reacting system, which is [CH_4(g) - H_2O(l) – Sediment - MGH(s)]

From the practical viewpoint of the natural gas industry, gas production from hydrates was found to be more economical through the use of the depressurization technique. Hence it becomes important to produce natural gas from hydrates through the depressurization technique.

Yousif (1994) investigated the kinetics of hydrate formation in bulk water and reported induction times for the onset of hydrate formation based on the first nucleation of the hydrate crystals. It was concluded that the formation of nuclei seeds is essential for the complete growth of the hydrate crystals. However, through our experimental results it was found that the formation of nuclei seeds is not always essential for the complete growth of hydrate crystals.

Sloan (1991) reported some experimental data on the formation and dissociation of methane hydrates within Berea sandstone cores, however the well-defined distribution of water within the cores is not clearly studied. Circone et al (1998) reported the decomposition rates of methane hydrates formed using solid ice at temperatures as low as 272.5 K. However neither of these studies reported reaction engineering data and the studies did not suggest any kinetic equation or the overall order for the reactions.

The importance of studying the kinetic behavior of hydrates formed within sediments stems from the fact that hydrates exist in Mother Nature either in permafrost or in deep sea sediments and not just in free water. In most of the studies carried out so far, hydrates have been formed in a bulk volume of water and consequently the formation and decomposition studies performed on these samples do not exactly represent the actual kinetic behavior of the hydrate samples existing in nature. Therefore we propose to study the kinetics of methane hydrate formation and decomposition within consolidated sediments.

Finally it is emphasized that the formation and decomposition of hydrates within sediments is important and significant since these synthetic samples could almost exactly reproduce the actual hydrates existing in Mother Nature either in permafrost or in deep sea sediments.

CHAPTER II

TECHNICAL BACKGROUND
&
LITERATURE REVIEW

2.1 Background

2.1.1 Gas Hydrates

Natural Gas Hydrates (NGH) are solid, porous, ice-like crystalline inclusion compounds (also called clathrates) of a host water lattice with cavities which contain guest gases. They are frequently referred to as solid solutions and are bonded by Van der Waals forces under low temperature and high pressure. The guest molecule is necessary to support the cavities in the water lattice. The host water molecules on account of hydrogen bonding form a three-dimensional lattice into whose voids the guest gas molecules penetrate. The structure formed by the water molecules depends on the shape and size of the molecules of the gas, which is in contact with the water. The degree to which the water structure is filled with gas molecules depends on the operating pressure and temperature. Further detailed description of the characteristics and nature of gas hydrates could be obtained from several literatures of Sloan (1991) and Makogon (1997).

2.1.2 Hydrate Structure

Gas hydrates are crystalline inclusion-compounds (clathrates) and are characterized by uniquely different structures for different gases. Fig 2.1 shows the hydrate unit cell structure for methane which has a structure named SI. Structure I is cubic and the unit cell consists of 46 water molecules, which form 2 small (dodecahedra) and 6 large (tetradecahedra) cages. In other words, 2 small cages and 6 large cages are combined to give a unit cell of structure I hydrate. In Fig 2.1, the black circles indicate small cages while the white circles indicate large cages. The small cages of structure I hold gas molecules with a molecular diameter less than

5.2 Å while the large cages hold gas molecules with a molecular diameter less than 5.9 Å. The molecular diameter of methane is between 4 and 5 Å and hence it forms structure I as shown in Fig 2.2.

In addition to structural differences, there are several properties that are unique to gas hydrates through which it is possible to distinguish between a hydrate and ice. One such property is the increase in specific volume of water during the hydrate formation process. The specific volume of water increases by about 26-32% during the hydrate formation process whereas during the formation of ice the increase is only about 9% (Makogon 1997). Further detailed analysis of the hydrate structure could be obtained from several literatures of Sloan (1991) and Makogon (1997).

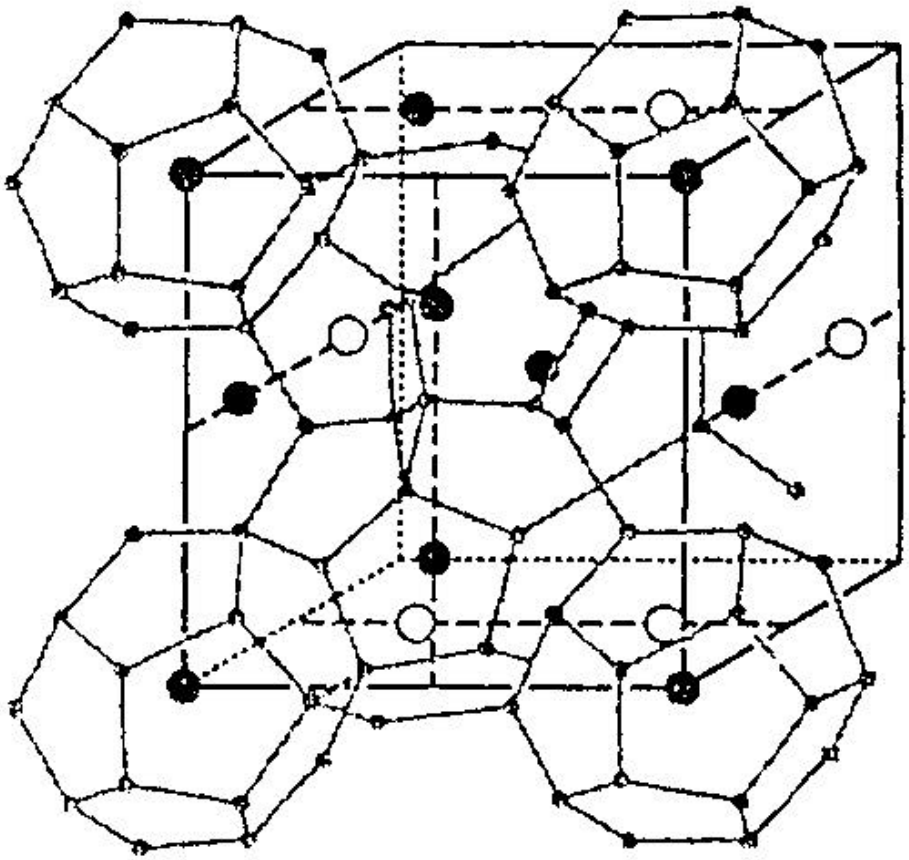

Figure 2.1 Lattice crystal structure of methane hydrate (sI hydrate) with a unit cell dimension of 1.2 nm.

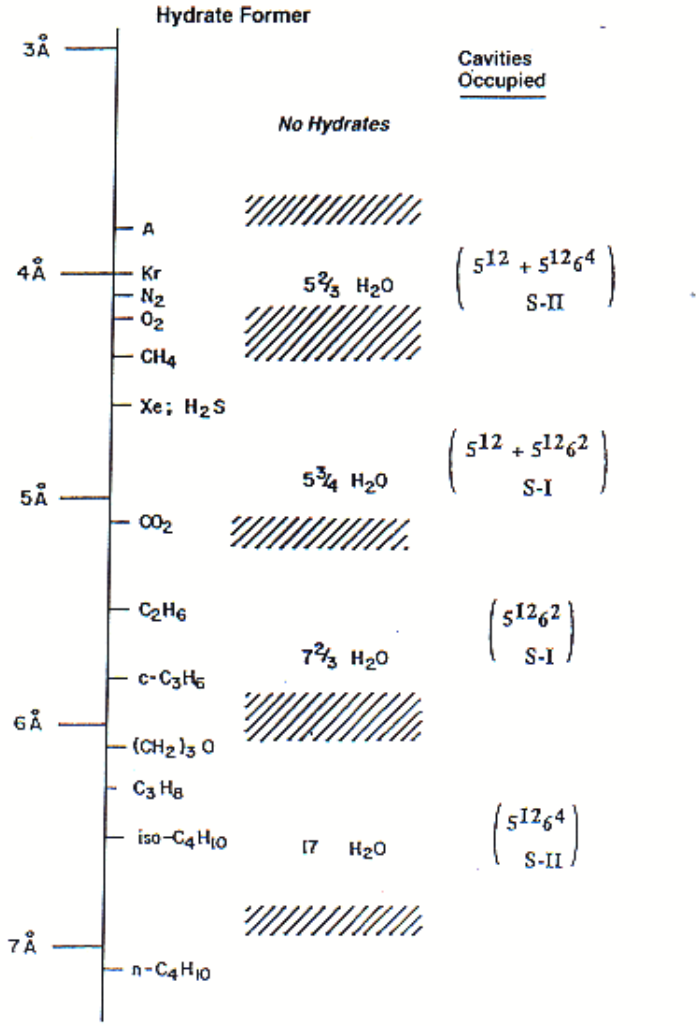

Figure 2.2 Guest (gas) size and hydrate structure relationships for several hydrocarbons.

2.1.3 Formation of Gas Hydrates

The formation of gas hydrates is a non-stoichiometric, exothermic reaction between a gas and water and can be represented by the following equation,

$$\text{Gas} + n\text{H}_2\text{O}\ (\text{L}_w \text{ or I}) \longrightarrow \text{Hydrate (H)} + \Delta h$$

Where n is called the hydration number (number of water molecules per mole of gas) and Δh is the associated enthalpy change which is negative by sign convention. L_w and I denote liquid water and ice respectively (Sloan 1991).

The ratio of water to gas in the hydrate molecule (hydration number) is commonly referred to as the composition of the hydrate. The composition of a gas hydrate is substantially determined by the composition of the guest gas, the formation pressure and temperature. However, during the formation process this ratio of water to gas keeps changing because of a different degree of filling of the voids by the hydrate-forming gas. But at the end of the formation process, the value of n remains constant. The most accurate experimental data on hydrate composition could be obtained by a controlled static growth of hydrates with control over the feed gas composition and the pressure and temperature of formation.

The beginning of hydrate formation is actually a transition phenomenon from the point of equilibrium of forces. Hydrate formation begins when the orienting forces of mutual attraction between water and gas molecules overcome the disrupting forces of thermal motion of molecules. Substantial thermal motion of molecules hinders the mutual attracting forces between the gas and water and this is the main reason for maintaining isothermal operating condition during the formation of hydrates.

2.1.4 Kinetics of Gas Hydrate Formation

The kinetics of gas hydrate formation is a multi step process and the study involves the understanding of the mechanisms of several elementary steps. The kinetics of hydrate formation could be best understood in terms of the following steps:

a. Formation of seed nuclei.

b. Growth of this seed nuclei to a crystal.

c. Diffusion of the gas within the sediments to the growing hydrate surface.

d. Dissipation of the heat of crystal formation.

Hydrate formation begins by the formation of crystallization seed nuclei at the gas-water interface if the reaction is carried out in a bulk volume of water. In general, hydrate can be formed under two different conditions, namely the static and dynamic condition. The static condition corresponds to a batch operation where specific proportions of water and gas are fed into the batch reactor and the reaction is then started. In this type of reaction, the reacting components are not agitated, but random molecular collision between water and gas molecules continuously take place. Under this condition, the hydrate that is formed assumes the shape of long crystals. The dynamic condition corresponds to a continuous operation where there is mixing of the reacting components during the reaction. The mixing of the gas could be either by the bubbling of gas through water or by mechanical agitation by means of various electromagnetic stirrers.

Fig 2.3 shows the pressure temperature diagram for methane indicating clearly the zones of hydrate formation and decomposition. In the figure the co-ordinate (T_e, P_e) indicates the equilibrium temperature and pressure for hydrate formation whereas the co-ordinates (T_f, P_f) indicate the operating conditions of our experiments.

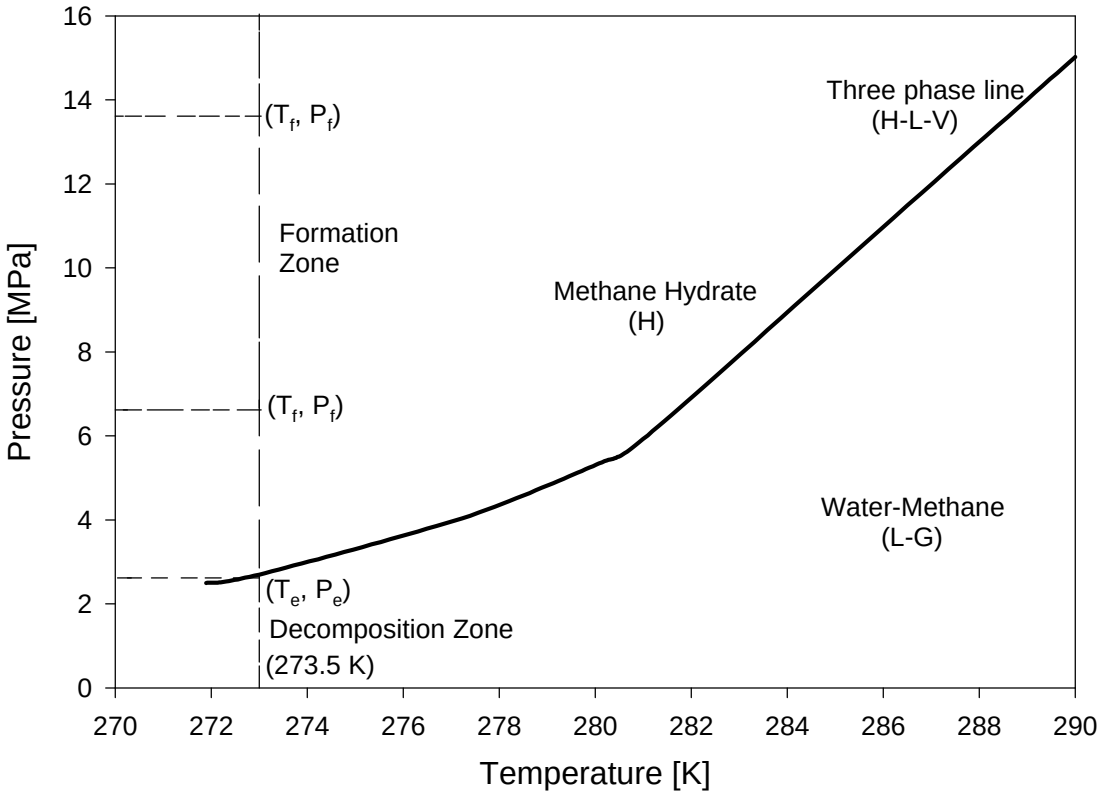

Figure 2.3 Three-phase equilibrium curve for hydrate-liquid water-methane gas system

2.1.5 Decomposition of Gas Hydrates

Decomposition of gas hydrates is an endothermic reaction and could be accomplished either by depressurization or heating of the reactor. In this work, hydrate decomposition was accomplished by controlled depressurization of the reactor at the experimental temperature of 273.5 K.

2.2 Literature Review

Vysniauskas and Bishnoi (1983) investigated the kinetics of methane hydrate formation using a semibatch stirred tank reactor. The experiments were carried out in bulk water under the operating conditions of 274-284 K and 3-10 MPa. It was concluded through their experiments that the formation kinetics were dependent on the interfacial area, pressure, temperature and degree of supercooling. The formation rate of the hydrates was correlated with the stirring speed. Also, a semi-empirical model was formulated to correlate the experimental data.

Englezos et al (1987) investigated the formation kinetics of methane and ethane gas hydrates in bulk water and proposed a mechanistic model based on the crystallization theory, with one adjustable parameter to determine the rate constant for the growth of hydrate particles. The operating conditions were 274-282 K and 0.636-8.903 MPa and the experiments were carried out at various stirring rates.

Kim et al (1987) studied the kinetics of methane hydrate decomposition by reducing the pressure on hydrate slurry in water to a value below the three-phase equilibrium pressure at the reactor temperature. The experiments were carried out under the operating conditions of 274-283 K and 0.17-6.97 MPa. The conclusions of the experiments were that the hydrate decomposition rate was proportional to the particle surface area and to the difference in the fugacity of methane at the equilibrium pressure and the decomposition pressure.

Yousif (1994) investigated the kinetics of methane hydrate formation in bulk water with a special focus on hydrate nucleation, simultaneously defining induction times for various types of water used. Methane with a purity of 87.3% was used, and the operating conditions were in the range of 277.6-288.3 K, at two different pressures of 6.9

and 9.7 MPa. The onset of hydrate formation was detected using the change in the frequency of a scattered laser beam and by the increase in the reactor temperature.

Yousif and Sloan (1991) investigated the formation and decomposition of methane hydrate in Berea sandstone cores using a flow reactor system. The operating conditions of the experiments were 273.7 K and 7-8 MPa and a 1.5% NaCl solution was used as the source of water. The onset of hydrate formation was determined by the drop in the reactor pressure and by the change in electric resistance along three cores of different permeabilities. Both linear and non-linear decomposition rates were reported depending on the percentage of water saturation in the core.

Ullerich et al (1987) investigated the kinetics of methane hydrate decomposition without sediments under the operating conditions of 274 K and 4.1 MPa. The decomposition of hydrate was confirmed by combustion bomb calorimetry and gravimetric determination. A mathematical model without adjustable parameters was proposed based upon first principles for the hydrate decomposition. The model assumes that the water formed during decomposition is blown away by the methane gas generated due to decomposition.

As could be seen from the previous research of several workers, numerous data are existing for the kinetics of methane hydrate formation and decomposition. However, there have been only a few data corresponding to the formation and decomposition of methane hydrates within porous sediments. In the nature, hydrates exist not only in bulk water but also within porous rocky sediments. Therefore we propose to study the kinetics of methane hydrate formation and decomposition within porous sediments.

CHAPTER III

RESULTS & DISCUSSION

3.1 Experimental

Studies of the formation of crystallization seed nuclei and of the rate of hydrate formation and decomposition processes within porous sediments were carried out under static conditions for methane gas hydrates.

For the case of methane hydrate, the experiments were carried out in a batch reactor made of carbon steel with a total volume of 188 cm^3. Fig 3.1 shows the sketch of the experimental apparatus used for methane hydrate formation and decomposition kinetic studies.

The experimental apparatus consists of a nearly cylindrical packed bed reactor within which known amounts of different sediments and distilled water were added to a certain constant level before the start of reaction as shown in Fig 3.1. The reactor was equipped with a thermocouple at the center to measure the temperature of the packed bed. The pressure of the reactor was measured at two different points as indicated by P_1 and P_2. The experimental set up was also equipped with a stainless steel pressure relief valve to ensure safety of the high-pressure reacting system. All flow pipelines were made of stainless steel SS 304. For the formation reaction, high purity methane gas (99.90%) was used. The methane gas enters the bottom of the reactor through a high-pressure regulator and a needle valve connected in series. The decomposition set up consists of two needle valves connected in series along with a gas flow stabilizer and a water tank with an inverted graduated cylinder that was used as a gas receiver.

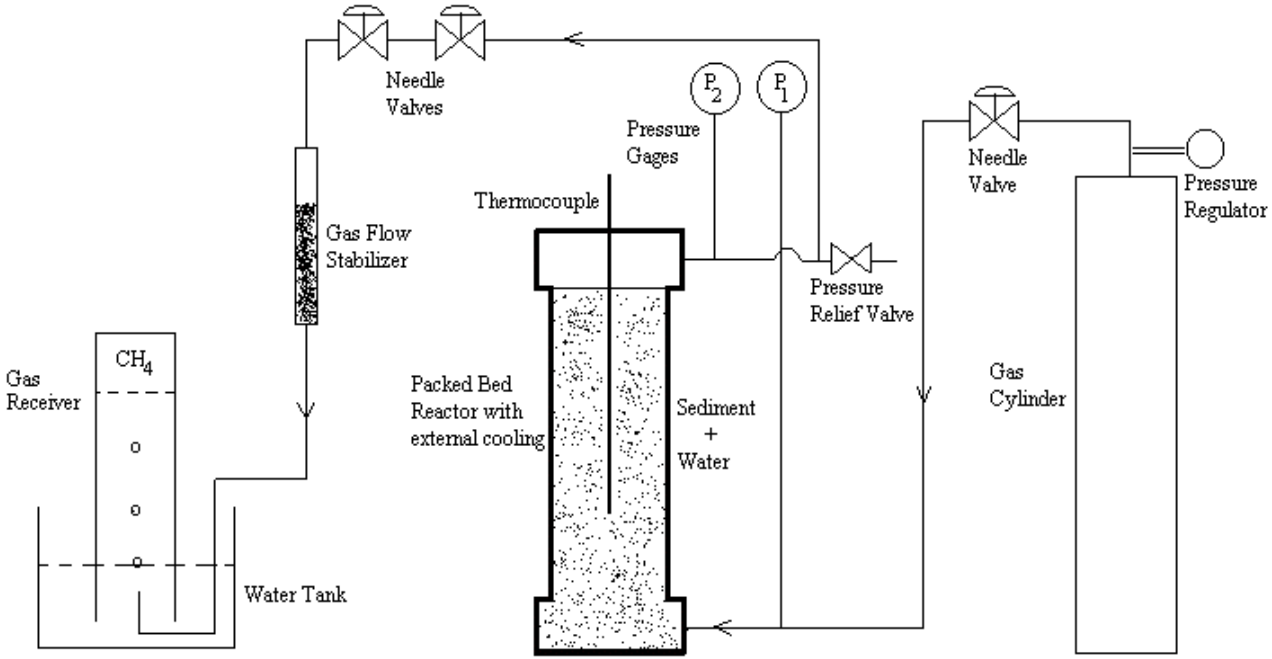

Figure 3.1 Experimental equipment for the synthesis and decomposition of methane gas hydrate with and without sediments.

3.2 Experimental Procedure

As a first step in the experimental procedure, known amounts of a sediment and distilled water were mixed in a separate container and fed into the reactor. The amounts of sediment and water added into the reactor were based upon simple reactor design calculations dictated by the total volume of the reactor and by the water saturation coefficient of the granules in the packed bed. Then the reactor was cooled completely to attain thermal equilibrium at 273.5 K using ice and water. The coolant water and ice were contained in a well-insulated plastic container. The volume of the coolant ice and water was several times larger than the volume of the reactor so that the heat evolved during the exothermic hydrate formation reaction did not really affect the progress of the reaction.

After thermal equilibrium was reached, high purity methane gas was fed into the bottom of the reactor as shown in Fig 3.1. The operating pressure for the formation of methane hydrate was varied in the range of 6.8 - 13.6 MPa and the temperature was kept at 273.5 K. Continuous monitoring of the temperature of the reactor was done using a Fe - CuNi Type J thermocouple (Model: Omega HH-26J) to confirm isothermal reacting conditions.

Since the reaction was carried out at T > 273 K, the reaction system clearly consists of only three phases at any time t. Methane forms the gas phase, water forms the liquid phase and the product gas hydrate forms the solid phase. The progress of the reaction was monitored by recording two different pressures at regular intervals of time, one at the bottom and the other at the top of the reactor indicated respectively as P_1 and P_2 .

3.3 Hydrate Formation

A partial three-phase equilibrium curve for the system methane hydrate-liquid water-methane gas is as shown in Fig 3.2. The region above the three phase H-L-V line

corresponds to the region where methane hydrate could be formed. The region below the three phase H-L-V line corresponds to the region where liquid water and gaseous methane exist. The co-ordinate (T_e, P_e) corresponds to the equilibrium point for hydrate formation at a temperature of 273.5 K. In the scope of our study, the temperature was always maintained at 273.5 K, thereby leaving only the pressure as the controlling variable. The operating pressures were 6.8 MPa and 13.6 MPa for our experiments and this operation zone is schematically represented as the co-ordinate (T_f, P_f) in Fig 3.2. It could be clearly seen that the formation pressure in our operation was much higher than the equilibrium pressure of hydrate formation. Therefore, this selection justifies the operating conditions of our experiment to form hydrates.

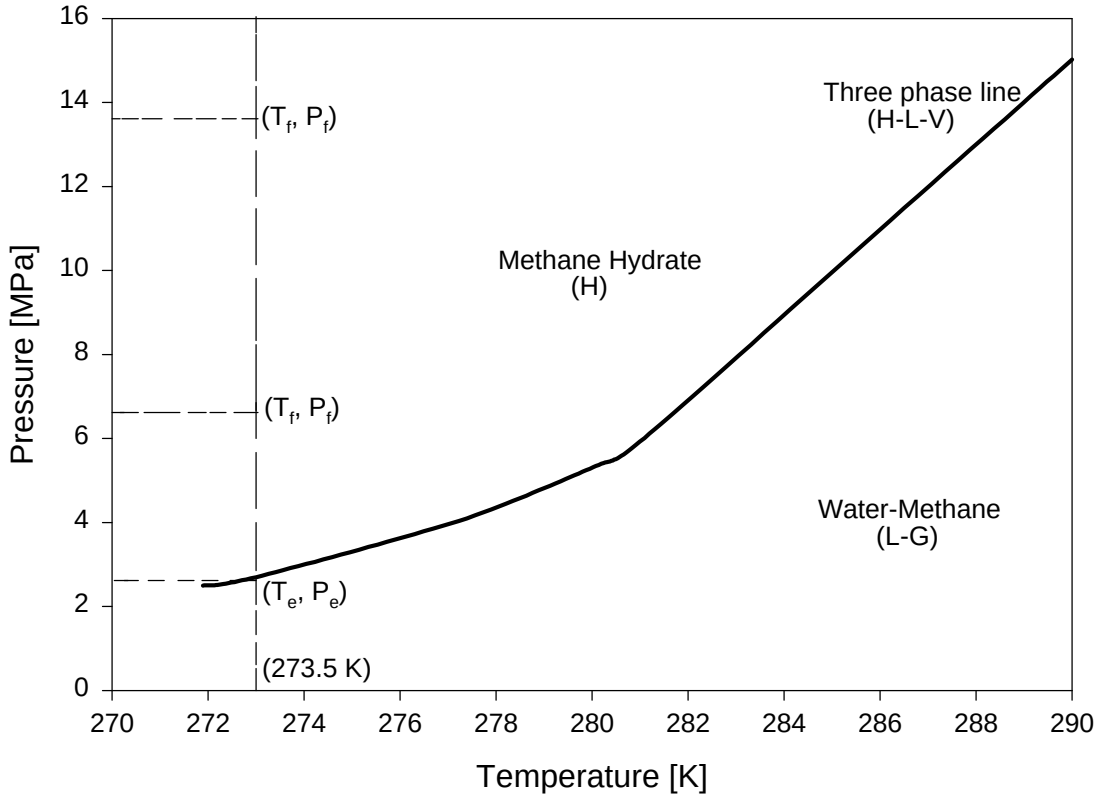

Figure 3.2 Three-phase equilibrium curve for hydrate-liquid water-methane gas system

3.4 Experimental Results

The analysis of the experimental results starts with the governing material balance equation for the reactor, which could be expressed as

$$\begin{pmatrix} volume\ of \\ reactor \end{pmatrix} = \begin{pmatrix} volume\ of \\ water \end{pmatrix} + \begin{pmatrix} volume\ of \\ gas\ space \end{pmatrix} + \begin{pmatrix} volume\ of \\ sedi\ ment \end{pmatrix}$$

$$V_R = V_w + V_{gs} + V_s$$

The number of moles of gas in the reactor at any time is a function of the pressure, temperature and the volume of gas inside the reactor. Hence the number of moles of gas could be calculated from the equation

$$n = \frac{V_{gs}\,[lit]}{v[lit/mole]}$$

where v is the specific volume of methane at a certain pressure and temperature. This value of the specific volume was obtained from the Van der waals equation of state.

Fig 3.2a shows the schematic representation of various packed beds used in this study with several different sediments. Table 3.1 shows the summary of the operating conditions and the amount of gas converted to hydrate for the formation of methane hydrate for various sediments tested. Fig 3.3 shows the behavior of the reactor pressure and the number of moles of methane consumed as a function of time for methane hydrate formation within a mixture of two different sediments, namely glass beads (100μ) and synthetic ceramic. The sediment mixture consisted of 84.5% glass beads and 15.5% synthetic sediment by weight. The packed bed had a capillary water saturation level of 53% (volume percent). The capillary water saturation level is defined as the ratio of the volume of water to the total volume of voids within the packed bed. The starting pressure for this reaction was 13.6 MPa and the temperature was maintained at 273.5 K. The total

reaction time for this experiment was 330 hrs. It could be observed that the formation reaction in this case was exponential with a conversion of 66%.

Fig 3.4 shows the behavior of the reactor pressure and the number of moles of methane consumed as a function of time for methane hydrate formation within two different sediments, namely glass beads (100μ) and glass beads (5000μ). In this case the packed bed with sediments and water was contained in a plastic cylindrical cage with a uniform mesh size of 2mm. The sediment mixture consisted of 76% glass beads (100μ) and 24% glass beads (5000μ) by weight. The packed bed had a capillary water saturation level of 29% (volume percent). The starting pressure for this reaction was 6.8 MPa and the temperature was maintained at 273.5 K. It could be observed from Fig 3.4 that the reactor pressure decreased exponentially, while the gas consumption increased exponentially. In this case, the conversion of the hydrate based on feed methane was experimentally found out to be 57%.

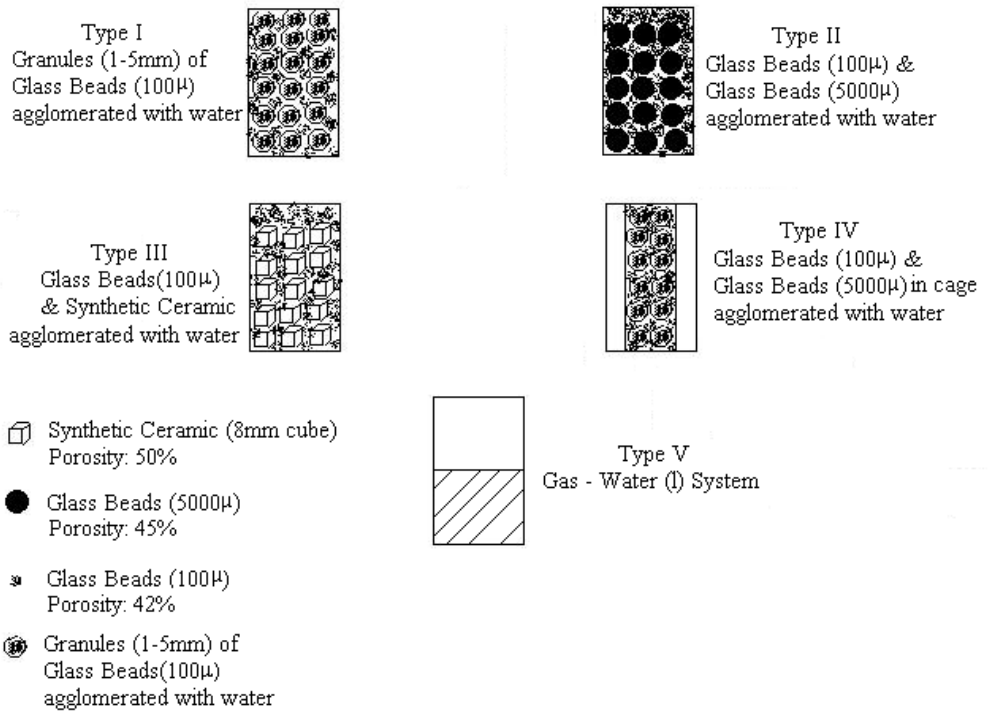

Figure 3.2a Schematic representation of several packed bed types based on various sediments

Run	Sediment	Capillary Water Saturation [%]	Reactor Pressure at t = 0 [MPa]	Reactor Pressure at $t = t_{end}$ [MPa]	Reactor Temperature [K]	Reaction Time [hrs.]	Methane converted to Hydrate [%]
1	Glass Beads (100μ) & Synthetic Ceramic	53	13.60	5.50	273.5	330	66
2	Glass Beads (100μ) & Glass Beads (5000μ) in cage	29	6.80	4.10	273.5	44	46
3	Glass Beads (100μ)	28	13.30	10.10	273.5	127	19
4	Gas - Liquid System	-	11.63	11.16	273.5	22	5
5	Glass Beads (100μ) & Glass Beads (5000μ)	18	10.20	2.90	273.5	137	78
6	Glass Beads (100μ) & Glass Beads (5000μ)	18	13.60	3.20	273.5	137	76

$$Capillary\ Water\ Saturation\,[\%] = \frac{Volume\ of\ Water}{Volume\ of\ Voids} x100$$

$$Methane\ Converted\ to\ Hydrate\,[\%] = \frac{moles\ of\ methane\ consumed}{moles\ of\ methane\ fed} x100$$

Table 3.1 Summary of operating conditions for methane hydrate formation using various sediments.

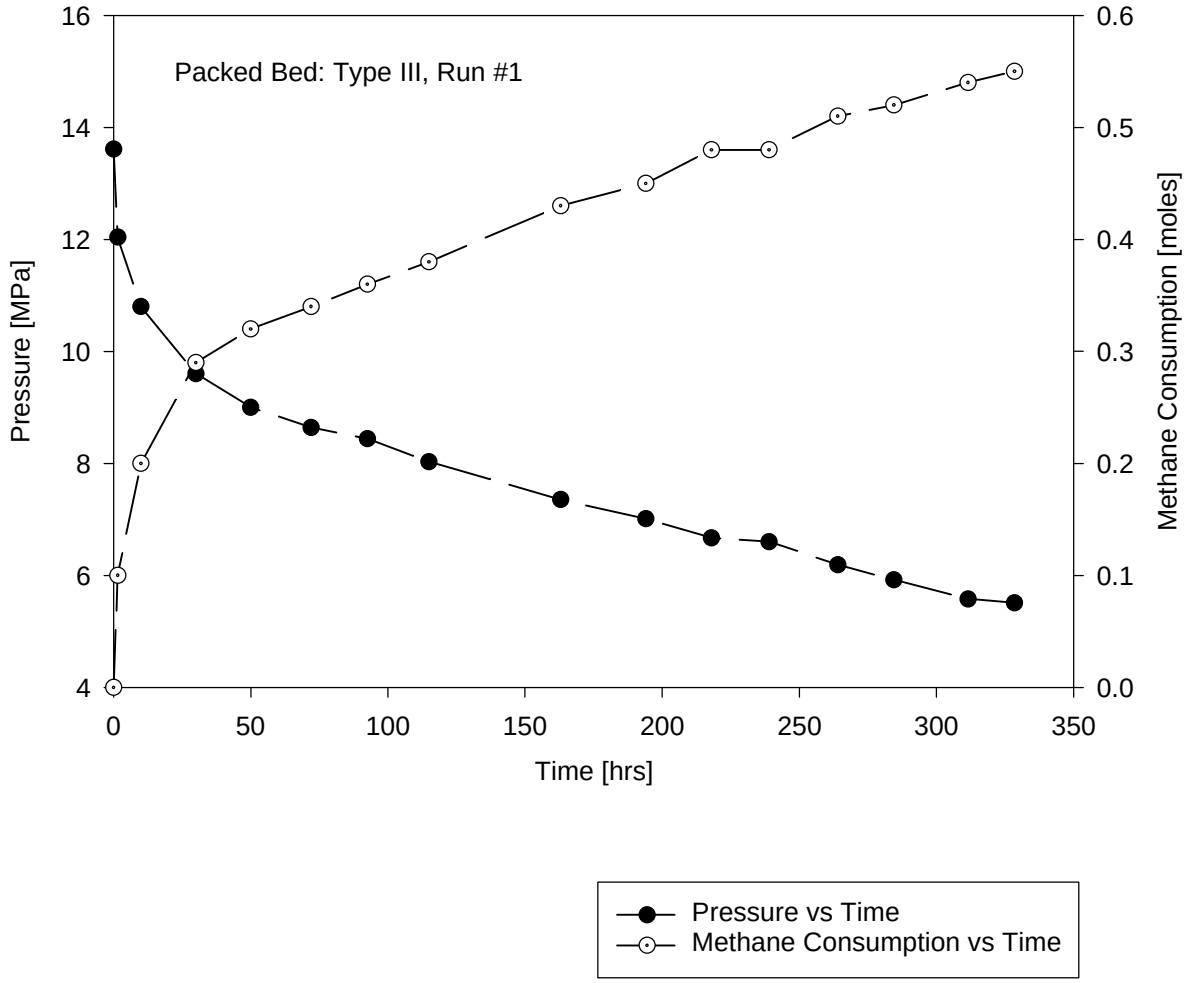

Figure 3.3 Kinetics of methane hydrate formation using the sediment mixture: glass beads (100μ) & synthetic ceramic.

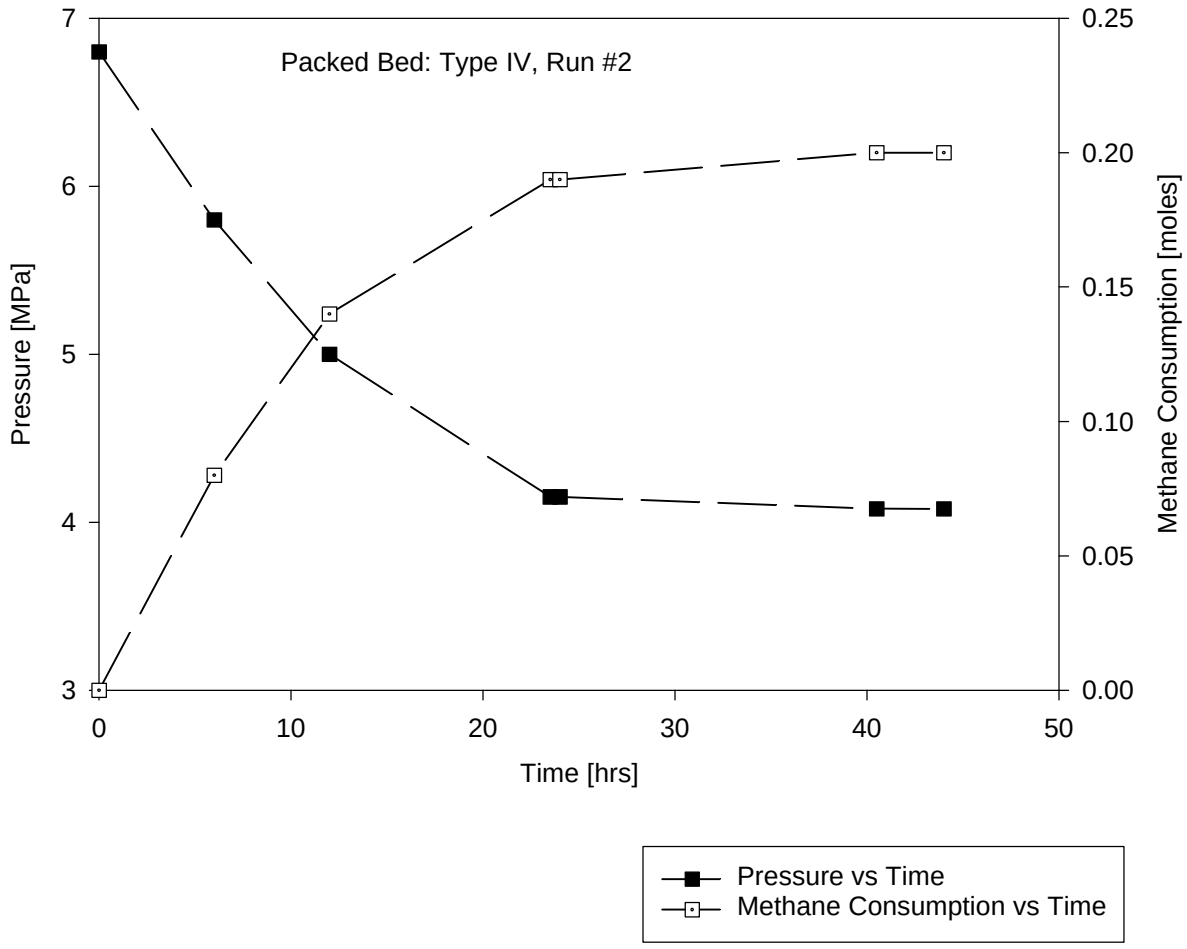

Figure 3.4 Kinetics of methane hydrate formation using the sediment mixture: glass beads (100μ) & glass beads (5000μ) in cage.

Fig 3.5 shows the behavior of the reactor pressure and the number of moles as a function of time for methane hydrate formation using a mixture of sediments containing glass beads (100μ) and glass beads (5000μ) . The sediment mixture consisted of 54% glass beads (100μ) and 46% glass beads (5000μ) by weight. The packed bed had a water saturation level of 18% (volume percent) The starting pressure for this reaction was 10.2 MPa and the temperature was maintained at 273.5 K. It could be observed from Fig 3.5 that the formation rate was found to be sigmoidal with a conversion of 78%.

Fig 3.6 shows the behavior of the reactor pressure and the number of moles as a function of time for methane hydrate formation with identical conditions as Fig 3.5 except for the starting pressure which was 13.6 MPa. Even in this case the formation rate was found to be sigmoidal with a conversion of 76%.

Fig 3.7 shows the behavior of the reactor pressure and the number of moles as a function of time for methane hydrate formation within the sediment glass beads with a mean diameter of 100μ. The packed bed had a water saturation level of 28% (volume percent). The starting pressure for this reaction was 13.3 MPa and the temperature was 273.5 K and the formation rate was exponential with a conversion of 19%.

Fig 3.8 shows the behavior of reactor pressure and the number of moles as a function of time for methane hydrate formed in a bulk volume of water. The starting pressure was 11.63 MPa and the temperature was 273.5 K. It could be observed from Fig 4.6 that the formation behavior was exponential with a conversion of 5%.

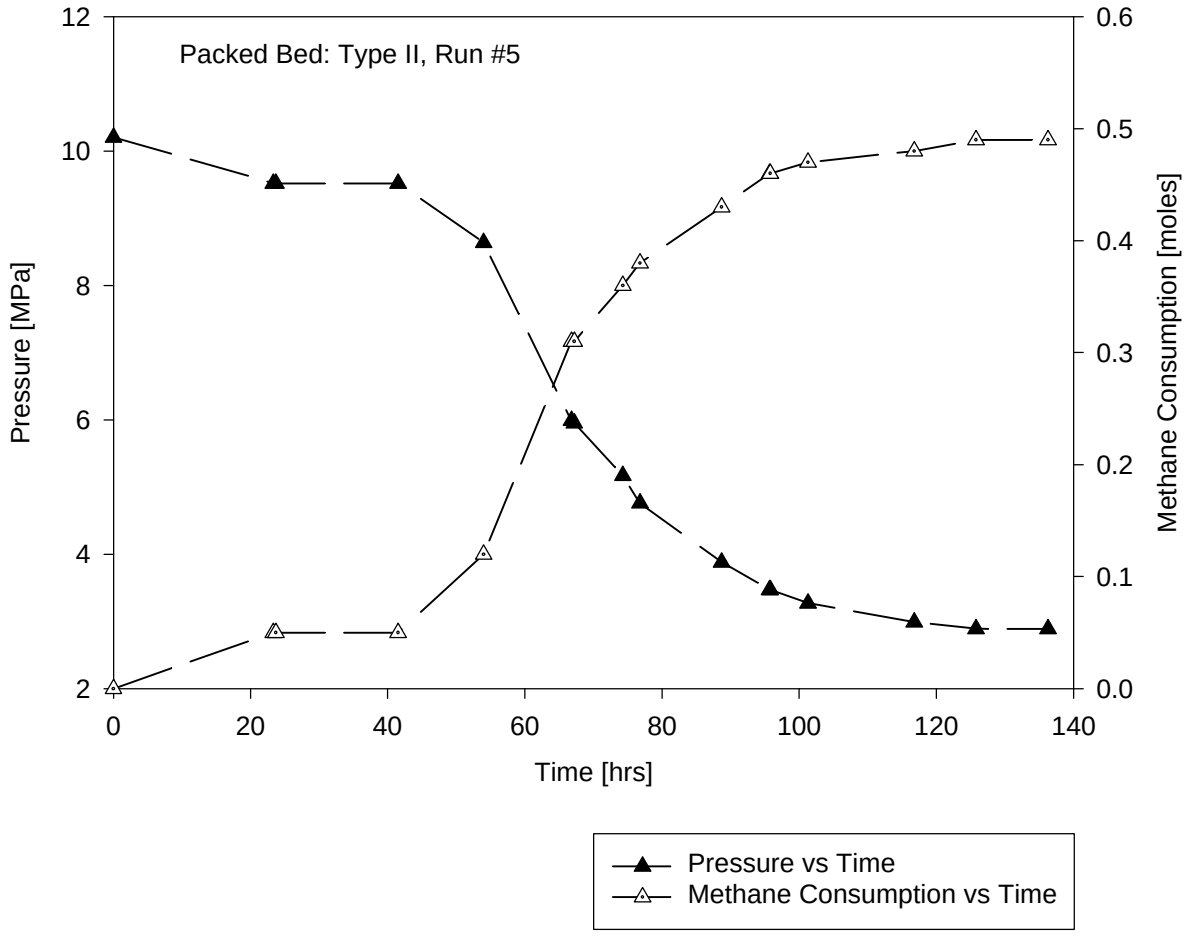

Figure 3.5 Kinetics of methane hydrate formation using the sediment mixture: glass beads (100μ) & glass beads (5000μ).

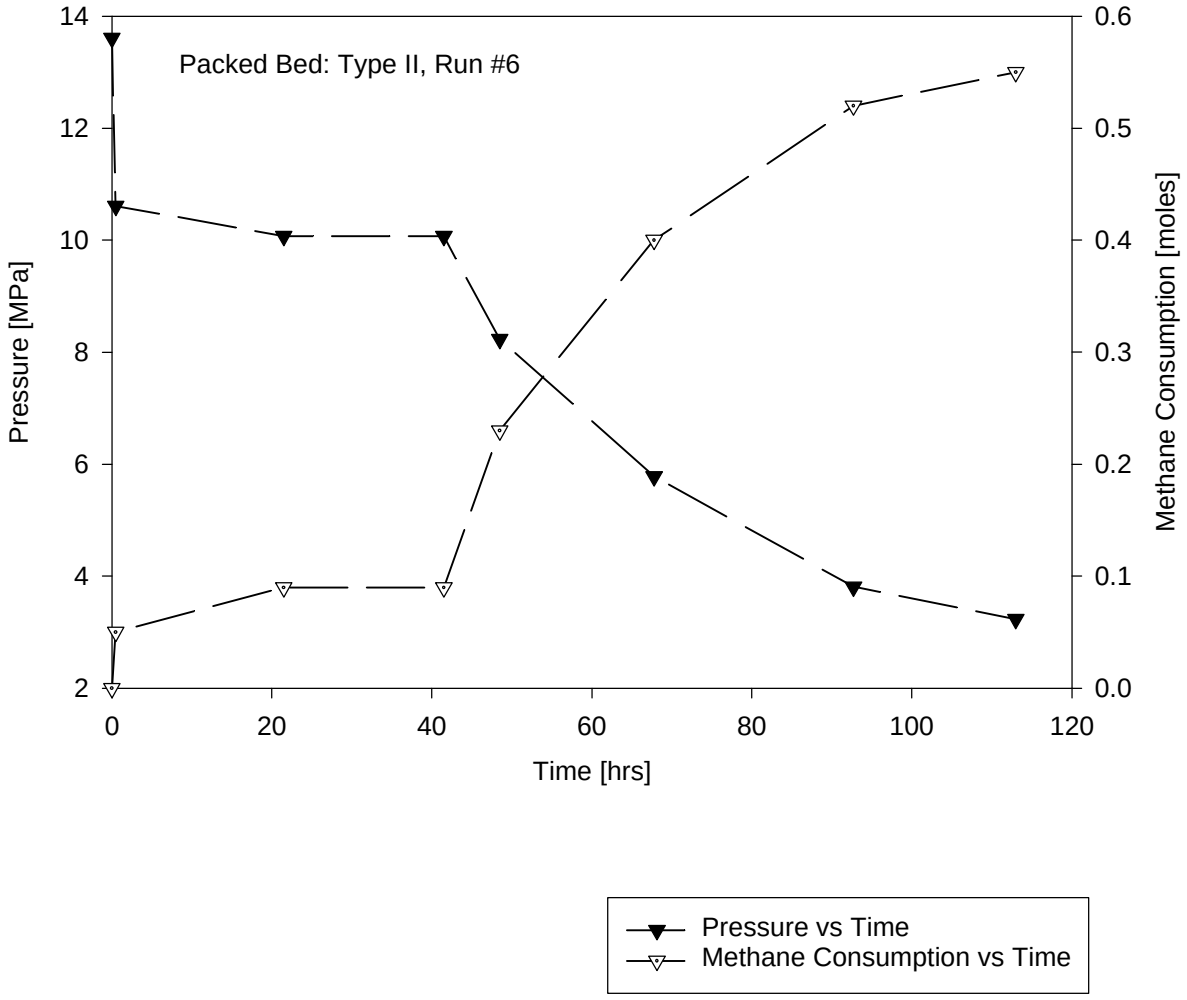

Figure 3.6 Kinetics of methane hydrate formation using the sediment mixture: glass beads (100μ) & glass beads (5000μ).

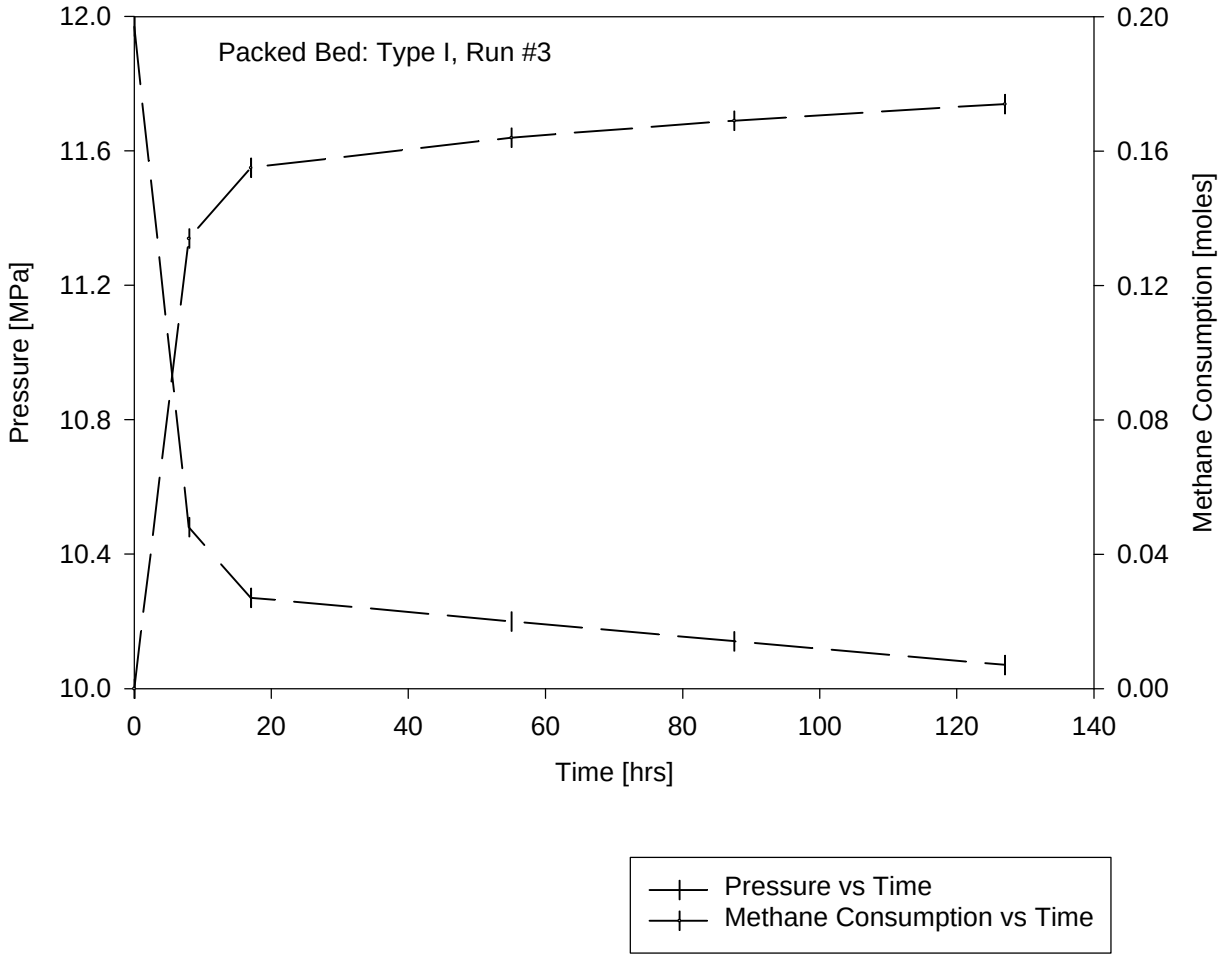

Figure 3.7 Kinetics of methane hydrate formation using the sediment: glass beads (100μ).

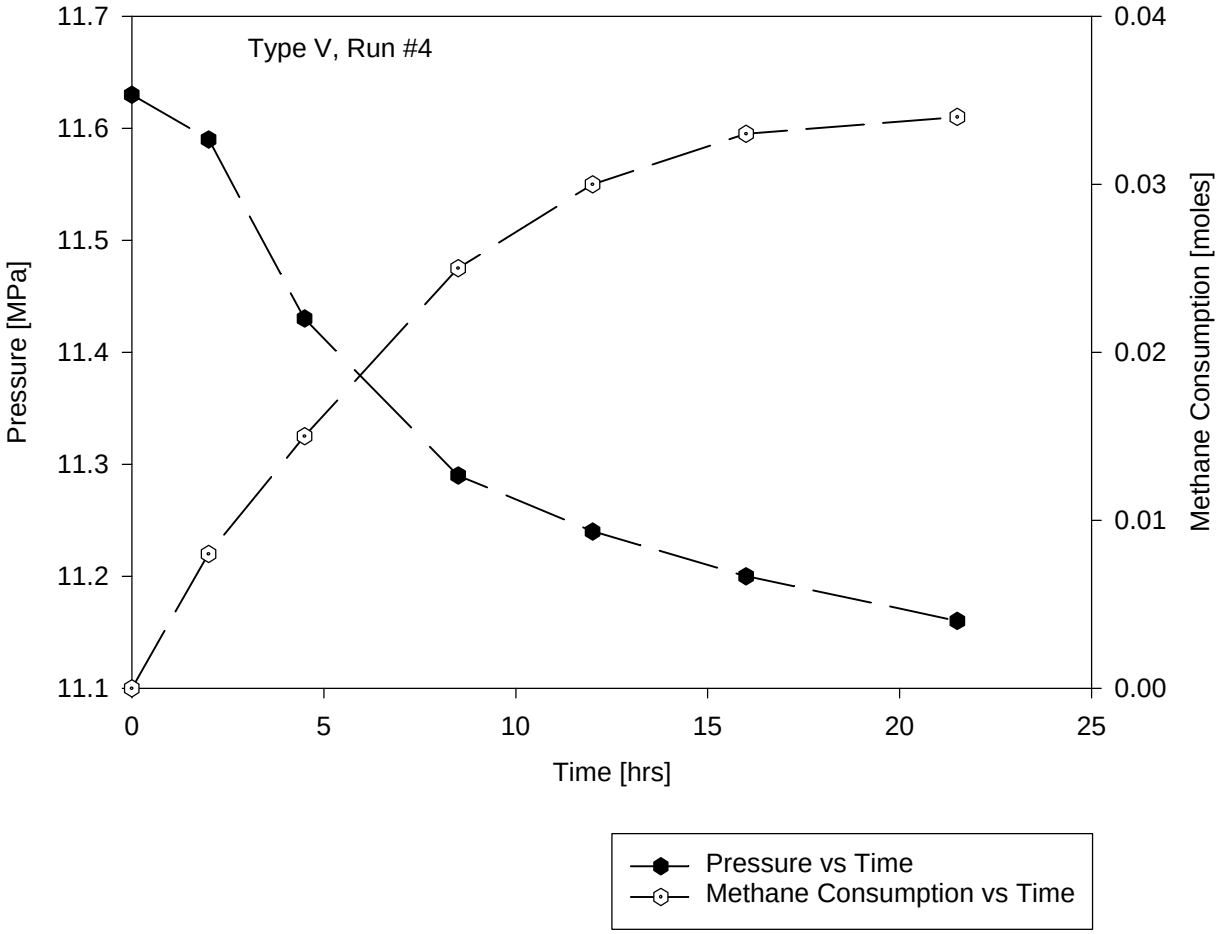

Figure 3.8 Kinetics of methane hydrate formation in a bulk volume of water

3.5 Formation rate constant

Based on the experimental results, it could be concluded that the formation of methane hydrate is a very complex exothermic crystallization reaction. This crystallization reaction is controlled by several different variables. The important variables that affect the crystallization reaction are:

1. Driving force available for reaction ($P_f - P^*$); This driving force is the difference between the experimental pressure (P_f) of the hydrate formation reaction and the pressure (P^*) corresponding to the three phase equilibrium point on the phase diagram at the experimental reactor temperature.
2. Capillary water saturation coefficient; This water saturation coefficient is defined as the ratio of the volume of water to the volume of voids in the packed bed. This ratio is very important in view of the granulation water balance of the sediments in the packed bed.
3. Sediment Type; Hydrate formation starts at the point where there is a large contact surface area for nucleation. Hence in view of enhancing the surface area available for reaction, the selection of the type of sediment with appropriate porosity is very important.
4. Reaction Time; The conversion of the hydrate that is formed is critically affected by the reaction time. Ideally the formation reaction should be carried out until the reactor pressure approached the value corresponding to the equilibrium point on the three-phase diagram. However, since the diffusion resistance increases as the reaction proceeds, the time required to attain the equilibrium pressure may be very large.

The overall rate constant for the formation of hydrates could be expressed as

$$k_{formation} = F(P_f, T_f, W_s, S/V)$$

The variables controlling the rate constant are the starting pressure of reaction P_f, temperature T_f, capillary water saturation coefficient W_s and the surface to volume ratio of packed bed S/V. It was inferred from the experimental data that the formation reaction was first order with respect to the concentration of methane and figures 3.3a through 3.8a describe the estimation of the overall formation reaction rate constant (k_f). This overall formation rate constant could be expressed by the following equation

$$-\frac{dn_{CH_4}}{dt} = k_f . n_{CH_4}{}^{n^*}$$

where n* is the overall order of the hydrate formation process and n* = 1.

Table 3.2 shows typical values for the overall formation reaction rate constant for the sediments tested. It should be very clearly understood that this formation reaction rate constant is not the same as the intrinsic rate constant of a chemical reaction. On the other hand this is the overall rate constant including the effects of heat transfer, mass transfer and reaction.

Run	Sediment	Rate Constant, k_f $[min]^{-1}$	Regression Equation
1	Glass Beads (100μ) & Synthetic Ceramic	1.50×10^{-4}	$n = n_o + a(1 - e^{-k_f t})$
2	Glass Beads (100μ) & Glass Beads (5000μ) in cage	12.05×10^{-4}	$n = n_o + a(1 - e^{-k_f t})$
3	Glass Beads (100μ)	25.47×10^{-4}	$n = a(1 - e^{-k_f t})$
4	-	19.92×10^{-4}	$n = a(1 - e^{-k_f t})$
5	Glass Beads (100μ) & Glass Beads (5000μ)	21.20×10^{-2}	$n = \frac{a}{1 + e^{-\frac{(t - t_o)}{k_f}}}$
6	Glass Beads (100μ) & Glass Beads (5000μ)	29.00×10^{-2}	$n = \frac{a}{1 + e^{-\frac{(t - t_o)}{k_f}}}$

Table 3.2 Formation rate constants of methane hydrate as a function of several different sediments.

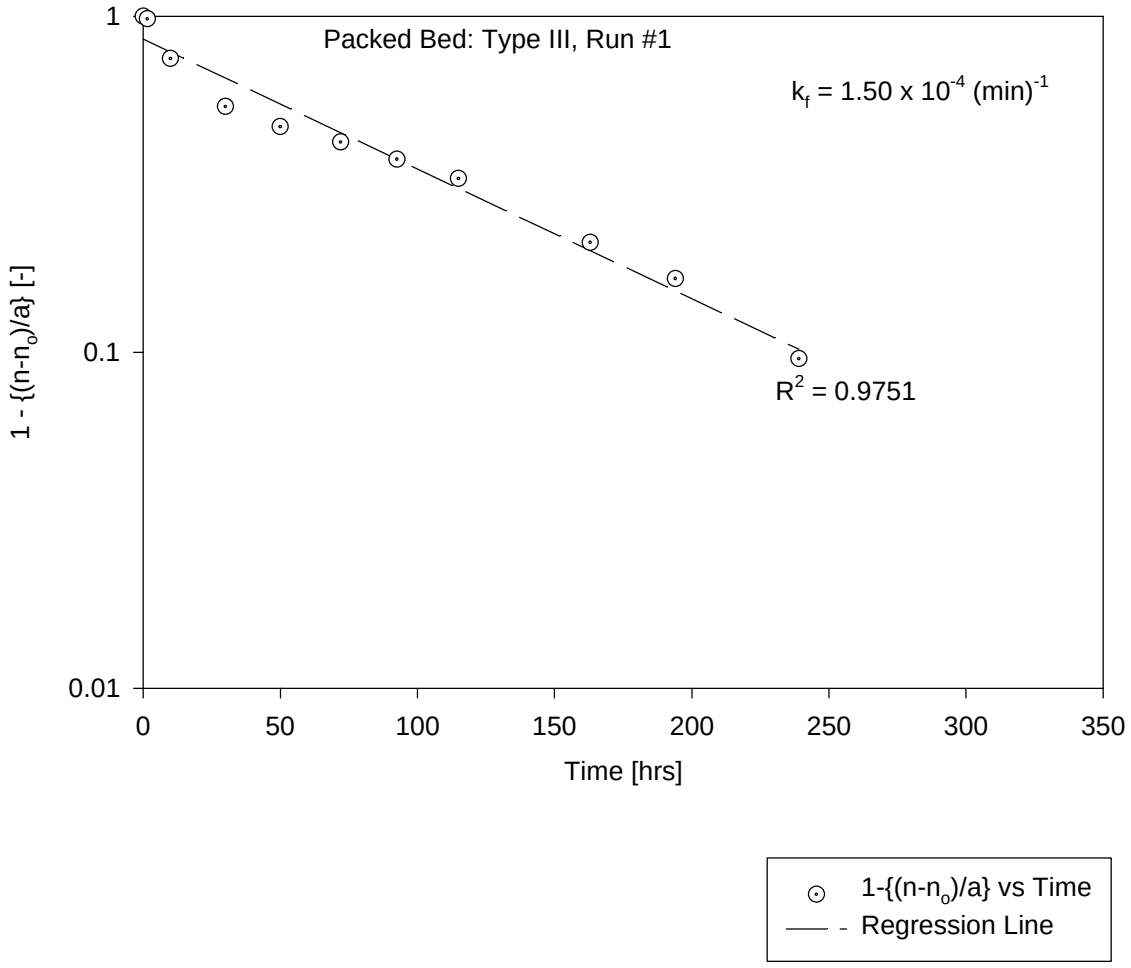

Figure 3.3a Determination of rate constant of methane hydrate formation using the sediment mixture: glass beads (100μ) & synthetic ceramic.

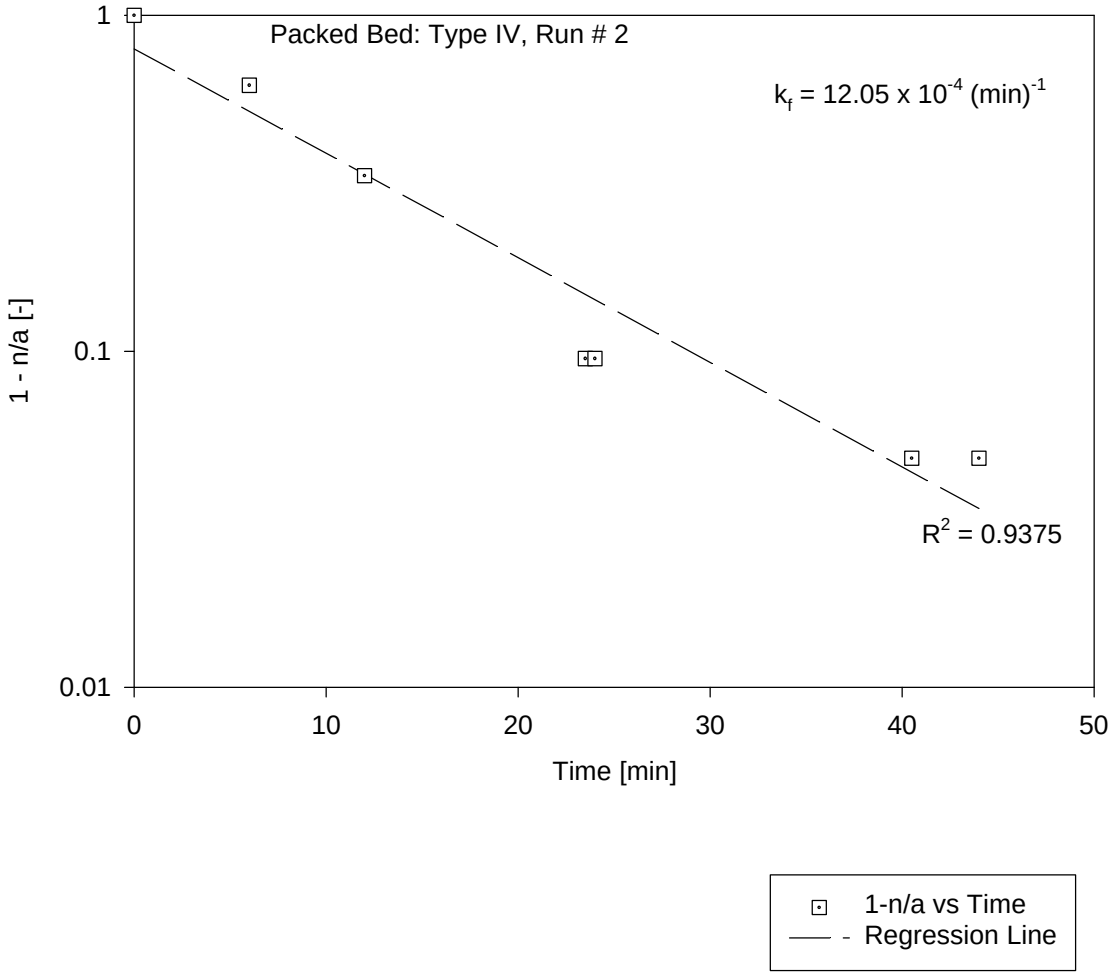

Figure 3.4a Determination of rate constant of methane hydrate formation using the sediment mixture: glass beads (100μ) & glass beads (5000μ) in cage.

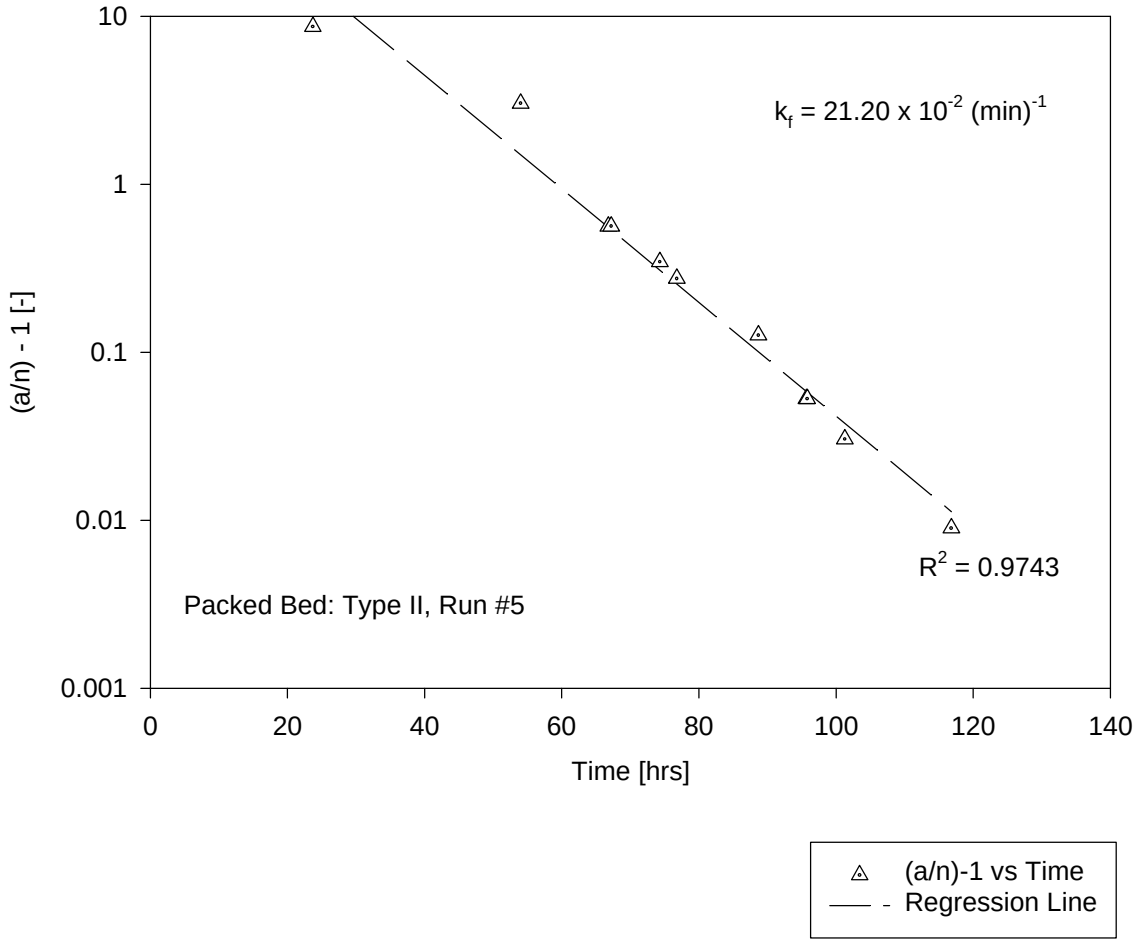

Figure 3.5a Determination of rate constant of methane hydrate formation using the sediment mixture: glass beads (100μ) & glass beads (5000μ).

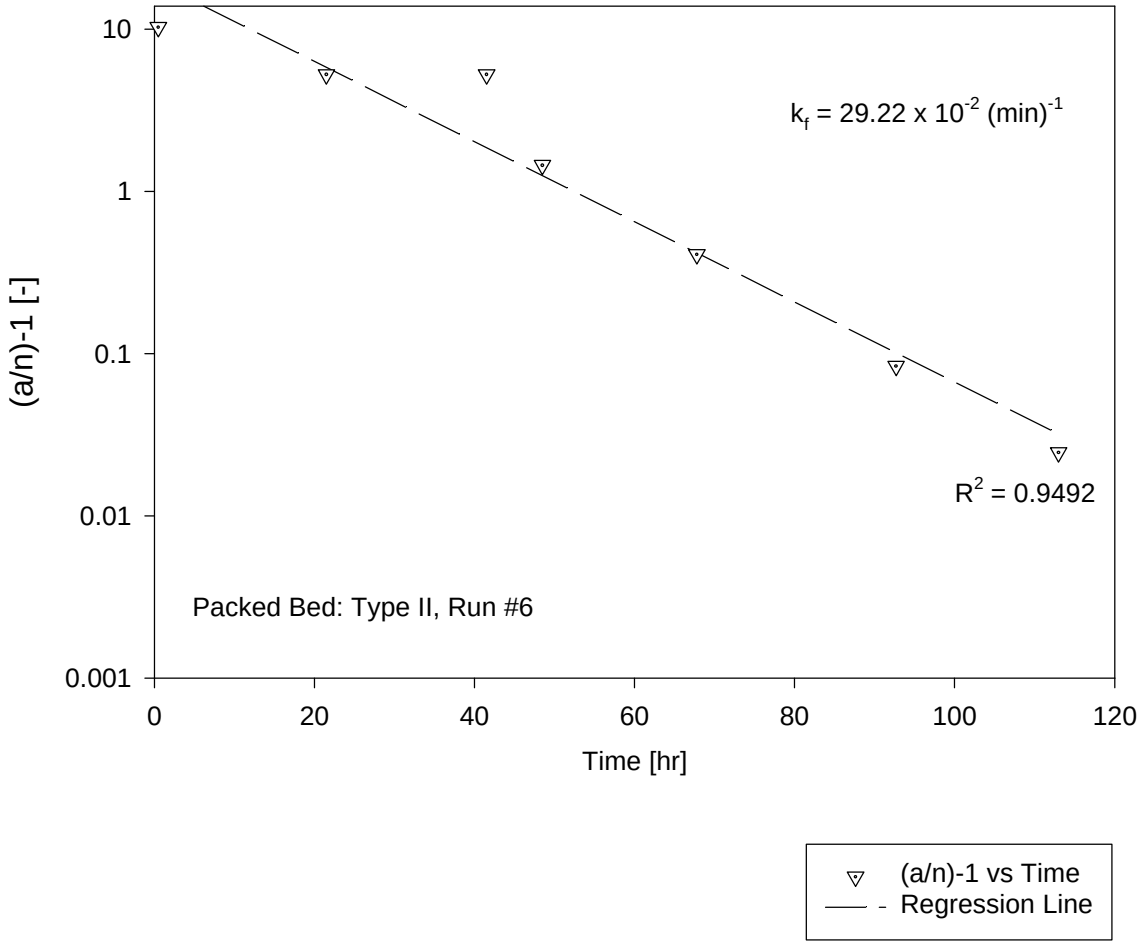

Figure 3.6a Determination of rate constant for methane hydrate formation using the sediment mixture: glass beads (100μ) & glass beads (5000μ).

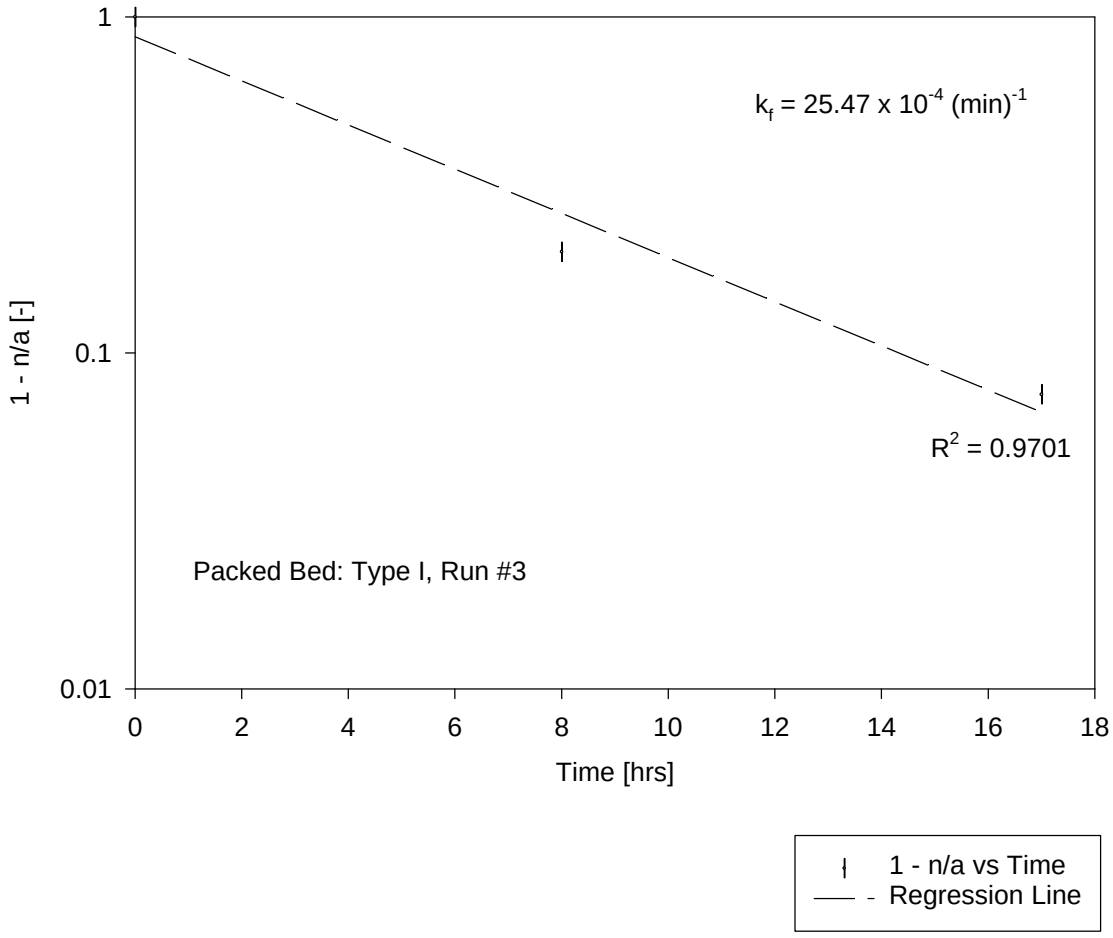

Figure 3.7a Determination of rate constant of methane hydrate formation using the sediment: glass beads (100μ).

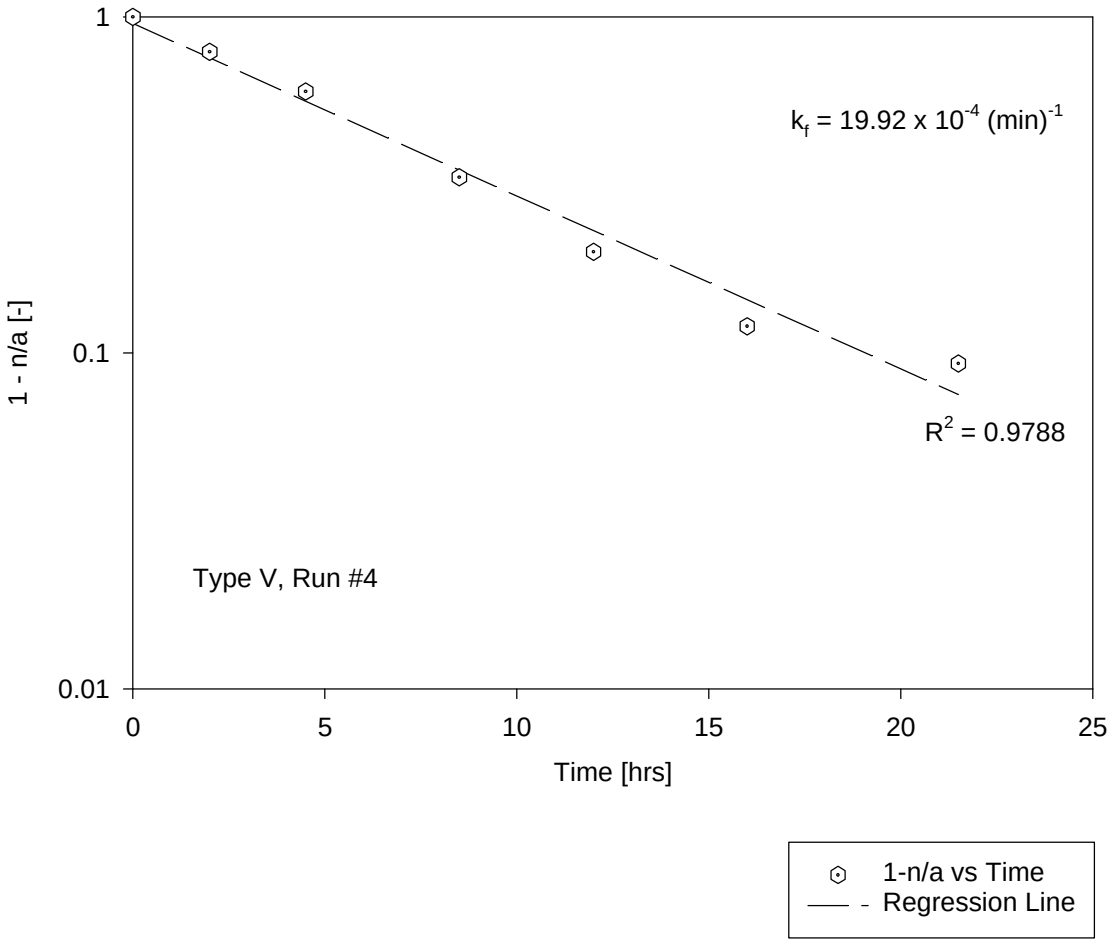

Figure 3.8a Determination of rate constant of methane hydrate formation in a bulk volume of water.

3.6 Hydrate Decomposition

Hydrate decomposition was accomplished by controlled depressurization starting at a pressure of 2.72 MPa when the temperature was maintained at 273.5 K. The decomposition rates were found be both zero order and first order based on the concentration of methane depending on the type of sediment. Figures 3.9 through 3.14 show the decomposition behavior in terms of the number of moles of methane generated. Material balance of methane was found to be within 10% for all the decomposition experiments. Hydrate decomposition is an endothermic reaction and the variables that control the overall rate constant (k_d) for the decomposition reaction could be expressed as

$$k_{decomposition} = F(P_d, T_d, e_{bed})$$

The controlling variables are the starting pressure of decomposition P_d, temperature T_d and the voidage of the packed bed ε_{bed}. The overall decomposition rate was found to be both zero order and first order depending on the type of sediment and other variables. This overall decomposition rate could be expressed by the following equation

$$\frac{dn_{CH_4}}{dt} = k_d \, .m_{hydrate}^{\ n^*}$$

where n* is the overall order of the decomposition reaction and n* = 0 or 1. It should be very clearly understood that this rate constant k_d is not the same as the rate constant of an intrinsic chemical reaction. On the other hand this rate constant simply represents the overall rate including heat transfer and mass transfer effects.

Run	Sediment	Rate Constant, k_d	Regression Equation
1	Glass Beads (100μ) & Synthetic Ceramic	15.1×10^{-2} $(min)^{-1}$	$n = a(1-e^{-k_d t})$
2	Glass Beads (100μ) & Glass Beads (5000μ) in cage	2.96×10^{-2} moles/min	$n = k_d t$
3	Glass Beads (100μ)	0.25×10^{-2} moles/min	$n = k_d t$
4	-	23.0×10^{-2} $(min)^{-1}$	$n = a(1-e^{-k_d t})$
5	Glass Beads (100μ) & Glass Beads (5000μ)	3.71×10^{-2} moles/min	$n = k_d t$
6	Glass Beads (100μ) & Glass Beads (5000μ)	5.97×10^{-2} moles/min	$n = k_d t$

Table 3.3 Decomposition rate constants of methane hydrate as a function of several different sediments.

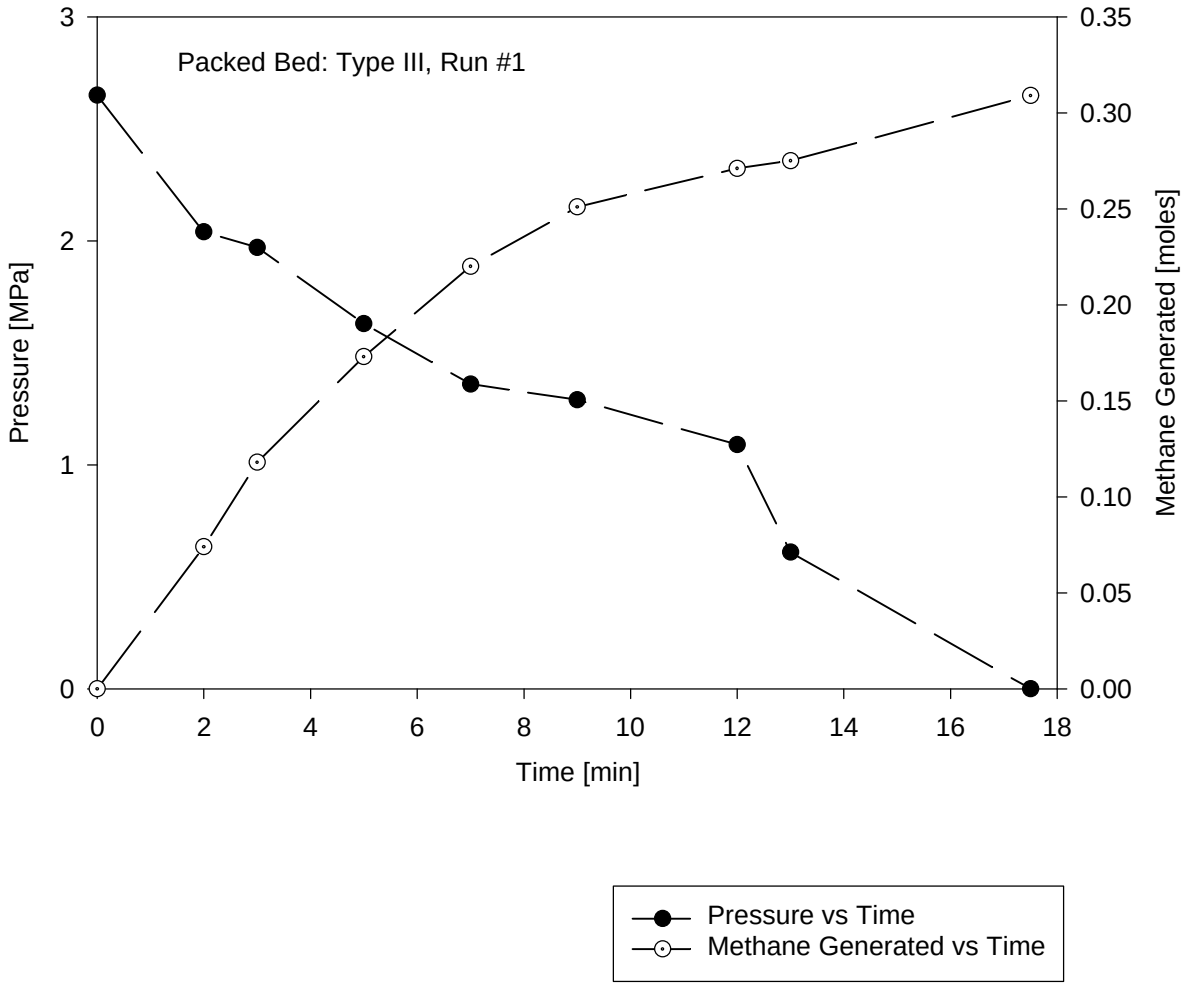

Figure 3.9 Kinetics of methane hydrate decomposition using the sediment mixture: glass beads (100μ) & synthetic ceramic.

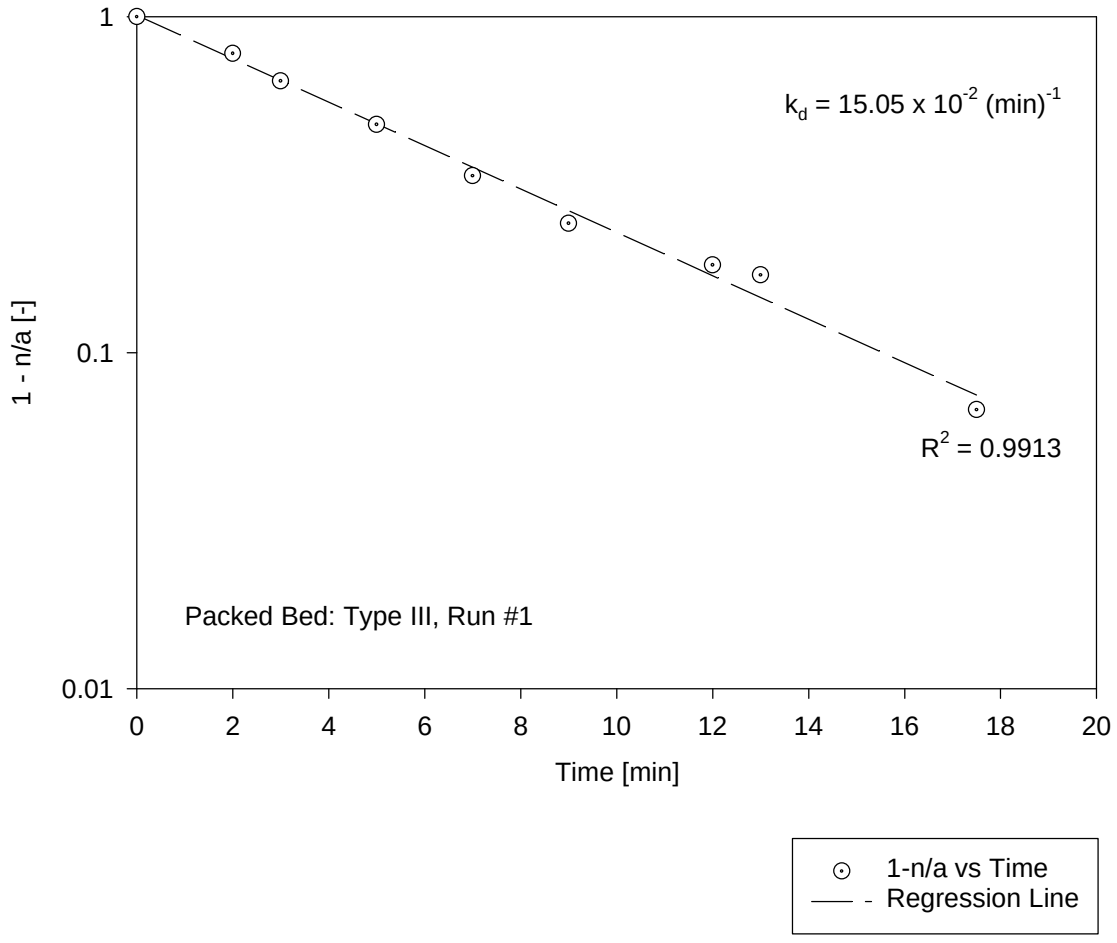

Figure 3.9a Determination of rate constant for methane hydrate decomposition using the sediment mixture: glass beads (100μ) & synthetic ceramic.

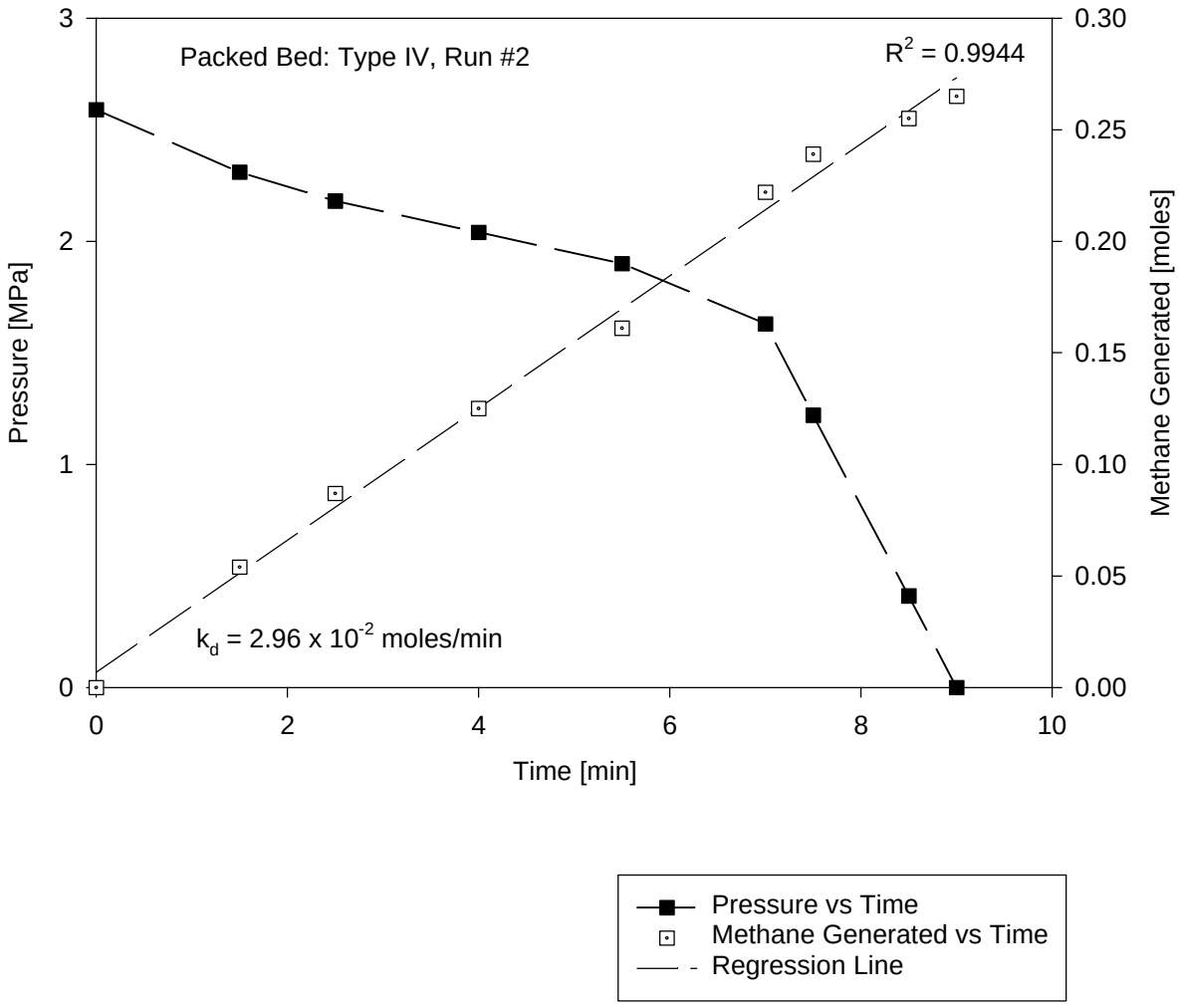

Figure 3.10 Kinetics of methane hydrate decomposition using the sediment mixture: glass beads (100μ) & glass beads (5000μ) in cage.

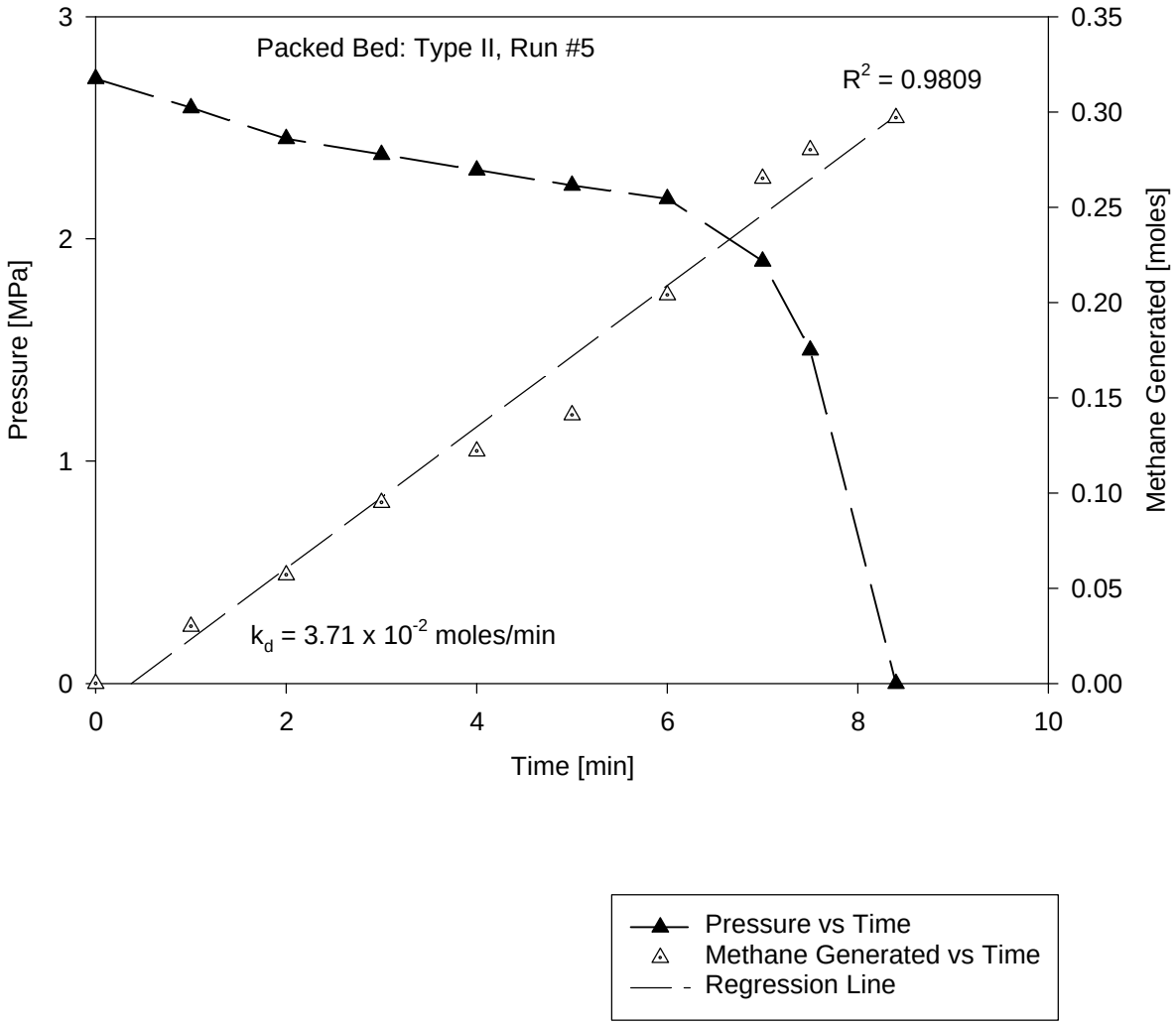

Figure 3.11 Kinetics of methane hydrate decomposition using the sediment mixture: glass beads (100μ) & glass beads (5000μ).

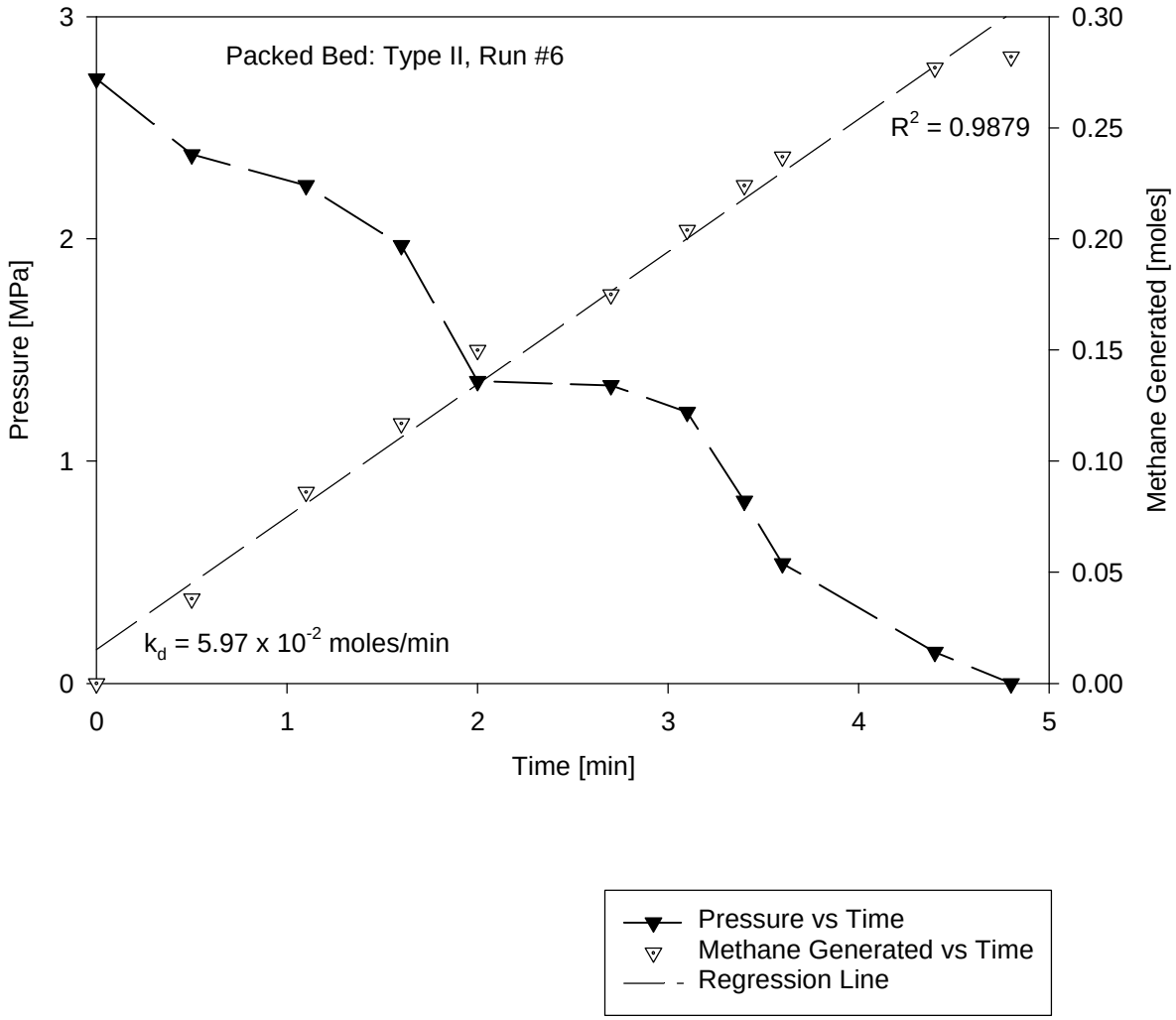

Figure 3.12 Kinetics of methane hydrate decomposition using the sediment mixture: glass beads (100μ) & glass beads (5000μ).

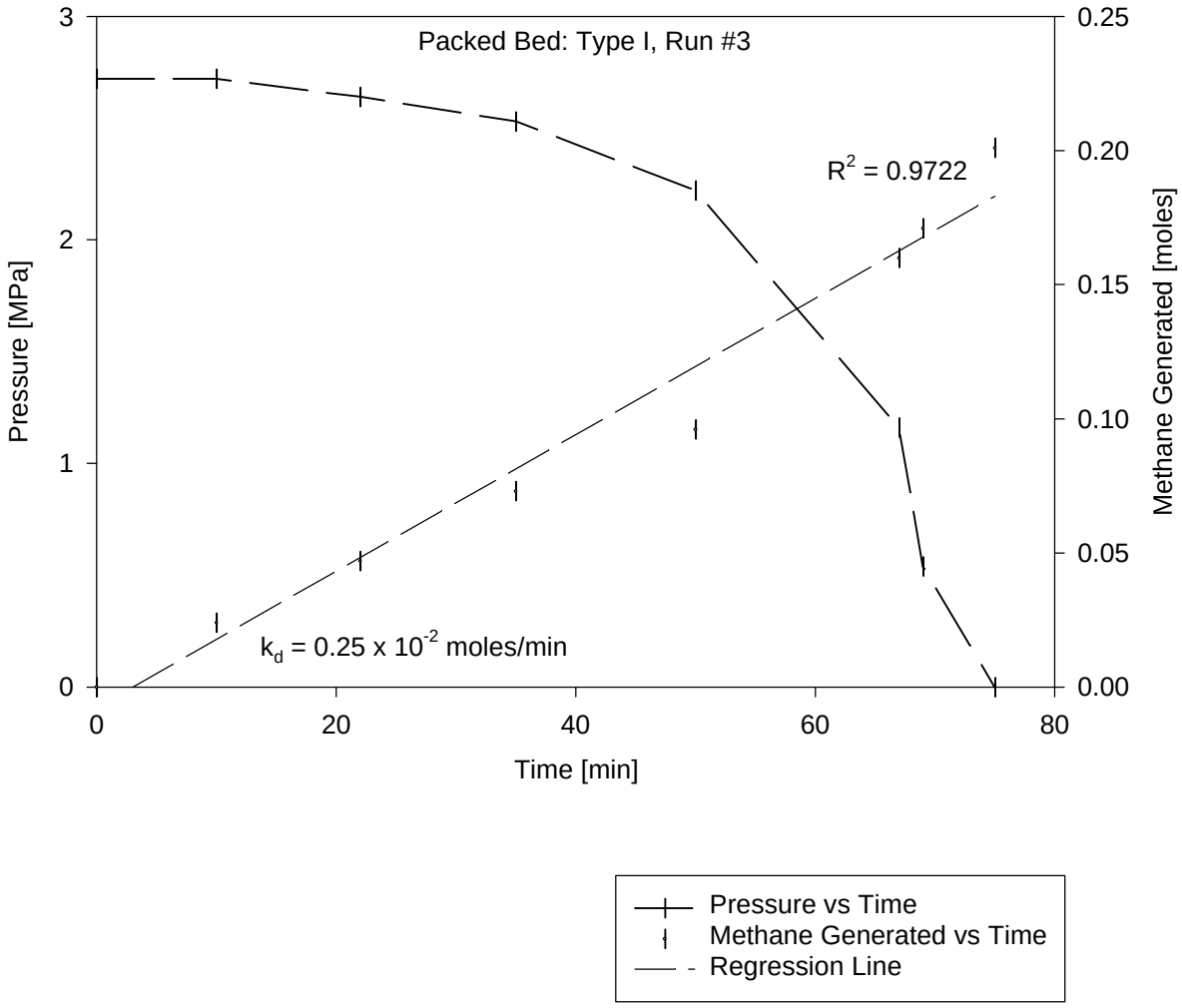

Figure 3.13 Kinetics of methane hydrate decomposition using the sediment: glass beads (100μ).

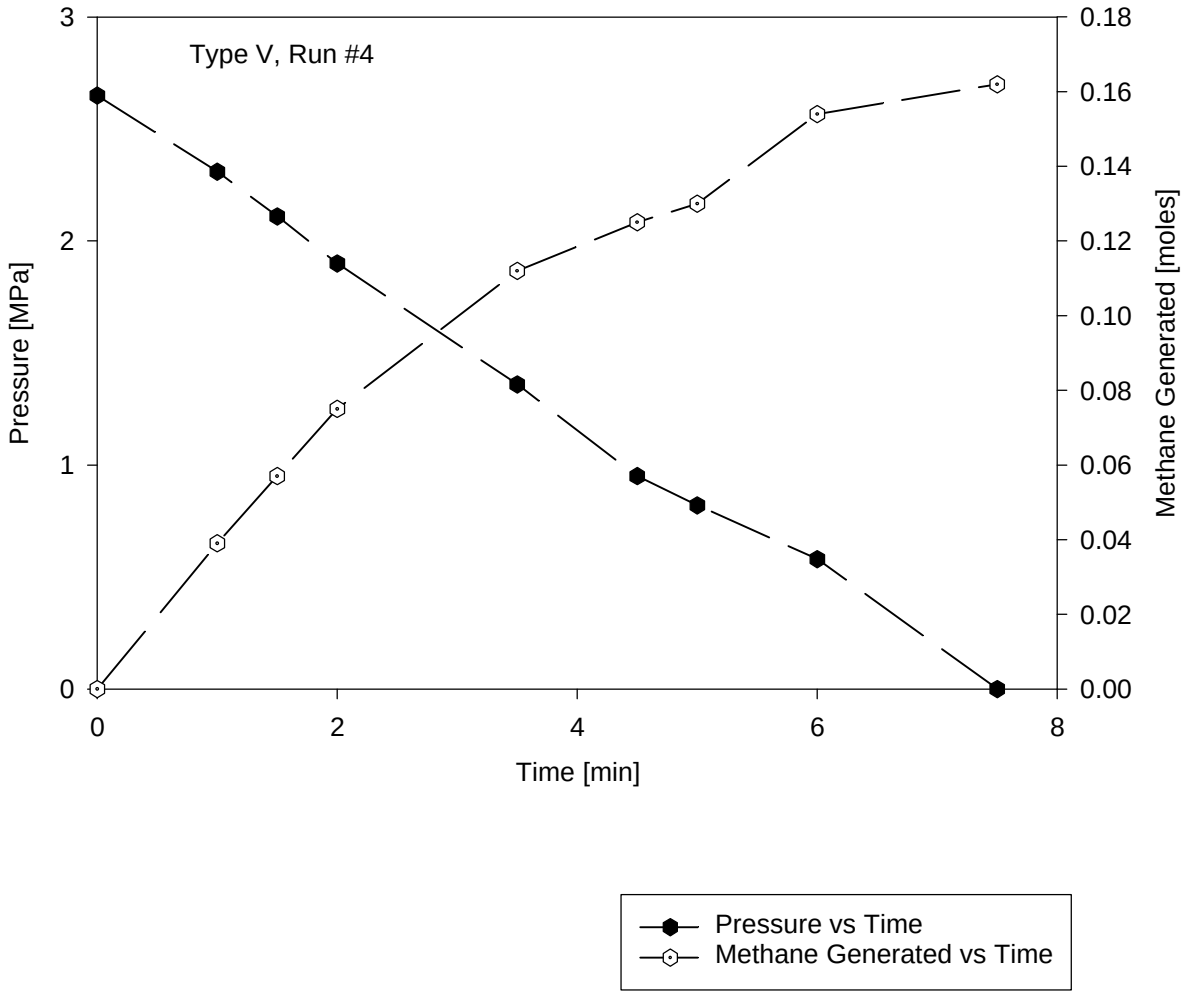

Figure 3.14 Kinetics of methane hydrate decomposition in a bulk volume of water.

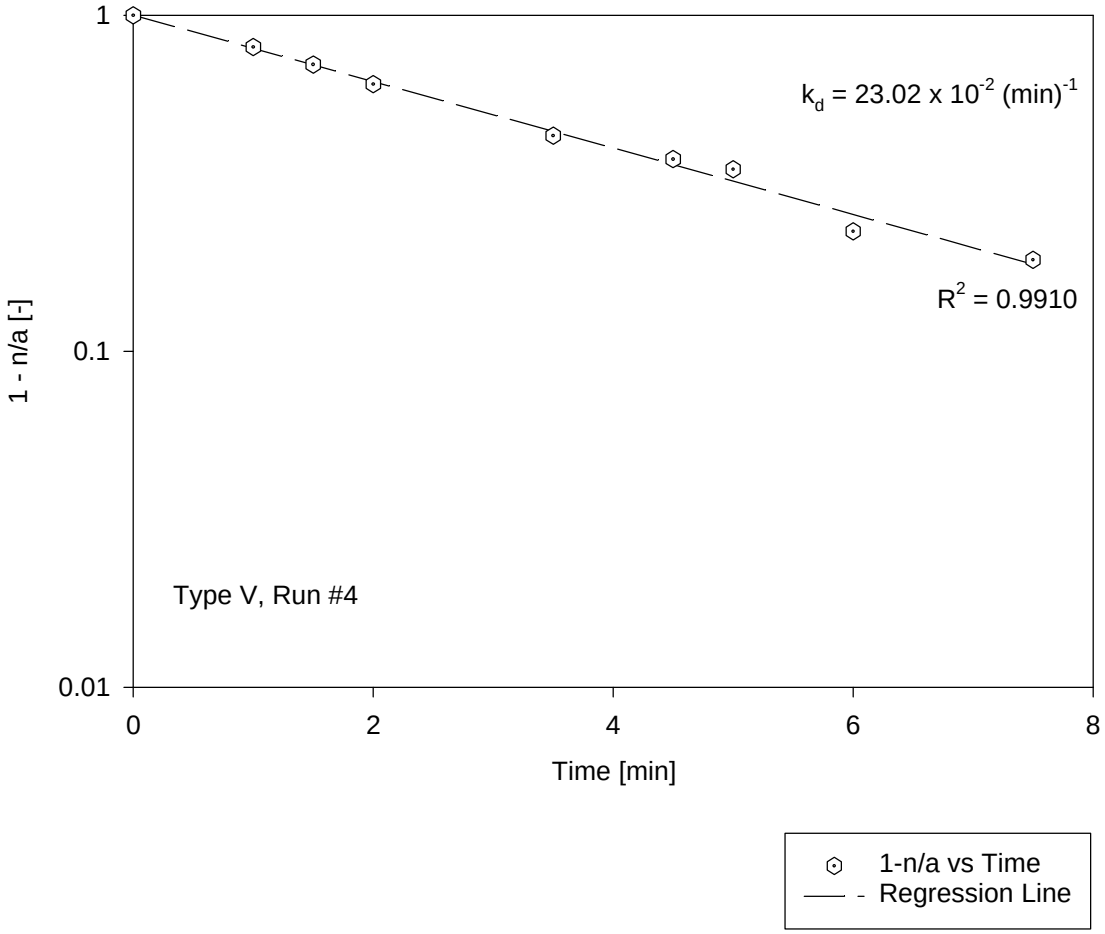

Figure 3.14a Determination of rate constant of methane hydrate decomposition in a bulk volume of water.

Fig 3.15 shows the amount of methane that was converted to hydrate at the end of the formation reaction for several different sediments. It also shows the same data for hydrates manufactured from a bulk of water. This data could be visualized as the extent of reaction and it could be clearly observed that the extent of reaction was much higher for experiments carried out with sediments as opposed to those carried out in a bulk volume of water.

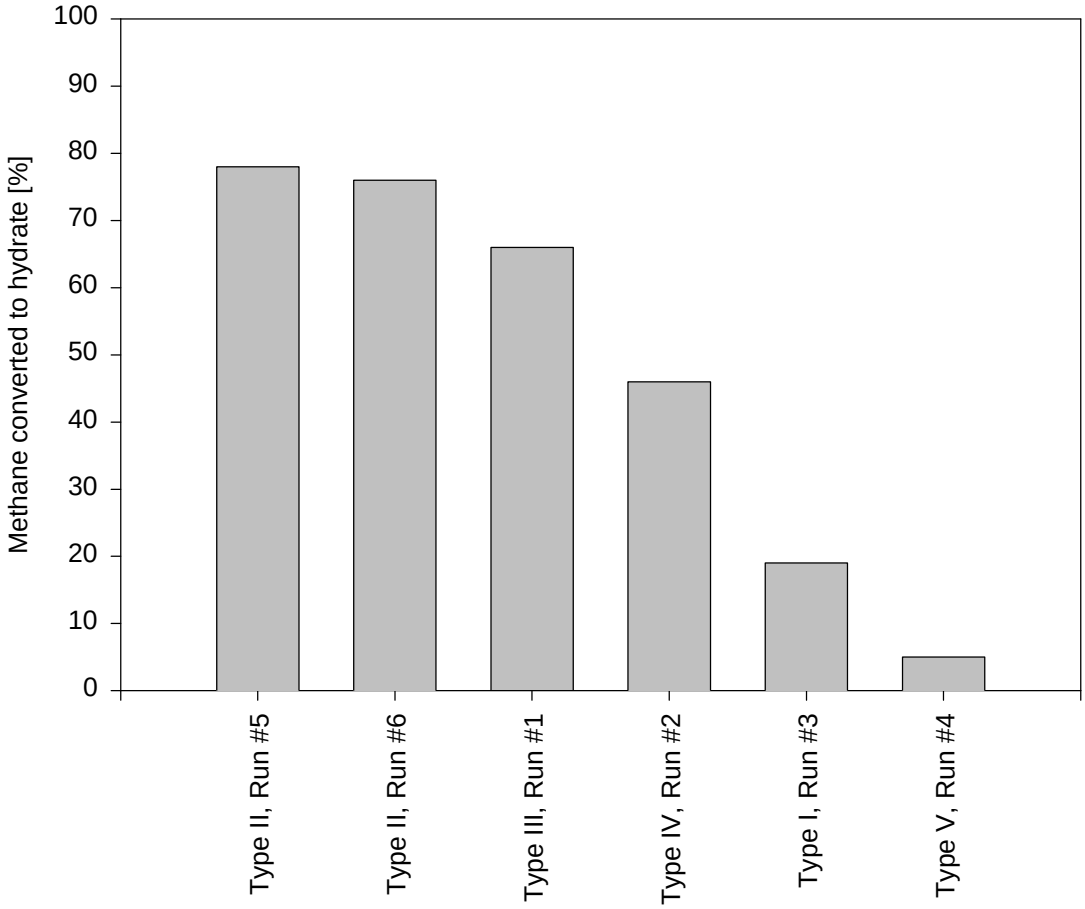

Figure 3.15 Amount of methane converted to hydrate as a function of several different sediments.

CHAPTER IV

CONCLUSION

Conclusions

Following are the conclusions derived based on the series of experiments carried out in our custom-built high-pressure reactor.

1. An experimental procedure based on our custom-built high-pressure reactor was presented for the formation and decomposition of methane gas hydrates with and without sediments.
2. The formation reaction was monitored based on a drop in the reactor pressure while decomposition reaction was accomplished through controlled depressurization of the reactor.
3. Overall kinetic rate constants were reported based on our experiments both for formation and decomposition of methane hydrates. This overall rate constant includes heat transfer, mass transfer and reaction effects and it is emphasized that this rate constant is not the same as the intrinsic rate constant of a chemical reaction. Kinetic reaction rate equations were proposed for both formation and decomposition reactions.
4. Based on the experiments, formation rates were found to be either exponential or sigmoidal while the decomposition rates were found to be either linear or exponential. Also formation rates were found to be first order in methane concentration while the decomposition rates were either zero order or first order depending on the type of sediment used.
5. Based on the experimental results it is evident that the formation of seed nuclei is not always necessary for the complete growth of hydrate crystals as claimed by Yousif (1994). This conclusion seems to be justified from a few

our experiments where the formation rate was very fast even at the beginning of the reaction.

6. The amount of methane converted to hydrate (in terms of the percentage of methane fed at t = 0) was found to be much larger for the case of hydrates formed within sediments as opposed to those formed in a bulk volume of water. This is reasonable because of the larger contact surface area that is available for reactions carried out within sediments. In the case of reactions carried out in a bulk volume of water, the reaction takes place only at the interface since the gas-water contact surface area is limited.
7. Formation and decomposition rate constants were found to be strongly dependent on the type of sediment used.

CHAPTER V

REFERENCES

References

1. Bishnoi, P. R. and Natarajan, V. “Formation and Decomposition of Gas Hydrates”, Fluid Phase Equilibria, 117, 168-177, 1996.
2. Circone, S., et al, “Methane Hydrate Dissociation Rates at 0.1 MPa and Temperatures above 272 K”, Annals of the New York Academy of Sciences, vol 912, 544-555, 2000.
3. Englezos, P., et al, “Kinetics of Formation of Methane and Ethane Gas Hydrates”, Chemical Engineering Science, Vol. 42, No.11, 2647-2658, 1983.
4. Katz, D.L., et al, “Handbook of Natural Gas Engineering”, McGraw-Hill Book Company, New York, 1959.
5. Kim, H. C., et al, “Kinetics of Methane Hydrate Decomposition”, Chemical Engineering Science, Vol. 42, No. 7, 1645-1653, 1987.
6. Makogon, Y. F. “Hydrates of Hydrocarbons”, PennWell Books, Tulsa, Oklahoma, 1997.
7. Selim, M. S. and Sloan, E. D. “Hydrate Decomposition in Sediment”, SPE Reservoir Engineering, 245-251, May 1990.
8. Sloan, E. D. “Clathrate Hydrates of Natural Gases”, Marcel Dekker Inc., New York, 1991.
9. Uchida, T., et al, “Decomposition Condition Measurements of Methane Hydrate in Confined Small Pores of Porous Glass”, Journal of Physical Chemistry, 103, 3659-3662, 1999.
10. Uchida, T., et al, “Summary of physicochemical properties of natural gas hydrate and associated gas-hydrate-bearing sediments”, JAPEX Report, 205-215, 1998.
11. Ullerich, J. W., et al, “Theory and Measurement of Hydrate Decomposition”,

AIChE Journal, Vol. 33, No. 5, 747-752, May 1987.

12. Vysniauskas, A.and Bishnoi, P.R. “A Kinetic Study of Methane Hydrate Formation”, Chemical Engineering Science, Vol. 38, No. 7, 1061-1072, 1983.

13. Yousif, M. F. “The Kinetics of Hydrate Formation”, SPE 28479, 169-177.